

AUS Repository

Shear Strength of Concrete Beams Reinforced with Steel Welded Wire Fabric

Item Type	Thesis
Authors	Alhoubi, Yazan L.
Download date	2026-06-08 17:46:15
Link to Item	http://hdl.handle.net/11073/16575

SHEAR STRENGTH OF CONCRETE BEAMS REINFORCED WITH
STEEL WELDED WIRE FABRIC

by

Yazan L. Alhoubi

A Thesis presented to the Faculty of the
American University of Sharjah
College of Engineering
In Partial Fulfillment
of the Requirements
for the Degree of
Master of Science in
Civil Engineering

Sharjah, United Arab Emirates

November 2019

Approval Signatures

We, the undersigned, approve the Master's Thesis of Yazan L. Alhoubi.

Thesis Title: Shear Strength of Concrete Beams Reinforced with Steel Welded Wire Fabric.

Signature

Date of Signature
(dd/mm/yyyy)

Dr. Sami Tabsh
Professor, Department of Civil Engineering
Thesis Advisor

Dr. Farid Abed
Professor, Department of Civil Engineering
Thesis Committee Member

Dr. Samir Emam
Professor, Department of Mechanical Engineering
Thesis Committee Member

Dr. Irtishad U. Ahmad
Head, Department of Civil Engineering

Dr. Lotfi Romdhane
Associate Dean for Graduate Affairs and Research
College of Engineering

Dr. Naif Darwish
Acting Dean, College of Engineering

Dr. Mohamed El-Tarhuni
Vice Provost for Graduate Studies

Acknowledgement

I would like to express my sincere gratitude to my supervisor and mentor, Dr. Sami Tabsh, who provided me with constant support and guidance during my M.Sc. degree in Civil Engineering at the American University of Sharjah. I would also like to extend my gratitude to all my colleagues and professors of the Department of Civil Engineering. I appreciate the effort and time spent on reviewing and commenting on this dissertation by the committee members, Dr. Farid Abed from the Civil Engineering Department and Dr. Samir Emam from the Mechanical Engineering Department. I am thankful to the American University of Sharjah for granting me the graduate teaching assistantship, which was a huge aid in fulfilling my master's degree. Many thanks to Engineer Arshi Faridi and Engineer Mohammad Ansari for their assistance in the laboratory work.

I would like to acknowledge the financial support provided by AUS faculty research grant EFRG18-MSE-CEN-28, which made completing this research study possible. Special thanks to Emirates Stones Co. Ltd. and its General Manager Mr. Jawdat Bargawi for providing material and labor for the experimental part of the study.

Last but not least, I would like to send special thanks to my family and friends who provided me with encouragement and support during my graduate degree.

Abstract

Reinforced concrete (RC) beams are typically reinforced transversely with steel stirrups to resist shear. However, this form of reinforcement requires extended time and considerable labor to make and place the stirrups, and results in large tolerances. Such shortcomings have encouraged researchers to seek alternatives methods of shear reinforcement. This study aims at researching the viability of using welded wire fabric (WWF), cold formed into the shape of a steel cage as shear reinforcement. A comprehensive literature review on this topic revealed scarce research about the use of WWF as shear reinforcement in RC beams. To accomplish the objective of the study, 23 half-scale beams that are 1900 mm or 2050 mm long with 200 mm x 300 mm cross-section are tested at AUS under a single-load configuration with consideration of different wire diameters (4, 6 and 8 mm), grid openings (25, 50 and 100 mm, concrete compressive strengths (30 and 35 MPa), shear span-to-thickness ratios (2.5 and 3.0), and transverse steel reinforcement ratios (251 and 505 N/mm). A comparison is carried out between the test results of WWF reinforced beams and corresponding stirrup reinforced beams in terms of the shear strength and ductility. The experimental study was complemented by a theoretical investigation utilizing the shear design provisions in North American and European structural design codes. Results of the study showed that not all the vertical shear reinforcement in the WWF and stirrup reinforced beams reach yielding at ultimate and the shear span-to-depth ratio has no impact on the shear strength of such beams. The WWF reinforced beams possess 2-17% higher shear strength than corresponding stirrup reinforced beams and the ductility index of WWF reinforced beams matches the ductility index of corresponding stirrup reinforced beams. Beams containing WWF cages that consist of smaller diameter wires at narrow spacing exhibit slightly higher shear strength than corresponding ones containing larger diameter wires at wide spacing. The predicted shear strength by the ACI 318, Eurocode2, CSA23.3 and BS 8110 is within 6% of the strength obtained by the experiments. This shows that the current approaches for computing the shear strength of stirrup reinforced beams can be reliably used for WWF reinforced beams.

Keywords: *Welded Wire Fabric, Welded Wire Mesh, Concrete, Beam, Confinement, Shear, Ductility, Stiffness.*

Table of Contents

Abstract.....	5
List of Figures.....	9
List of Tables.....	14
Chapter 1. Introduction.....	15
1.1. Introduction.....	15
1.2. Research Significance.....	17
1.3. Problem Statement.....	19
1.4. Proposed New Concept.....	19
1.5. Objectives of the Study.....	20
1.6. Scope of Study.....	21
1.7. Thesis Framework.....	21
Chapter 2. Welded Wire Fabric.....	23
2.1. Introduction.....	23
2.2. Manufacturing Process.....	25
2.3. Specification and Properties.....	26
2.4. Application in Construction.....	27
2.5. Structural Building Code Requirements.....	28
Chapter 3. Background on Shear.....	29
3.1. General.....	29
3.2. ACI 318 Code.....	30
3.3. Eurocode 2.....	32
3.4. CSA 23.3-04.....	33
3.5. BS 8110.....	34
3.6. Modified Compression Field Theory.....	35
3.7. Examples.....	37
3.7.1. ACI 318-14.....	39
3.7.2. ACI 318-19.....	39
3.7.3. Eurocode 2.....	40
3.7.4. CSA 23.3-04.....	41
3.7.5. BS code.....	41
3.7.6. Modified compression field theory.....	42

3.7.7. Summary of results.....	43
Chapter 4. Literature Review.....	44
4.1. Shear Reinforcement Alternative to Stirrups.....	44
4.2. Shear Performance of Beams Reinforced with WWF.....	50
4.3. Flexural Performance of Beams Reinforced with WWF.....	54
4.4. Axial Compression Performance of Columns Reinforced with WWF.....	55
4.5. Confinement Models and Reinforcing Methods.....	58
4.6. Final Remarks on the Literature Review.....	62
Chapter 5. Experimental Program.....	63
5.1. Details of Beam Specimens.....	63
5.1.1. Experimental plan.....	63
5.1.2. Test setup and instrumentation.....	68
5.2. Material.....	70
5.2.1. Concrete.....	70
5.2.1.1. High f'_c	71
5.2.1.2. Low f'_c	73
5.2.2. Steel.....	73
5.2.2.1. WWF.....	76
5.2.2.2. Stirrups.....	77
5.2.2.3. Strands.....	79
5.3. Laboratory Work.....	80
5.3.1. Bending bench.....	80
5.3.2. Specimen fabrication.....	80
5.3.3. Finishing of specimens.....	84
Chapter 6. Experimental Results.....	86
6.1. Introduction.....	86
6.2. Load-Deflection Relationships.....	88
6.3. Shear Force.....	112
6.4. Load-Strains Relationships.....	112
6.5. Load-Crack Width Relationships and Cracking Patterns.....	118
Chapter 7. Analysis of Results.....	126
7.1. Shear Force-Deflection Relationships.....	126
7.2. Shear Strength.....	130

7.2.1. Effect of grid size.....	131
7.2.2. Effect of transverse steel reinforcement ratio.....	134
7.2.3. Effect of shear span-to-depth ratio.....	135
7.2.4. Effect of concrete compressive strength.....	136
7.3. Ductility	137
7.4. Theoretical Studies.....	139
Chapter 8. Conclusions and Recommendations	149
8.1. Summary.....	149
8.2. Conclusions.....	150
8.3. Recommendations.....	152
8.4. Suggested Future Research.....	152
References.....	154
Vita.....	157

List of Figures

Figure 1: Typical concrete beam failures.....	16
Figure 2: Conventional beam reinforcement.	17
Figure 3: Stress-Strain curve of WWF versus Rebar.....	18
Figure 4: WWF concept as a steel cage.	20
Figure 5: Fabrication of a steel cage from WWF sheet in the laboratory.....	20
Figure 6: Plane and deformed WWF [12].....	23
Figure 7: Representation of a WWF sheet [11].	24
Figure 8: Manufacturing process [14].....	25
Figure 9: Available meshes in the UAE.	26
Figure 10: Difference between galvanized and epoxy coated WWF [15].....	26
Figure 11: Usage of WWF in the construction industry [11, 20].	27
Figure 12: Anchorage of U-stirrups made of WWF [11].	28
Figure 13: Sources of shear strength.....	30
Figure 14: Table 5.2-1 from AASHTO LRFD bridge design Specifications [21].	37
Figure 15: Beam example detailing.	38
Figure 16: Shear-moment diagram of beam example.....	38
Figure 17: Shear-deflection curves for beams tested by Karayannis [25].	45
Figure 18: Sample reinforcement of beams considered [26].	45
Figure 19: Load versus Deflection curves of study by Lee et al. [26].....	46
Figure 20: Sample ISSSB reinforced beam versus a stirrups reinforced beam [27]. ..	46
Figure 21: Sample of load versus deflection curve of Ahmed's study [27].	47
Figure 22: CFRP grid considered in Suwanpanjasil et al. study [28].....	47
Figure 23: Load versus displacement results of Suwanpanjasil et al. study [28].	48
Figure 24: Maximum shear recorded in Deivanai and Sathia study [29].	48
Figure 25: Beams reinforced with swimmer bars in the transverse direction [30].	49
Figure 26: load-elongation relationships for stirrups and WWF [4].....	50
Figure 27: Results of Xuan et al. study [4].	51
Figure 28: Results of Pincheira et al. study [31].....	51
Figure 29: Cold-drawn WWF versus Rebar stress-strain curve [3].....	52
Figure 30: Summary of results of the work of Griezic et al. [3].....	52
Figure 31: process of beam jacketing [32].....	53
Figure 32: Buckling of vertical wires of WWF cage [33].	53

Figure 33: Load-Deflection graph of all tested specimens [34].	54
Figure 34: Mode of failures witnessed in Ajin and Gokulram’s study [34].	54
Figure 35: Different WWF reinforcement configurations [35].	55
Figure 36: Reinforcement configuration of columns [36].	56
Figure 37: summary of results of study by Lambert-Aikhionbare and Tabsh [36].	56
Figure 38: Previous models, proposed model and experimental results [37].	57
Figure 39: Summary of results presented by Kusuma [38].	57
Figure 40: Confinement model proposed by Mander et al. [39].	58
Figure 41: Confinement model proposed by Hoshikuma et al. [40].	59
Figure 42: Confinement model proposed by Legeron and Paultre [41].	59
Figure 43: Predicted versus experimental comparison using proposed model [41].	60
Figure 44: Previous models of concrete confinement [42].	60
Figure 45: Detailing of sections [43].	61
Figure 46: Experimental results of study by Delalibera and Giongo [43].	61
Figure 47: Experimental results versus modelled results of Jaafar’s study [44].	62
Figure 48: Summary of design approaches.	64
Figure 49: Experimental study.	66
Figure 50: Sample beam detailing containing WWF (W-6-50-2.5-35).	67
Figure 51: Sample beam detailing containing stirrups (S-8-91.5-2.5-35).	67
Figure 52: Sample beam detailing with no shear reinforcement (N-2.5-35).	67
Figure 53: UTM available at the AUS’s Materials and Structures lab.	68
Figure 54: Beam support used made from structural steel chair and steel roller.	69
Figure 55: Typical test set-up and instrumentations.	69
Figure 56: Crushing machine used available in the AUS’s asphalt lab.	70
Figure 57: Stress-Strain relations of cylinders belonging to Group 1.	72
Figure 58: Stress-Strain relations of cylinders belonging to Groups 2.	72
Figure 59: Typical cubes and cylinders failures of high f'_c specimens.	73
Figure 60: Stress-Strain relations of cylinders belonging to Group 3.	74
Figure 61: Typical cubes and cylinders failures of Group 3.	74
Figure 62: Types of steel used in this study.	75
Figure 63: UTM machine used for testing the steel bars.	75
Figure 64: Test setup of steel coupons.	76
Figure 65: Tested wire specimens.	76

Figure 66: Stress versus strain curve for WWF coupons.....	77
Figure 67: Stress versus strain curve for deformed bars.....	78
Figure 68: Tested stirrups samples.	78
Figure 69: Stress versus strain curve for strands.	79
Figure 70: Tested strands samples.	80
Figure 71: Preparing the WWF cages using the old method.	81
Figure 72: A metal brake machine used to bend thin metal sheets.....	81
Figure 73: Parts used in the assembly.....	82
Figure 74: Manufacturing process.	82
Figure 75: Preparing the WWF cages using the new method.....	82
Figure 76: Preparing WWF steel cages using bending bench.	83
Figure 77: Attaching strain gauges to steel cages.....	83
Figure 78: Formwork prepared on top of the vibrating bench.....	83
Figure 79: Casting of beams, cubes and cylinders specimens.	84
Figure 80: Curing of demolded specimens.	84
Figure 81: Painting and constructing gridlines process.	84
Figure 82: Typical finished beam.	85
Figure 83: Typical testing setup.....	85
Figure 84: Experimental details of beam W-4-25-2.5-35.....	89
Figure 85: Experimental details of beam W-6-50-2.5-35.....	90
Figure 86: Experimental details of beam W-8-100-2.5-35.....	91
Figure 87: Experimental details of beam S-8-91.5-2.5-35.....	92
Figure 88: Experimental details of beam W-4-50-2.5-35.....	93
Figure 89: Experimental details of beam S-6-103.5-2.5-35.....	94
Figure 90: Experimental details of beam S-10-73-2.5-35.....	95
Figure 91: Experimental details of beam N-2.5-35.....	96
Figure 92: Experimental details of beam W-4-25-3.0-35.....	97
Figure 93: Experimental details of beam W-6-50-3.0-35.....	98
Figure 94: Experimental details of beam W-8-100-3.0-35.....	99
Figure 95: Experimental details of beam S-8-91.5-3.0-35.....	100
Figure 96: Experimental details of beam W-4-50-3.0-35.....	101
Figure 97: Experimental details of beam S-6-103.5-3.0-35.....	102
Figure 98: Experimental details of beam S-10-73-3.0-35.....	103

Figure 99: Experimental details of beam N-3.0-35	104
Figure 100: Experimental details of beam W-4-25-3.0-30	105
Figure 101: Experimental details of beam W-6-50-3.0-30	106
Figure 102: Experimental details of beam W-8-100-3.0-30	107
Figure 103: Experimental details of beam S-8-91.5-3.0-30	108
Figure 104: Experimental details of beam W-4-50-3.0-30	109
Figure 105: Experimental details of beam S-6-103.5-3.0-30	110
Figure 106: Experimental details of beam N-3.0-30	111
Figure 107: Shear-Moment diagram of beams with $a/h=2.5$	113
Figure 108: Shear-Moment diagram of beams with $a/h=3.0$	113
Figure 109: Placement of strain gauges.	115
Figure 110: Load versus strain in transverse steel for beams of Group 1.....	116
Figure 111: Load versus strain in transverse steel for beams of Group 2.....	117
Figure 112: Load versus strain in transverse steel for beams of Group 3.....	118
Figure 113: Placement of LVDTs.....	119
Figure 114: Adjustment of crack width.	119
Figure 115: Load versus average crack width for beams of Group 1.....	120
Figure 116: Load versus average crack width for beams of Group 2.....	121
Figure 117: Load versus average crack width for beams of Group 3.....	122
Figure 118: Crack inclination of beams belonging to Group 1.	123
Figure 119: Crack inclination of beams belonging to Group 2.	124
Figure 120: Crack inclination of beams belonging to Group 3.	124
Figure 121: Summary of comparison network.	126
Figure 122: Shear-deflection graphs of beams belonging to Group 1.	127
Figure 123: Shear-deflection graphs of beams belonging to Group 2.	128
Figure 124: Shear-deflection graphs of beams belonging to Group 3.	129
Figure 125: Effect of grid size on shear strength based on equivalent $(A_{st}f_{yst}/s)_v$	133
Figure 126: Effect of grid size on shear strength based on equivalent $(A_{st}f_{yst}/s)_{v+h}$. .	134
Figure 127: Effect of vertical steel reinforcement ratio on shear strength.	135
Figure 128: Effect of shear span-to-depth ratio on shear strength.....	136
Figure 129: Effect of concrete compressive strength on shear strength.	137
Figure 130: Points considered for determining ductility of a typical beam.....	138
Figure 131: Ductility indices of the WWF and stirrup reinforced beams.....	140

Figure 132: Normalized ductility indices of the WWF reinforced beams..... 141
Figure 133: Predicted versus actual shear capacities for ACI 318-14 model..... 143

List of Tables

Table 1: Summary of results of solved example.....	43
Table 2: Fineness modulus of fine aggregate.	71
Table 3: Coarse aggregate properties.....	71
Table 4: Mix proportions for high strength concrete used in the study.	71
Table 5: Summary of results of high f'_c specimens.	72
Table 6: Mix proportions for low strength concrete used in the study	73
Table 7: Summary of results of low f'_c specimens.	74
Table 8: Mechanical properties of WWF steel wire	77
Table 9: Mechanical properties of deformed bars steel test.	78
Table 10: Summary of strands steel test.	79
Table 11: Beams details and identification scheme.	87
Table 12: Maximum recorded values of load and shear.	114
Table 13: Summary of crack width and inclination of tested specimens.	125
Table 14: Shear Strength of all tested specimens	130
Table 15: Shear strength of beams with $A_{st}f_{yst}/s = (A_w f_{yw}/g)_v$	132
Table 16: Shear strength of beams with $A_{st}f_{yst}/s = (A_w f_{yw}/g)_{v+h}$	132
Table 17: Details of the calculations of ductility indices.....	140
Table 18: Experimental and predicted shear strength results based on actual f_y	142
Table 19: Experimental to predicted shear strength results based on actual f_y	144
Table 20: Experimental and predicted shear strength results based on nominal f_y . ..	145
Table 21: Ratio of experimental to predicted shear strength based on nominal f_y	146
Table 22: Average experimental-to-predicted shear strength.....	147
Table 23: Shear strength contribution of concrete and shear reinforcement.	147

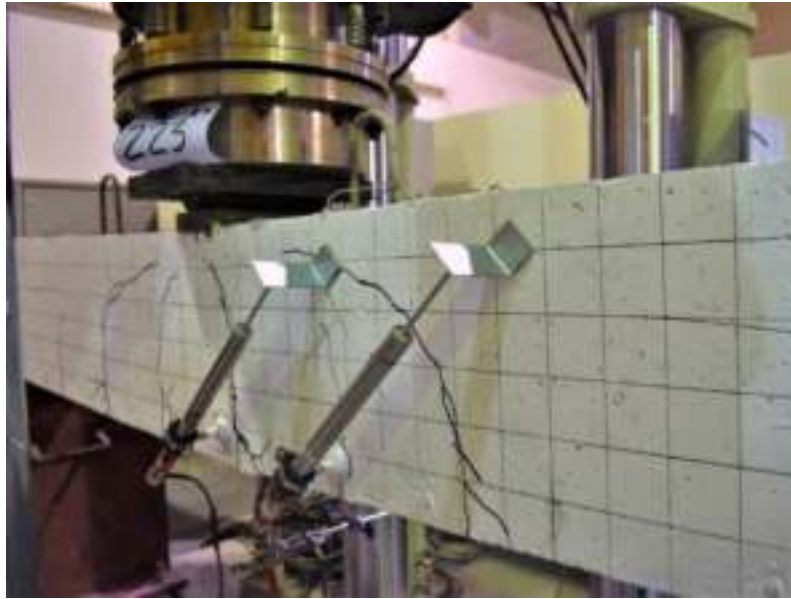
Chapter 1. Introduction

In this chapter, a brief introduction to the research is provided. This chapter includes background information to the topic, objectives and scope of the study, and thesis framework.

1.1. Introduction

In general, reinforced concrete (RC) beams may fail in two different modes, which are flexure or shear. The mode of failure depends on several factors such as the length of the beam, type of loading subjected to the beam, location of the applied load along the beam, cross-section dimensions of the beam, amount of longitudinal and transverse reinforcement present, and material properties. Flexural failure is the type of failure associated with the bending of the beam, causing one extreme part to be in compression and the other extreme part to be in tension. Shear failure is a failure that happens in the plane that is parallel or at some angle to the applied load causing the beam to split into two parts. In reinforced concrete, shear failures are usually accompanied with diagonal tension cracks that occur at roughly 20 to 50-degree angle from the centerline of the member. In most cases, they propagate from flexural cracks at the extreme tension side of the beam and extend towards the neutral axis and beyond. For members with thin webs (e.g. I-section), these cracks can even initiate near the neutral axis in regions of high shear and low bending moment along the beam. In members that do not contain shear reinforcement, shear failures are characterized by sudden collapse with little or no warning prior to failure. Typical beam failures in flexure and shear of RC beams tested in the material and structures laboratory at AUS are shown in Figure 1.

One of the shortcomings of concrete as a building material is its weakness in tension. To overcome this weakness, concrete members are usually reinforced with a stronger material in regions along the member in which tension occurs. Steel is a very suitable material not only because of its high strength and ductility, but also for its compatible thermal expansion with concrete. To overcome flexural and shear failures, concrete beams are respectively reinforced with longitudinal deformed rebars and transverse stirrups made from steel, that are placed in critical flexural and shear regions. Figure 2 shows the conventional way of reinforcing beams for flexure and shear.



a) Typical flexure failure.



b) Typical shear failure.

Figure 1: Typical concrete beam failures.

Past research and experience have demonstrated the great benefits of using conventional rectilinear steel stirrups as shear reinforcement in concrete beams. However, there are some problems associated with the use of stirrups, such as extensive labor requirement, time consumption and congestion of reinforcement in steel cages. Moreover, concrete cover on reinforcement may spall off at high load levels leaving

the stirrups vulnerable to losing their effectiveness due to deboning [1]. This raises a need to research alternative methods to reinforce concrete beams for shear.

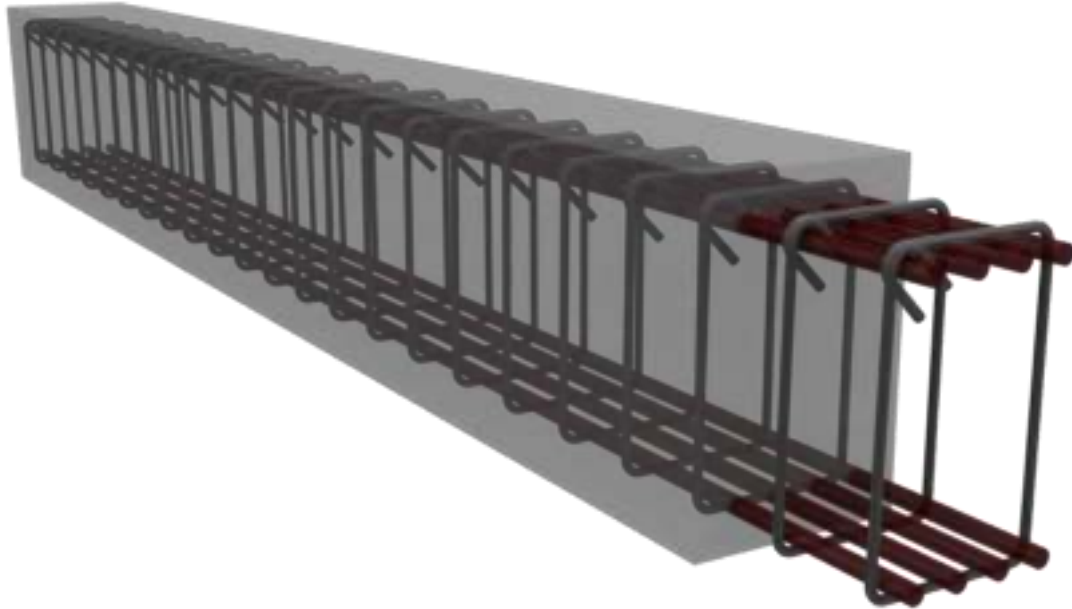


Figure 2: Conventional beam reinforcement.

1.2 Research Significance

Welded wire fabric (WWF) can be a suitable alternative to reinforce concrete beams for shear. WWF, also known as welded wire mesh (WWM), consists of a series of steel wires along two orthogonal directions that are tack welded at their crossing. Popularity of WWF in the construction field has increased in recent years, although its application in the construction field has been limited to pavements and slabs-on-grade for the purpose of controlling the effects of shrinkage and temperature [2]. Use of WWF as in reinforcement in concrete members has many advantages, including saving in time of steel cage assembly, reduction in labor requirement during construction, and more accurate placement of reinforcement within the member. According to Griezic et al. [3] the use of WWF can save up to 75% of on-site construction time. Further, WWF comes in variety of diameters and spacing, and it can be smooth surfaced or deformed.

The process by which WWF is manufactured is called cold-drawn process, where the steel is pulled through a die at room temperature which reshapes it into thin

wires that are then tack-welded in an orthogonal configuration. While the process of cold-drawing increases the strength of the steel, it reduces its ductility. Xuan et al. [4] noticed that WWF exhibits a strain at ultimate that is 5-7.5 times smaller than that of conventional steel rebars. Figure 3 shows the results of tested steel wire from WWF and conventional steel rebar performed at AUS laboratory.

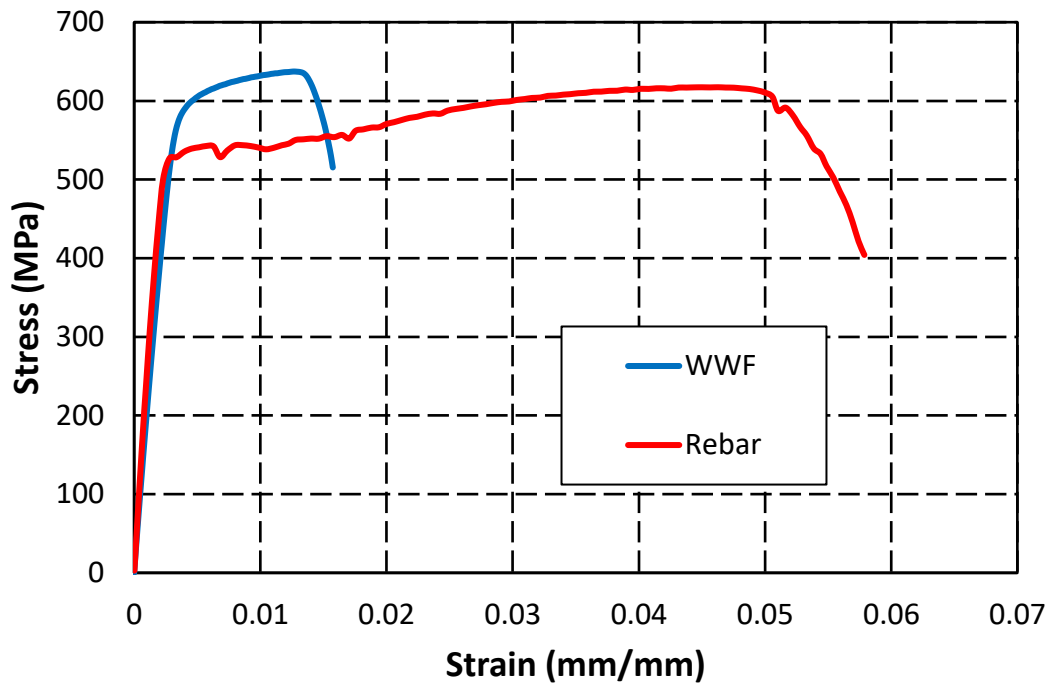


Figure 3: Stress-Strain curve of WWF versus Rebar.

Although the steel wires used in a WWF has lower ductility than corresponding steel rebars, it is expected that promising results due to concrete confinement caused by the tight grid of the WWF may more than compensate for this shortcoming. The enhanced confinement in a WWF reinforced beam relative to a stirrup reinforced beam can result in higher ductility and reduction in crack width of concrete within the core; thus, increasing the shear strength provided by concrete.

A preliminary literature review on the subject shows limited published research on this concept. While some research studied the effect of using WWF as U-shaped cage, or sheets placed perpendicular to the centerline of the member, none of them proposed the use of WWF as closed boxes and made use of the confinement effect on

the concrete. Further, none of the published work addressed altering different parameters such as the concrete compressive strength, shear span-to-depth ratio, grid size of the WWF sheet, etc.

1.3. Problem Statement

In general, the strength and ductility of concrete under shear is limited due to its weakness in tension and brittleness at the onset of failure. Thus, it requires proper reinforcing materials to overcome those deficiencies. Conventional shear reinforcement of concrete in the form of rectilinear stirrups has some drawbacks with regard to time and effort of placement, quality control, congestion of steel cage, and their effectiveness in carrying high loads once the concrete cover spalls off. Moreover, recent research [1] has shown that stirrups may not reach yielding even at ultimate loads. They merely act as confining elements to the concrete core over small distances where they are located; hence, a more effective method of transverse reinforcement is deemed necessary. This raises the need to explore an alternative reinforcement in shear for concrete beams that is more effective than stirrups.

1.4. Proposed New Concept

The aim of this study is to investigate the effectiveness of replacing conventional steel stirrups with WWF. The proposed reinforcement consists of a sheet of WWF that will be cold bent into the shape of a steel cage. Presence of longitudinal and transverse wire reinforcement within the resulting steel cage contributes towards the flexural and shear reinforcement. Unlike the case of conventional stirrups in which mainly the transverse steel mainly resists the shear, the transverse and longitudinal steel wires from the WWF both contribute in a major way to the resistance of shear. In addition, the close spacing of the transverse and longitudinal steel wires is expected to confine the concrete in the core resulting increase in its strength and enhancement in its ductility; thus, increasing the shear strength contributed by the concrete. The longitudinal steel wires may also add to the flexural capacity and flexural ductility of the member. The availability of WWF in various wire diameters and different grid spacing offers valuable flexibility for the structural design engineer. Figure 4 shows a schematic drawing of the new concept and Figure 5 shows the fabrication process done with the help of a manual forming machine constructed in the manufacturing laboratory at AUS.

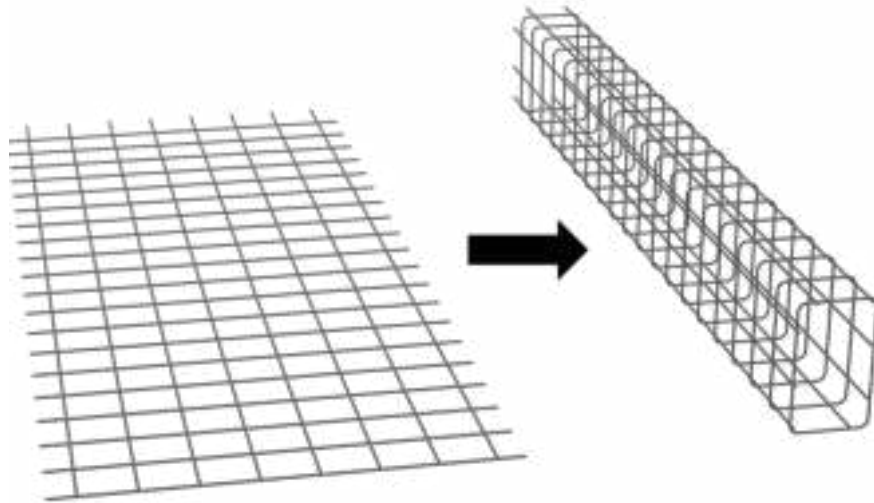


Figure 4: WWF concept as a steel cage.



Figure 5: Fabrication of a steel cage from WWF sheet in the laboratory.

1.5. Objectives of the Study

This research is primarily focused on studying the shear behavior of RC beams reinforced with steel WWF as shear reinforcement instead of conventional rectilinear steel stirrups. The main objectives of this study are to:

1. investigate the feasibility of using WWF in reinforced concrete beams for shear enhancement.
2. compare the performance of beams reinforced with WWF with corresponding beams reinforced with conventional stirrups in relation to

crack propagation, stiffness, shear capacity and ductility when the beams are subjected to predominantly shear forces.

3. determine the effects of the concrete compressive strength, shear span-to-depth ratio, transverse steel volumetric ratio, wire diameter and grid spacing on the performance of concrete beams transversely reinforced with WWF in terms of shear strength and ductility.
4. check whether the current shear design provisions in structural codes and specifications for stirrups are applicable for WWF; if not then develop new design guidelines for this type of reinforcement.

1.6. Scope of Study

The scope of this study addresses the shear performance of concrete beams reinforced with WWF as transverse reinforcement and compares the results with beams reinforced with rectilinear steel stirrups. This study consists of two main parts, an experimental program and a theoretical component. In the experimental program, a total of 23 half-scale beams with rectangular cross-sections 200 mm x 300 mm are tested under one-point loading scheme. The beams are divided into 3 groups in which one group (7 beams) has a shear span-to-total depth ratio, a/h of 2.5 and the other two groups (16 beams, 8 beams each) have a shear span-to-total depth ratio, a/h of 3.0. Two concrete compressive strengths of about 30 MPa and 35 MPa are used in this study. In addition, three different wire sizes (4, 6, and 8 mm) and three grids spacing (25, 50 and 100 mm) are considered. The beams are tested in the AUS materials and structures laboratory inside a Universal Testing Machine (UTM) through a displacement-controlled loading at a rate of 1.0 mm/min. Instrumentation of the tested beams consists of strain gauges placed on the transverse steel and linear variable differential transformers (LVDTs) installed diagonally on the side of the beams. The purpose of the LVDTs is to monitor the average diagonal shear crack width. The theoretical part of the study uses formulations to predict the shear strength of the beams and compares them with the experimental outcome. The methods considered in the theoretical component of the study include the ACI 318 code approach [5, 6], Eurocode 2 [7], CSA 23.3-04 code [8], BS 8110 standard [9], and modified compression field theory [10].

1.7. Thesis Framework

This thesis is organized into seven chapters, divided as follows:

1. **Chapter 1: Introduction.** Introduces the topic, states the problem and proposes a solution. In addition, the objectives and scope are defined, and the outline of the thesis is presented.
2. **Chapter 2: Welded Wire Fabric.** Presents a quick overview on the manufacturing process of WWF, available standards and specifications concerning testing of the product, uses in construction, and structural design requirements in buildings.
3. **Chapter 3: Background on Shear.** Provides a theoretical foundation on the shear strength of reinforced concrete members from different models and codes available in the literature.
4. **Chapter 4: Literature Review.** Presents a comprehensive literature review of the various research conducted on WWF as reinforcement material for concrete, and addresses the different confinement models that exist.
5. **Chapter 5: Experimental Program.** Covers the geometric and mechanical properties of the RC beams considered in the study. The breakdown of the test matrix and different variables considered are discussed and explained. It outlines the fabrication, casting, instrumentation, test setup and procedures for the beam specimens.
6. **Chapter 6: Experimental Results.** This chapter presents the results of the experimental and theoretical work.
7. **Chapter 7: Analysis of Results.** Results pertaining to stiffness, strength and ductility for the WWF and stirrups reinforced beams are compared and discussed.
8. **Chapter 8: Conclusions and Recommendations.** Findings are summarized, conclusions are drawn, design recommendations are outlined, and future research work on the subject are proposed.

Chapter 2. Welded Wire Fabric

In this chapter, a background on the manufacturing process, steel mechanical properties and application in construction of Welded Wire Fabric (WWF) is presented. The design criteria addressed in the relevant design codes concerning WWF with concrete are also discussed.

2.1. Introduction

Welded Wire Fabric, also known as welded wire mesh, refers to a type of steel that is readily available in the industry and used for various applications. It consists of a series of parallel steel wires that are welded across another set of parallel wires through the process of electric fusion. The steel wires that are used come in different sizes and can be either plain or deformed, as shown in Figure 6. They can be used for fencing or structural applications [11].



Figure 6: Plane and deformed WWF [12].

Welded Wire Reinforcement was first introduced in 1901 by John C. Perry who invented a machine capable of welding steel wires into large sheets [13]. This invention was intended to serve as a fencing material and was intended to expand to the construction industry as a reinforcing material in 1906. However, it was impractical in the early 1900s since technological advances were not as effective nowadays, in terms

of welding and rolling technology. The popularity of WWF in Europe grew by the end of World War II, when it was successful in the post-war reconstruction of the infrastructure which was done in a short time. The use of welded wire reinforcement is widespread in Europe where it is utilized in 50% of all reinforced concrete projects. Nowadays, less than 10% of concrete projects in the United States uses welded wire reinforcement as a reinforcing material. Many building codes allow the use of WWF in construction with some limitations and criteria; however, research on the topic of WWF is limited.

The common nomenclature of WWF is “ $S_L \times S_T - T A_L \times T A_T$ ”, in which “ S_L ” is the longitudinal wire spacing, “ S_T ” is the transverse wire spacing, “ A_L ” is the cross-sectional area of longitudinal wires, “ A_T ” is the cross-sectional area of transverse wires, and “ T ” is the type of wire where “ D ” refers to deformed and “ W ” for plain. For example, 200x100-D78.5xW50.3 refers to a sheet with deformed longitudinal wires of diameter 10 mm (corresponding to area 78.5 mm²) spaced at 200 mm and plain transverse wires of diameter 8 mm (corresponding to area 50.3 mm²) spaced at 100 mm. In case English units are used, the common practice is to specify the cross-sectional area of the wire in square inch and multiplying it by 100 [11]. When WWF is compared to conventional reinforcement, it can be noticed that both types meet ASTM standards with respect of mechanical and chemical properties. Figure 7 shows a representation of a WWF sheet.

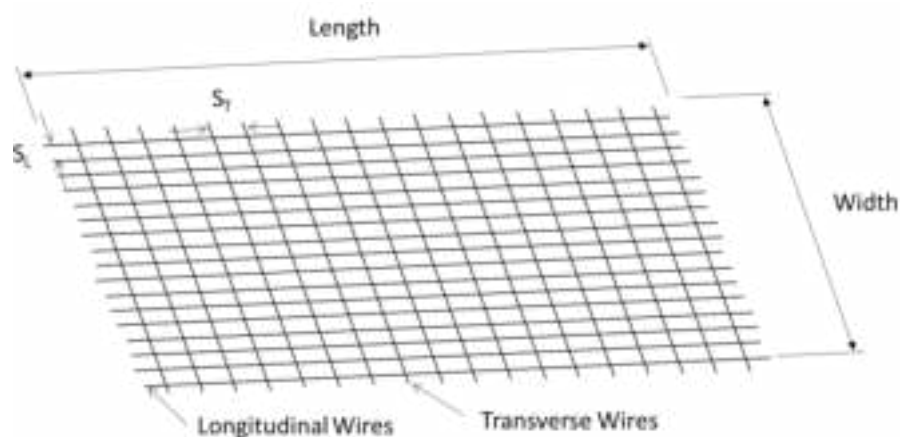


Figure 7: Representation of a WWF sheet [11].

Furthermore, there are some advantages associated with using WWF over conventional stirrups in construction applications. WWF is more flexible in handling and placing which results in time and labor cost saving due to ease of installment. It also has higher design strength that can be utilized which results in saving of material. The presence of steel in both directions and weld connections instead of wire ties provides better bonding between the concrete and steel.

2.2. Manufacturing Process

The process by which WWF wires are manufactured is referred to as cold-drawn process, where a large diameter steel rod (usually hot-rolled) is pulled through a die at room temperature causing it to reshape into thin wires. The method of cold-drawing results in an increase in the strength of the steel but at the cost of reduction in its ductility [11]. The WWF assembly is usually performed by special automated machines to ensure good quality of work and consistency. Longitudinal wires are straightened and spaced according to desired spacing. They are then drawn into the machine where transverse wires are dropped at the desired angle and welded through electric resistance with applied pressure, as shown in Figure 8. This results in a continuous flow of WWF sheet that can be cut according to needed lengths or can be revolved into rolls if smaller diameters are used.



Figure 8: Manufacturing process [14].

In construction, contractors prefer to use sheets over rolls due to their easy handling and no problems associated with the curl. Figure 9 shows the different types of meshes found in a local shop in the UAE. The whole process is computerized, and

variations can be implemented with respect to wire sizes, spacing in both directions, orientation of the wire, overhang of wires, and width and length of sheets. The wires used can be zinc-coated (galvanized), epoxy coated or left uncoated; however, it is not recommended to leave wires exposed to weather uncoated to avoid problems associated with corrosion. The coating process is done prior to welding in the case of zinc-coating and performed after welding if epoxy coating is used. Figure 10 shows zinc-coated (shiny surface) and epoxy coated WWF (green).



Figure 9: Available meshes in the UAE.



Figure 10: Difference between galvanized and epoxy coated WWF [15].

2.3. Specification and Properties

American and British standards are available that address the chemical composition, mechanical properties, and testing procedures for steel used in WWF, (ASTM1064 [16] and BS 4483 [17]). The chemical composition of the steel used is an important aspect when it comes to welding. In general, rebars used in the construction industry are made of carbon steel. The amount of carbon that is present varies between 0.3% to 2.1% by weight, in addition to other elements which are magnesium, silicon, and manganese, sulfur, phosphorus, and chromium. The level of carbon present is very important for the welding process, where the lower the carbon content the more suitable

the steel is for welding. Hence, WWF requires that the amount of carbon present should be as low as possible. According to ASTM A322 [18], the carbon content should be between 0.36-0.44%, silicon content between 0.1-0.4%, the manganese content between 0.65-1.1%, chromium content between 0.75-1.2 %, and phosphorus and sulfur should be limited to 0.04%.

The ASTM 1064 specifies that any WWF used as reinforcement needs to have a minimum yield strength of 450 MPa and ultimate yield strength of 520 MPa. Furthermore, the shear strength of the welds needs to be tested to meet the minimum allowable strength which 240 MPa. There are other standards that are available that require different criterion for the WWF properties. For example, the German standard DIN 488 [19] requires that the WWF wires have a nominal yield strength of 500 MPa. The yield strength of the wires can be obtained by cutting from a sheet a single wire sample and tested in a similar fashion of testing normal steel rebars. The standard mentions that the area of the reduced section, as a result of the welding process, to be used in the calculation of the stress. The yield strength can be obtained using one of two methods which are the 0.2% offset method or strength measured at a strain of 0.005 mm/mm.

2.4. Application in Construction

The applications mainly consist of shrinkage and temperature use in slabs and reinforcement for pavements and roads. Furthermore, WWF is more convenient for structures with curved elements such as arches, domes and lotus petals. The use of WWF is also more popular in precast industries due to the ease of handling and time saving gained from using it. WWF is also used for ferrocement or ferrocete works, where it is the only suitable option for reinforcement. Figure 11 shows some of the applications of WWF in the construction industry.



Figure 11: Usage of WWF in the construction industry [11, 20].

2.5. Structural Building Code Requirements

WWF has been around for many years; however, engineers preferred to not use it due to the limited available research. The ACI 318 code [5, 6] allows the use of welded wire reinforcement in some applications with limitations and conditions. For example, along with stirrups, hoops, ties, and spirals the code allows the use of WWF as shear reinforcement provided that wires that are perpendicular to longitudinal axis of member are present. On the other hand, the code does not permit the use of WWF in some applications such as flexural or axial reinforcement of a special seismic system and as spirals in shear design or special seismic systems. Further, the code does not allow the use of zinc and epoxy dual-coated welded wire reinforcement in no prestressed reinforcement applications. The AASHTO LRFD Specifications [21] permits the use of WWF in reinforcing concrete bridge and retaining wall structures. However, the transverse wires need to at least undergo elongation of 4%, measured over a gage length of at least 100 mm with a minimum of one crosswire.

Both design specifications provide the same guidelines with regards to anchorage of U-stirrups. If WWF is used as a U-stirrups, then the anchorage of each leg of welded wire reinforcement forming a single U-stirrup shall be in accordance with 2 conditions as shown in Figure 12, which are: (1) two longitudinal wires spaced at least 50 mm spacing along the member at the top of the U-stirrup, and (2) one longitudinal wire located not more than $d/4$ from the compression face and a second wire closer to the compression face and spaced not less than 50 mm from the stirrup leg beyond a bend, or on a bend with an inside diameter of bend of at least 8 times the diameter of the wire.

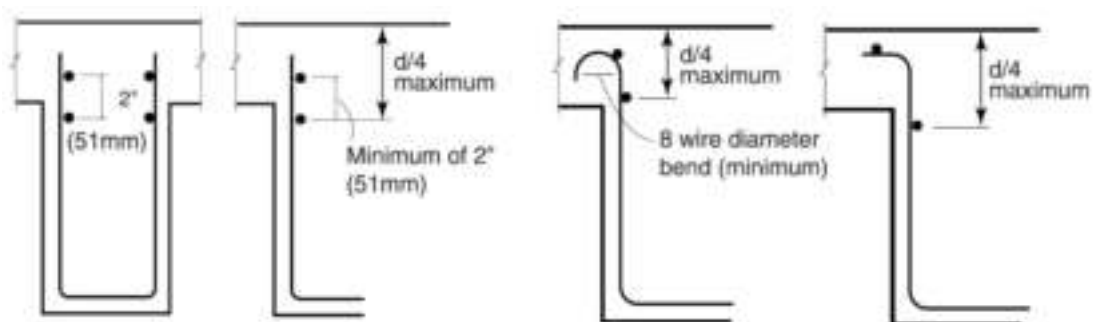


Figure 12: Anchorage of U-stirrups made of WWF [11].

Chapter 3. Background on Shear

In this chapter, a background on the available theory and formulations used to calculate the shear strength provided of reinforced concrete beams is provided. Five different approaches are considered: (1) ACI 318 code [5, 6], (2) Eurocode 2 [7], (3) CSA 23.3-04 code [8], (4) BS 8110 code [9], and (5) modified compression field theory [10]. A numerical example covering all the considered methods is included at the end of the chapter.

3.1. General

The strength provided by concrete in RC beams comes from three sources, as illustrated by Figure 13. The first contribution comes from shear carried by concrete in the compression zone above the crack, designated by V_1 . The second one arises from the aggregate interlock through the crack, denoted by V_2 . The third contribution originates from the dowel action of the flexural longitudinal reinforcing steel rebars, represented by V_3 . The mechanism by which a shear failure is reached is as follows: immediately post cracking, about 40-60 % of the shear stresses are resisted by V_2 and V_3 [22]. However, V_2 decreases as the crack widens until it reaches zero when the crack is wide enough. At higher loads, cracks along the longitudinal reinforcement start to develop due to the dowel shear resulting in the resistance by dowel action to decrease until V_3 reaches to zero. With V_2 and V_3 disappearing, the shear stresses cannot be resisted alone by V_1 since the section is too shallow at this point, resulting into the crack propagating through the remaining uncracked portion resulting in crushing and shear failure of the beam.

If required, transverse shear reinforcement can be added to the beam to help the concrete in resisting large shear forces, indicated in Figure 13, by V_4 [22]. The mechanism by which the transverse steel carries shear is based on tension. Hence, this type of reinforcement must be anchored well in the two concrete zones (above and below the crack) in order to avoid slippage. The transverse reinforcement act as a stitching element to the developed cracks, thus there is no contribution of V_4 to the shear to strength of the beam prior to cracking. As the load increase, the shear resistance due to stirrups increases, until the steel reaches the yield point. Once the yield point is reached, the opening of the diagonal crack becomes more rapid. Beyond this point the

shear resistance contribution by V_4 becomes constant. The response of all shear components is brittle, except the response of V_4 .

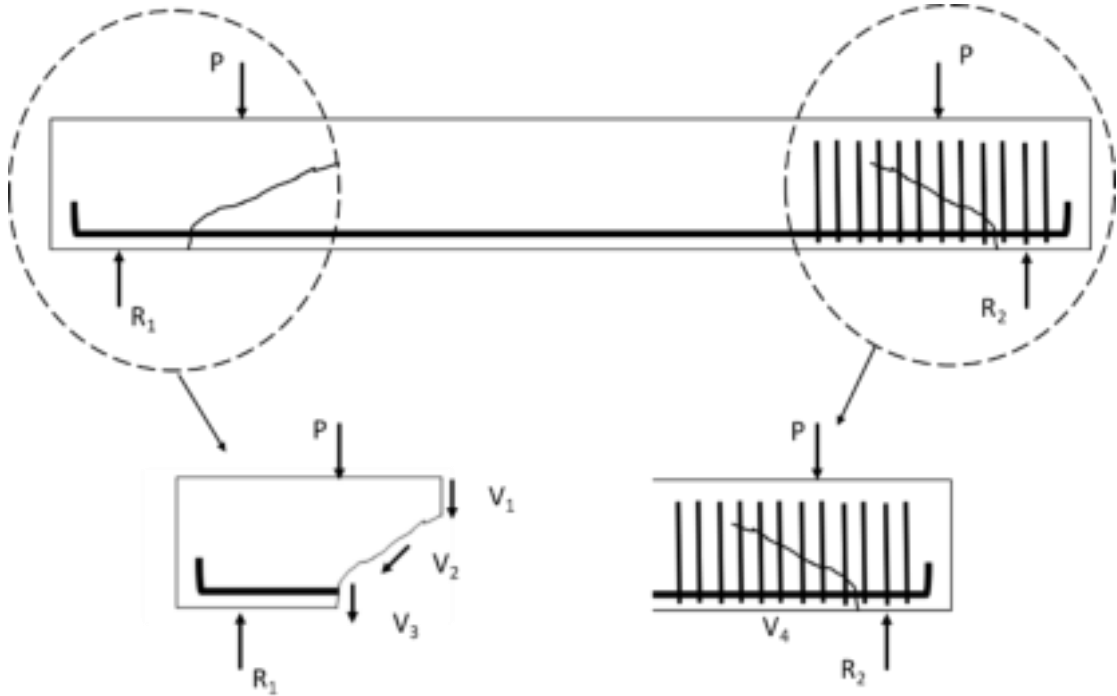


Figure 13: Sources of shear strength.

3.2. ACI 318 Code

Prior to 2019, the shear strength provisions in the ACI 318 code considered the effect of the shear span-to-depth ratio but did not account for the size effect of the member when specifying the contribution of concrete in carrying shear. For example, the ACI 318-14 code [5] provides two expressions for the shear strength of concrete in RC beams, V_c . The simple expression, shown in Equation 1, is solely based on the concrete material strength and cross-section dimensions, while the detailed expression, presented in Equation 2, considers additionally the shear span-to-depth ratio and the dowel action of the flexural reinforcement:

$$V_c = 0.17\lambda\sqrt{f'_c} b_w d \quad (1)$$

$$V_c = \left(0.16\lambda\sqrt{f'_c} + 17\rho_w \left(\frac{V_u d}{M_u} \right) \right) b_w d \leq 0.29\lambda\sqrt{f'_c} b_w d \quad (2)$$

where:

λ = light-weight reduction factor,

f'_c = concrete compressive strength (MPa),

b_w = narrowest width of the beam (mm),

d = effective depth of flexural reinforcement from the extreme concrete compression fibers (mm),

ρ_w = effective flexural steel reinforcement ratio = $\frac{A_s}{b_w d}$,

A_s = area of longitudinal flexural reinforcement (mm²),

V_u = maximum factored shear at the location considered (N), and

M_u = corresponding factored bending moment occurring at location of V_u (N-mm), and the quantity $\frac{V_u d}{M_u} \leq 1.0$.

For the case of axially loaded members, the ACI 318-14 [5] code provides expressions for V_c that lead to higher values when subjected to compression, given by Equation 3, and lower values when subjected to tension, given by Equation 4.

$$V_c = 0.17(1 + \frac{N_u}{14A_g})\lambda\sqrt{f'_c} b_w d \quad (3)$$

$$V_c = 0.17(1 + \frac{0.29N_u}{A_g})\lambda\sqrt{f'_c} b_w d \quad (4)$$

where:

N_u = factored axial load (N, > 0 for compression and < 0 for tensile), and

A_g = gross area of member (mm²).

Starting in 2019, the ACI 318 code [6] modified the shear strength provided by concrete provisions. If the size effect of the member is not considered, the code provided two expressions for finding V_c :

$$V_c = \left(0.17\lambda\sqrt{f'_c} + \frac{N_u}{6A_g}\right) b_w d \leq 0.42\lambda\sqrt{f'_c} b_w d \quad (5)$$

$$V_c = \left(0.66\lambda\rho_w^{1/3}\sqrt{f'_c} + \frac{N_u}{6A_g}\right) b_w d \leq 0.42\lambda\sqrt{f'_c} b_w d \quad (6)$$

If the size effect of the member is considered, then V_c can be computed from:

$$V_c = \left(0.66\lambda_s\lambda\rho_w^{1/3}\sqrt{f'_c} + \frac{N_u}{6A_g} \right) b_w d \leq 0.42\lambda\sqrt{f'_c} b_w d \quad (7)$$

where:

$$\lambda_s = \text{size factor} = \sqrt{\frac{2}{1+d/250}} \leq 1.0.$$

Note that: the value of $(N_u/6A_g)$ shall not be taken greater than $0.05f'_c$, and $\sqrt{f'_c}$ is taken ≤ 8.3 MPa (unless at least minimum shear reinforcement is present in the member).

The ACI 318-14 and ACI 318-19 codes' expression for the contribution of vertical steel stirrups in carrying shear is based on the conservative assumption that the shear crack is inclined at 45 degrees from the centreline of the member. This results in the expression shown by Equation 8 for the shear strength provided by transverse reinforcement [6] :

$$V_s = \frac{A_v f_y d}{s} \quad (8)$$

where:

A_s = total cross-sectional area of vertical stirrups reinforcement (mm^2),

f_y = yield strength of stirrups (MPa), limited to 420 MPa, and

s = spacing of stirrups (mm)

The nominal shear capacity of a reinforced concrete beam is computed using Equation 9, the ultimate load applied on the member must apply to Equation 10:

$$V_n = V_c + V_s \quad (9)$$

$$V_u \leq \phi V_n \quad (10)$$

where:

ϕ = strength reduction factor taken as 0.75.

3.3. Eurocode 2

The Eurocode 2 [7] provides an expression for the concrete shear strength displayed in Equation 11:

$$V_{Rd,c} = [C_{Rd,c} k (100 \rho_l f_{ck})^{1/3}] b_w d \quad (11)$$

where:

$$\rho_l = \rho_w \leq 0.02,$$

$$f_{ck} = f'_c,$$

$$C_{Rd,c} = \text{reduction factor} = \frac{0.18}{\gamma_c},$$

γ_c = partial safety factor taken as 1.5, and

$$k = \text{member size factor} = 1 + \sqrt{\frac{200}{d}} \leq 2.$$

The Eurocode 2 [7] provides a separate expression for the contribution of the transverse reinforcement in carrying shear is shown in Equation 12, and an upper limit for the shear contribution of transverse reinforcement provided by Equation 13:

$$V_{Rd,s} = \frac{A_{sw}}{s} z f_{ywd} \cot \theta \leq V_{Rd,max} \quad (12)$$

$$V_{Rd,max} = b_w z v f_{cd} \frac{1}{\cot \theta + \tan \theta} \quad (13)$$

where:

$$A_{sw} = A_s,$$

z = lever arm taken as 0.9d,

$$f_{ywd} = f_y,$$

θ = compression strut angle with the centerline of the member, to be chosen between 45° and 21.8° (i.e. $1 \leq \cot \theta \leq 2.5$),

v = is a reduction factor for the concrete compressive strength of the struts in the stress field taken as 0.6,

f_{cd} = reduced concrete compressive strength, equal to f_{ck}/γ_c .

3.4. CSA 23.3-04

The Canadian code [8] provides similar expressions for shear strength to the expressions provided by the ACI code [5]. The formula for shear strength provided by concrete is:

$$V_c = \lambda \beta \sqrt{f'_c} b_w d_v \quad (14)$$

where:

$$d_v = d;$$

$$\beta = \begin{cases} 0.18 \text{ if minimum transverse reinforcement is provided,} \\ \frac{230}{1000 + d_v} \text{ if no transverse reinforcement provided, and } a_g \geq 20\text{mm,} \\ \frac{230}{1000 + s_{ze}} \text{ if no transverse reinforcement provided, and } a_g \leq 20\text{mm.} \end{cases}$$

$$s_{ze} = \frac{35}{15 + a_g} s_z \geq 0.85s_z, \text{ and}$$

a_g = maximum aggregate size (mm).

s_z = parameter related to crack spacing (mm) conservatively taken as d_v .

The expression for shear strength provided by the transverse reinforcement is similar to that in the ACI 318 code:

$$V_s = \frac{A_v f_y d}{s} \quad (15)$$

Note that the quantity $\sqrt{f'_c}$ is taken less than or equal to 8.0 MPa (unless at least minimum shear reinforcement is present in the member).

The resistance shear capacity of a reinforced concrete beam is computed using Equation 16, the ultimate load applied on the member must apply to Equation 17:

$$V_r = V_c + V_s \quad (16)$$

$$V_u \leq \phi_c V_c + \phi_s V_s \quad (17)$$

where:

ϕ_c = strength reduction factor for concrete taken as 0.65.

ϕ_s = strength reduction factor for concrete taken as 0.9.

3.5. BS 8110

Similar to the ACI code, the BS [9] expression for shear strength of concrete accounts for the size effect and longitudinal reinforcement provided. The expression can be seen in Equation 18:

$$V_c = \frac{0.79 \left(\frac{100 A_s}{b_v d} \right)^{1/3} \left(\frac{400}{d} \right)^{1/4} \left(\frac{f_{cu}}{25} \right)^{1/3}}{\gamma_m} b_v d \quad (18)$$

The BS code provides limits for the following quantities:

$$\frac{100A_s}{b_v d} \leq 3.0,$$

$$\left(\frac{400}{d}\right)^{1/4} \geq 1.0,$$

$$\frac{f_{cu}}{25} \leq 1.6,$$

where:

$$b_v = b_w,$$

$$f_{cu} = f'_c, \text{ and}$$

$$\gamma_m = \text{taken as } 1.25.$$

The contribution of transverse reinforcement to shear strength is represented by Equation 19 [9]:

$$V_s = \frac{0.95 f_{yv} A_{sv} d}{s_v} \quad (19)$$

where:

$$f_{yv} = f_y,$$

$$A_{sv} = A_s, \text{ and}$$

$$s_v = s.$$

3.6. Modified Compression Field Theory

The modified compression field theory (MCFT) was adjusted by Vecchio and Collins [10] based on the compression field theory (CFT) that was developed earlier by Collins and Mitchell [23]. The CFT was developed by adopting three main conditions: (1) the compatibility condition; which states that any deformation or strain in the concrete is matched with the same deformation or strain in the reinforcement, (2) the equilibrium condition; where the applied external forces are resisted by internal stresses developed by the concrete and reinforcement, and (3) the stress-strain relationship of concrete and reinforcement; which relates the stress and strain in both the concrete and the reinforcement to their respective modulus of elasticity.

Although, the stress-strain relationships for the concrete and for the reinforcement are dependent, they were assumed to be independent for the sake of simplicity. While the CFT was successful in predicting behavior of beams, it resulted

in conservative predictions. This was because Collins and Mitchell's [24] model failed to capture the effect of the tensile stresses in the concrete between the cracks, which was introduced by Vecchio and Collins in their MCFT. The MCFT was developed using sing mechanics of materials principles and the three assumptions discussed above.

Based on the principles of the MCFT, buildings design codes, like AASHTO developed their own formulas to compute the capacity of beams. The general formula for calculating the beam shear capacity is presented by Equations 20 to 22 [21]:

$$V_n = V_c + V_s \quad (20)$$

$$V_c = 0.083\beta\sqrt{f'_c}b_vd_v \quad (21)$$

$$V_s = \frac{A_vf_yd_v \cot \theta}{s} \quad (22)$$

Using Equations 23 and 24, the values of β and θ can be computed in an iterative procedure from table B5.2-1 from the AASHTO LRFD bridge design specification [21] shown in Figure 14:

$$\frac{v_u}{f'_c} = \frac{V_u}{\phi b_v d_v} \left(\frac{1}{f'_c} \right) \quad (23)$$

$$\varepsilon_x = \frac{\frac{|M_u|}{d_v} + 0.5N_u + 0.5|V_u - V_p| \cot \theta}{2(E_s A_s + E_p A_{ps})} \quad (24)$$

If the value obtained of ε_x using Equation 24 is negative, then a slightly modified expression is used as shown in Equation 25:

$$\varepsilon_x = \frac{\frac{|M_u|}{d_v} + 0.5N_u + 0.5|V_u - V_p| \cot \theta}{2(E_c A_c + E_s A_s + E_p A_{ps})} \quad (25)$$

where:

d_v = effective shear depth (mm), measured as the distance between the resultants of tensile and compressive forces due to flexure,

ε_x = is the longitudinal strain at the mid-depth of the member,

β = factor indicating ability of diagonally cracked concrete to transmit tension,

θ = angle of inclination of diagonal compressive stresses,

M_u = factored moment (N-mm),

N_u = factored axial force, taken as positive if tensile and negative if compressive (N),

V_u = factored shear force (N),

E_c = modulus of elasticity of concrete, measured as $4700\sqrt{f'_c}$ (MPa),

A_c = area of concrete on the flexural tension side of the member (mm^2),

E_s = modulus of elasticity of flexural steel (MPa),

E_p = modulus of elasticity of prestressed steel (MPa), and

A_p = area of prestressing steel on the flexural tension side of the member (mm^2).

$\frac{V_u}{f'_c}$	$\rho_s \times 1,000$								
	≤ 0.20	≤ 0.10	≤ 0.05	≤ 0	≤ 0.125	≤ 0.25	≤ 0.50	≤ 0.75	≤ 1.00
≤ 0.075	22.3 6.32	20.4 4.75	21.0 4.10	21.8 3.75	24.3 3.24	26.6 2.94	30.5 2.59	33.7 2.38	36.4 2.23
≤ 0.100	18.1 3.79	20.4 3.38	21.4 3.24	22.5 3.14	24.9 2.91	27.1 2.75	30.8 2.50	34.0 2.32	36.7 2.18
≤ 0.125	19.9 3.18	21.9 2.99	22.8 2.94	23.7 2.87	25.9 2.74	27.9 2.62	31.4 2.42	34.4 2.26	37.0 2.13
≤ 0.150	21.6 2.88	23.3 2.79	24.2 2.78	25.0 2.72	26.9 2.60	28.8 2.52	32.1 2.36	34.9 2.21	37.3 2.08
≤ 0.175	23.2 2.73	24.7 2.66	25.5 2.65	26.2 2.60	28.0 2.52	29.7 2.44	32.7 2.28	35.2 2.14	36.8 1.96
≤ 0.200	24.7 2.63	26.1 2.59	26.7 2.52	27.4 2.51	29.0 2.43	30.6 2.37	32.8 2.14	34.5 1.94	36.1 1.79
≤ 0.225	26.1 2.53	27.3 2.45	27.9 2.42	28.5 2.40	30.0 2.34	30.8 2.14	32.3 1.86	34.0 1.73	35.7 1.64
≤ 0.250	27.5 2.39	28.6 2.39	29.1 2.33	29.7 2.33	30.6 2.12	31.3 1.93	32.8 1.70	34.3 1.58	35.8 1.50

Figure 14: Table 5.2-1 from AASHTO LRFD bridge design Specifications [21].

3.7. Examples

Determine the shear strength provided by concrete for a simply-supported RC beam having a span equal to 8 m and 300 mm x 600 mm rectangular cross-section. The beam is subjected to 50 kN/m uniform factored load along its entire length, which includes the self-weight). It is reinforced at the bottom for flexure with 3 No. 32 bars, as shown in Figure 15. It is also reinforced for shear with No. 10 stirrups at a spacing of 200 mm. Consider the section at d-away from the face of the support. Given: $f'_c = 40$ MPa (normal weight) and $f_y = 460$ MPa. The shear moment diagram of the beam is constructed and shown in Figure 16.

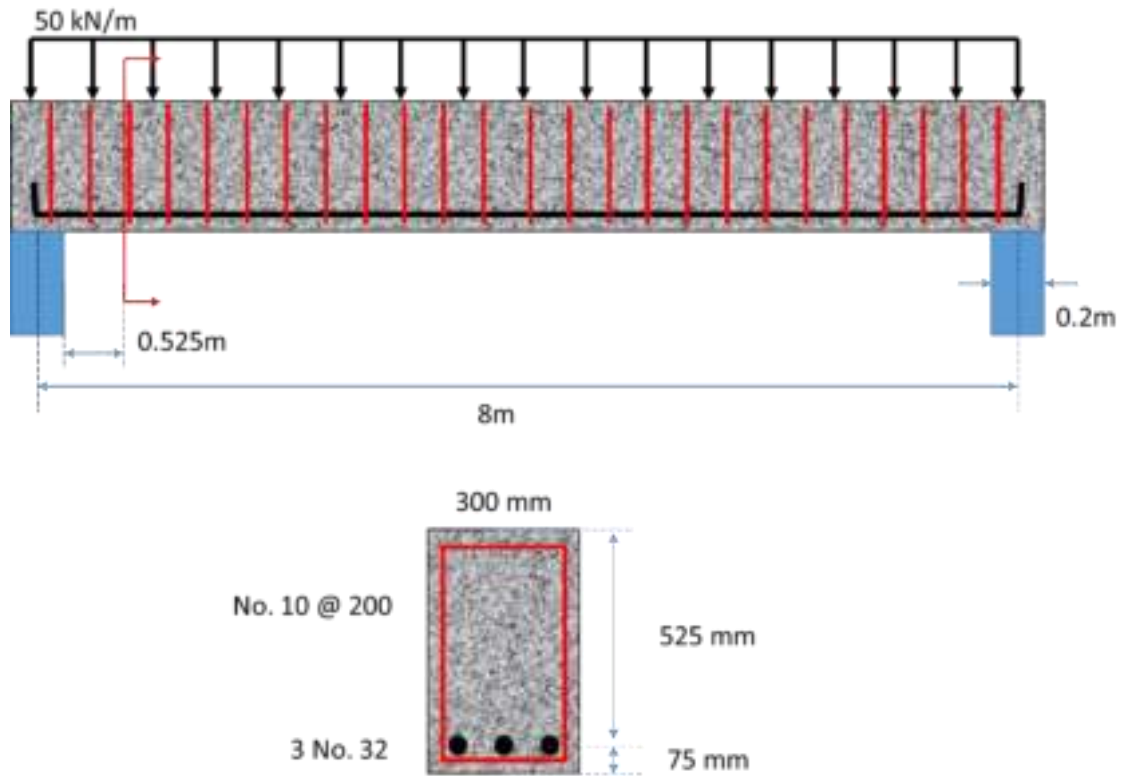


Figure 15: Beam example detailing.

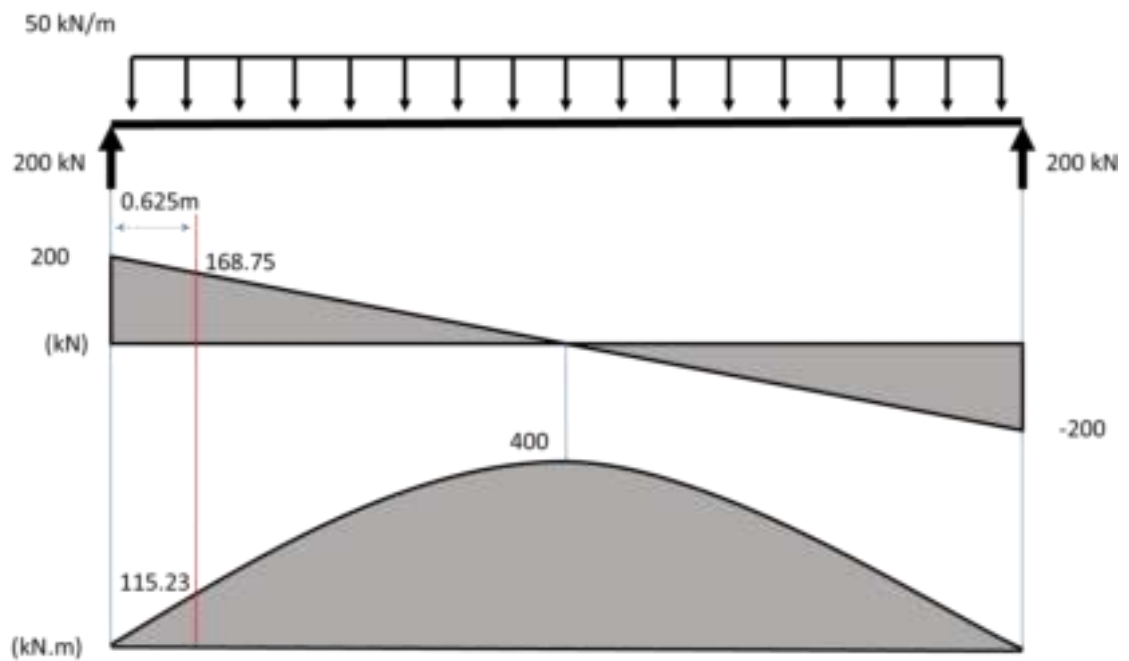


Figure 16: Shear-moment diagram of beam example.

3.7.1. ACI 318-14. The shear capacity of a reinforced concrete beam is computed as follows:

$$A_s = 3 * \pi * \frac{32^2}{4} = 2412 \text{ mm}^2$$

$$\rho_w = \frac{A_s}{b_w d} = \frac{2412}{300 * 525} = 0.0153$$

$$\begin{aligned} V_c &= \left(0.16\lambda\sqrt{f'_c} + 17\rho_w \left(\frac{V_u d}{M_u} \right) \right) b_w d \\ &= \left(0.16 * 1.0 * \sqrt{40} + 17 * 0.0153 * \left(\frac{168.75 * 525}{115.23 * 10^3} \right) \right) * 300 * 525 \\ &* 10^{-3} = 190.9 \text{ kN} \end{aligned}$$

$$\text{Limit} = 0.29\lambda\sqrt{f'_c} b_w d = 0.29 * 1.0 * \sqrt{40} * 300 * 525 * 10^{-3} = 288.9 \text{ kN}$$

$$A_v = 2 * \pi * \frac{10^2}{4} = 157 \text{ mm}^2$$

$$V_s = \frac{A_v f_y d}{s} = \frac{157 * 460 * 525}{200} * 10^{-3} = 189.6 \text{ kN}$$

$$V_n = V_c + V_s = 190.9 + 189.6 = 380.5 \text{ kN}$$

$$\phi V_n = \phi(V_c + V_s) = 0.75 * (190.9 + 189.6) = 285.4 \text{ kN}$$

3.7.2. ACI 318-19. The shear capacity of a reinforced concrete beam is computed as follows:

$$A_s = 3 * \pi * \frac{32^2}{4} = 2412 \text{ mm}^2$$

$$\rho_w = \frac{A_s}{b_w d} = \frac{2412}{300 * 525} = 0.0153$$

$$\lambda_s = \sqrt{\frac{2}{1 + d/250}} = \sqrt{\frac{2}{1 + 525/250}} = 0.803$$

$$\begin{aligned}
V_c &= (0.66\lambda_s\lambda\rho_w^{1/3}\sqrt{f'_c})b_wd \\
&= 0.66 * 0.803 * 1.0 * 0.0153^{\frac{1}{3}} * \sqrt{40} * 300 * 525 * 10^{-3} \\
&= 131.1 \text{ kN}
\end{aligned}$$

$$Limit = 0.42\lambda\sqrt{f'_c} b_wd = 0.42 * 1.0 * \sqrt{40} * 300 * 525 * 10^{-3} = 418.4 \text{ kN. OK}$$

$$A_v = 2 * \pi * \frac{10^2}{4} = 157 \text{ mm}^2$$

$$V_s = \frac{A_v f_y d}{s} = \frac{157 * 460 * 525}{200} * 10^{-3} = 189.6 \text{ kN}$$

$$V_n = V_c + V_s = 131.1 + 189.6 = 320.7 \text{ kN}$$

$$\phi V_n = \phi(V_c + V_s) = 0.75 * (131.1 + 189.6) = 240.5 \text{ kN}$$

3.7.3. Eurocode 2. The shear capacity of a reinforced concrete beam is computed as follows:

$$A_s = 3 * \pi * \frac{32^2}{4} = 2412 \text{ mm}^2$$

$$\rho_l = \frac{A_s}{b_w d} = \frac{2412}{300 * 525} = 0.0153$$

$$C_{Rd,c} = \frac{0.18}{\gamma_c} = \frac{0.18}{1.5} = 0.12$$

$$k = 1 + \sqrt{\frac{200}{d}} = 1 + \sqrt{\frac{200}{525}} = 1.617 \leq 2.0. \text{ OK}$$

$$\begin{aligned}
V_{Rd,c} &= \left(C_{Rd,c} k (100\rho_l f_{ck})^{\frac{1}{3}} \right) b_w d \\
&= \left(0.12 * 1.617 * (100 * 0.0153 * 40)^{\frac{1}{3}} \right) * 200 * 525 * 10^{-3} \\
&= 80.3 \text{ kN}
\end{aligned}$$

$$A_{sw} = 2 * \pi * \frac{10^2}{4} = 157 \text{ mm}^2$$

$$V_{Rd,s} = \frac{A_{sw}}{s} z f_{yw} d \cot \theta = \frac{157}{200} * 0.9 * 525 * 460 * \cot 45 * 10^{-3} = 170.6 \text{ kN}$$

$$V_{Rd,max} = b_w z v f_{cd} \frac{1}{\cot \theta + \tan \theta}$$

$$= 200 * 0.9 * 525 * 0.6 * \frac{40}{1.5} * \frac{1}{\cot 45 + \tan 45} * 10^{-3} = 756 \text{ kN OK}$$

$$\phi V_n = V_{Rd,c} + V_{Rd,s} = 80.3 + 170.6 = 250.9 \text{ kN}$$

For the nominal shear strength,

$$V_n = V_{Rd,c} * 1.5 + \frac{V_{Rd,s}}{0.9} = 80.3 * 1.5 + 180.1/0.9 = 320.6 \text{ kN}$$

3.7.4. CSA 23.3-04. The shear capacity of a reinforced concrete beam is computed as follows:

$$A_v = 2 * \pi * \frac{10^2}{4} = 157 \text{ mm}^2$$

$$\frac{A_v}{s} = \frac{157}{200} = 0.785 \geq 0.06 \frac{\sqrt{f'_c}}{f_y} b_w = 0.06 * \frac{\sqrt{40}}{460} * 200 = 0.165 \text{ OK}$$

$$\beta = 0.18$$

$$V_c = \lambda \beta \sqrt{f'_c} b_w d_v = 1.0 * 0.18 * \sqrt{40} * 200 * 525 * 10^{-3} = 119.5 \text{ kN}.$$

$$V_s = \frac{A_v f_y d}{s} = \frac{157 * 460 * 525}{200} * 10^{-3} = 189.6 \text{ kN}$$

$$V_r = V_c + V_s = 119.5 + 189.6 = 309.1 \text{ kN}$$

$$\phi V_r = \phi_c V_c + \phi_s V_s = 0.65 * 119.5 + 0.9 * 189.6 = 248.3 \text{ kN}$$

3.7.5. BS code. The shear capacity of a reinforced concrete beam is computed as follows:

$$A_s = 3 * \pi * \frac{32^2}{4} = 2412 \text{ mm}^2$$

$$\frac{100 A_s}{b_v d} = \frac{100 * 2412}{200 * 525} = 2.298 \leq 3.0 \text{ OK}$$

$$\left(\frac{400}{d}\right)^{1/4} = \left(\frac{400}{525}\right)^{1/4} = 0.934 \geq 1.0. \text{ Not OK, use } 1.0$$

$$\frac{f_{cu}}{25} = \frac{40}{25} = 1.6 \leq 1.6. \text{ OK}$$

$$\begin{aligned} \phi V_c &= \frac{0.79 \left(\frac{100A_s}{b_v d}\right)^{1/3} \left(\frac{400}{d}\right)^{1/4} \left(\frac{f_{cu}}{25}\right)^{1/3}}{\gamma_m} b_v d \\ &= \frac{0.79 * 2.298^{1/3} * 1.0^{1/4} * 1.6^{1/3}}{1.25} * 200 * 525 * 10^{-3} = 102.4 \text{ kN} \end{aligned}$$

$$A_{sv} = 2 * \pi * \frac{10^2}{4} = 157 \text{ mm}^2$$

$$\phi V_s = \frac{0.95 f_{yv} A_{sv} d}{s_v} = \frac{0.95 * 460 * 157 * 525}{200} * 10^{-3} = 180.1 \text{ kN.}$$

$$\phi V_n = V_c + V_s = 102.4 + 180.1 = 282.5 \text{ kN}$$

For the nominal shear strength,

$$V_n = V_c * 1.25 + \frac{V_s}{0.95} = 102.4 * 1.25 + 180.1/0.95 = 317.6 \text{ kN}$$

3.7.6. Modified compression field theory. The shear capacity of a reinforced concrete beam is computed as follows:

$$A_s = 3 * \pi * \frac{32^2}{4} = 2412 \text{ mm}^2$$

$$a = \frac{A_s f_y}{0.85 f'_c b} = \frac{2412 * 460}{0.85 * 40 * 200} = 163.2 \text{ mm}$$

$$d_v = d - \frac{a}{2} = 525 - \frac{163.2}{2} = 443.4 \text{ mm}$$

$$\frac{v_u}{f'_c} = \frac{V_u}{\phi b_v d_v} \left(\frac{1}{f'_c}\right) = \frac{168750}{0.9 * 200 * 443.4} * \frac{1}{40} = 0.0529$$

Initially, ϵ_x is assumed 0.

From the table, $\beta = 3.75$ and $\theta = 21.8$.

$$\begin{aligned}\varepsilon_x &= \frac{\frac{|M_u|}{d_v} + 0.5N_u + 0.5|V_u - V_p| \cot \theta}{2(E_c A_c + E_s A_s + E_p A_{ps})} \\ &= \frac{\frac{115230000}{443.4} + 0 + 0.5 * |168750 - 0| * \cot 21.8}{2 * (200000 * 2412)} = 0.000488\end{aligned}$$

From the table, $\beta = 2.59$ and $\theta = 30.5$.

$$V_c = 0.083\beta\sqrt{f'_c}b_vd_v = 0.083 * 2.59 * \sqrt{40} * 200 * 443.4 * 10^{-3} = 120.6 \text{ kN}$$

$$A_v = 2 * \pi * \frac{10^2}{4} = 157 \text{ mm}^2$$

$$V_s = \frac{A_v f_y d_v \cot \theta}{s} = \frac{157 * 460 * 443.4 * \cot 30.5}{200} * 10^{-3} = 271.8 \text{ kN}.$$

$$V_n = V_c + V_s = 120.6 + 271.8 = 392.4 \text{ kN}.$$

$$\begin{aligned}\phi V_n &= \phi(V_c + V_s) = 0.9 * (120.6 + 271.8) = 353.2 \text{ kN} \leq 0.25f'_c b_v d_v \\ &= 0.25 * 40 * 200 * 443.4 = 886.8 \text{ kN. OK.}\end{aligned}$$

3.7.7. Summary of results. The shear capacity of all the design methods considered are summarized in Table 1:

Table 1: Summary of results of solved example.

Method	V_n (kN)	ϕV_n (kN)
ACI 318-14	380.5	285.4
ACI 318-19	320.7	240.5
Eurocode2	320.6	250.9
CSA 23.3-04	309.1	248.3
BS 8110	317.6	282.5
MCFT	392.4	353.2

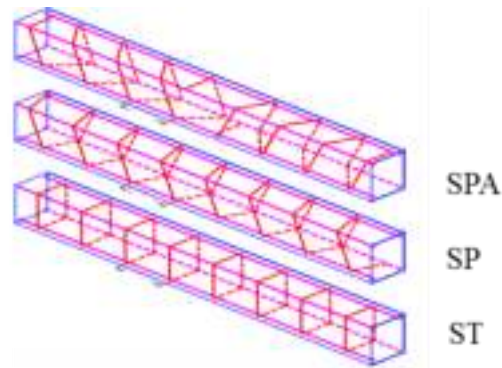
Chapter 4. Literature Review

In this chapter, an extensive literature review on the topic of shear reinforcement, WWF, and confinement of concrete cores is carried out. The findings are organized according to the addressed subject.

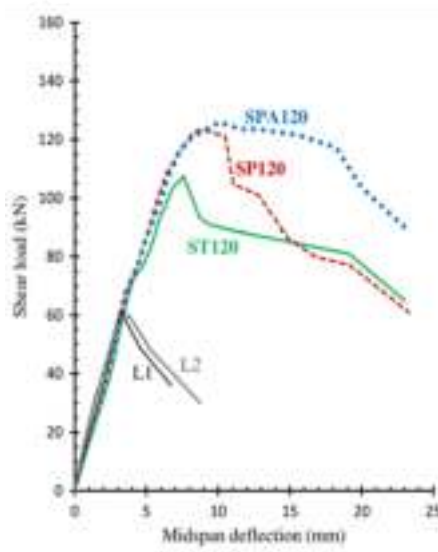
4.1. Shear Reinforcement Alternative to Stirrups

In the past decade, there have been some efforts to seek alternative methods for shear reinforcement to the conventional rectilinear steel stirrups. A study published by Karayannis and Chalioris [25] investigates the feasibility of replacing stirrups with spirals across the length of the beam. A total of 8 beams were tested in shear, in which 2 beams were not reinforced for shear denoted with “L”, 2 beams were reinforced with normal stirrups denoted with “ST”, 2 beams were reinforced with normal spirals denoted with “SP”, and 2 beams reinforced with spirals oriented at an angle perpendicular to the expected shear cracks denoted by “SPA.” All beams were tested using a displacement controlled 2-point loading scheme. One of the two beams in each set has shear reinforcement spaced at 80 mm and the other at 120 mm. The experiments showed that the use of spirals as shear reinforcement resulted in 14.7-21.7% enhancement in the shear strength of tested beams. Furthermore, enhancements in ductility and maximum deflection were observed on the beams that were reinforced with spirals. Figure 17 illustrates the shear force versus deflection graphs of the tested specimens.

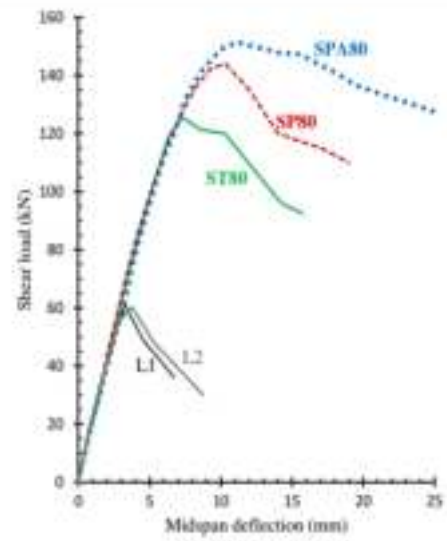
Another study conducted by Lee et al. [26] considered the use of composite fiber sheet strips (FSS) as an alternative to steel stirrups. A total of 10 beams were tested for shear under one-point loading, 6 of which were reinforced with carbon FSS, 1 reinforced with carbon rods stirrups, 2 with steel stirrups and 1 with no shear reinforcement. A sample of each type of reinforcement considered in this study is shown in Figure 18. All beams were casted with one concrete batch, and the tested cylinders resulted in an average concrete compressive strength of 32 MPa at 28-days. Overall, beams reinforced with FSS having the same reinforcement ratio as the control stirrup reinforced beam witnessed similar ultimate loads and deflections, as it can be noticed from Figure 19. Furthermore, it was noticed that all specimens reinforced with FSS experienced an increase of shear strength of about 30% to 64% in comparisons to the specimens tested with no shear reinforcement.



(a) Spiral and stirrups reinforced beams.



(b) 120 mm spacing.

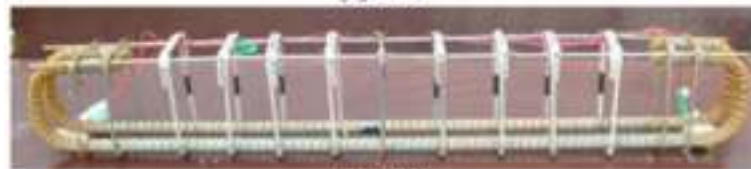


(c) 80 mm spacing.

Figure 17: Shear-deflection curves for beams tested by Karayannis [25].



(a) NS



(b) C06



(c) C15

Figure 18: Sample reinforcement of beams considered [26].

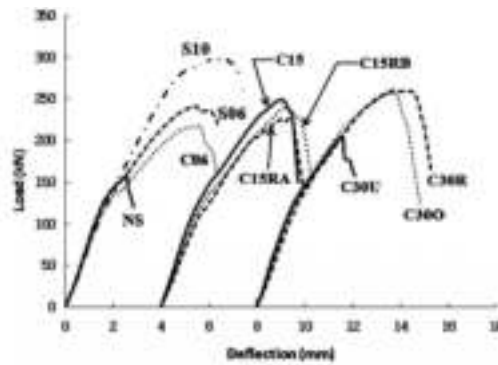


Figure 19: Load versus Deflection curves of study by Lee et al. [26].

A study conducted by Ahmad [27] investigated the use of Internal Structural Steel Strip Bands (ISSSB's) as a replacement of conventional rectilinear stirrups. The strips were obtained through cutting structural steel squares or rectangular tubes of desired thickness, and the size of the bands depends on the cross-section of the RC beam. Figure 20 shows a sample beam reinforced with ISSSB next to a conventionally reinforced beam with rectilinear stirrups. In their study, various cross-section dimensions, shear-span-to-depth ratios, transverse steel volumetric ratios, and strip band thickness-to-width ratios were considered. It was observed that the beams reinforced with ISSSB exhibited similar shear strength as the stirrups reinforced beams at low shear span-to-depth ratio, and higher shear strength as high shear span-to-depth ratio. Furthermore, it was also noticed that the beams reinforced with ISSSB exhibited higher ductility and residual strength than the corresponding beams that were reinforced with stirrups. A representative sample of the results obtained is shown in Figure 21.



Figure 20: Sample ISSSB reinforced beam versus a stirrups reinforced beam [27].

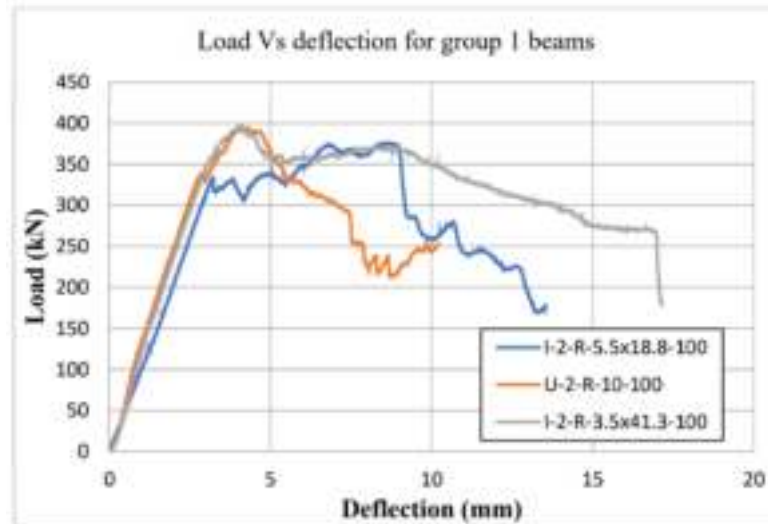


Figure 21: Sample of load versus deflection curve of Ahmed’s study [27].

Another study carried out by Suwanpanjasil et al. [28], investigates the use of carbon fiber reinforced polymer (CFRP) grids as a replacement of the conventional steel stirrups as transverse shear reinforcement. Figure 22 shows the suggested alternative shear reinforcement. A total of eight RC beams reinforced with CFRP grids with variation in the number of grids and the spacing of the grids were tested and compared against a concrete beam with no shear reinforcement. From the results shown in Figure 23, it was concluded that the shear carrying capacity of the beams reinforced with CFRP grids was significantly higher than the performance of beams with no shear reinforcement, however, the increase in strength was not proportional.

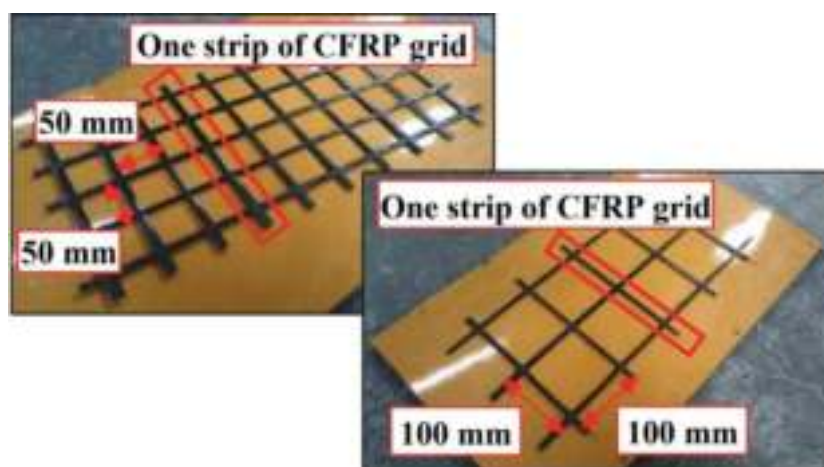


Figure 22: CFRP grid considered in Suwanpanjasil et al. study [28].

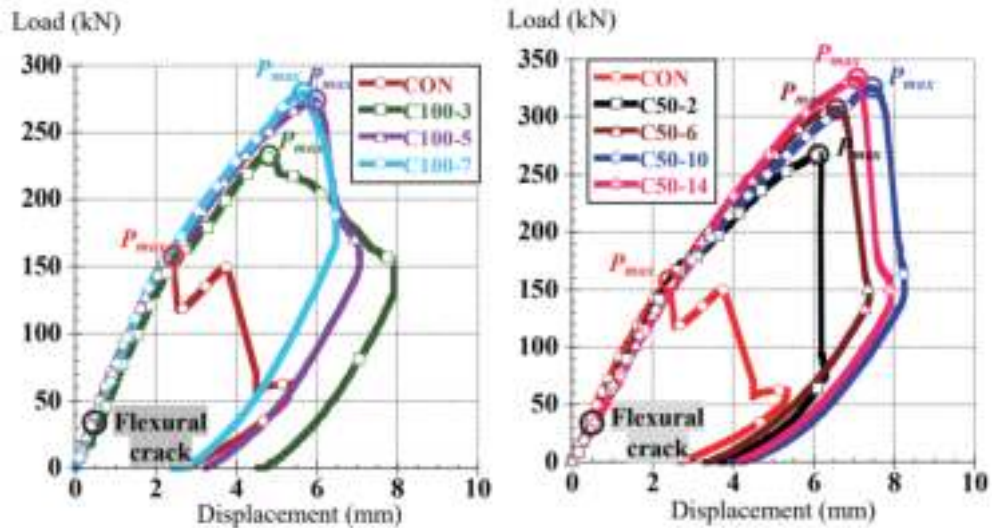


Figure 23: Load versus displacement results of Suwanpanjasil et al. study [28].

Deivanai and Sathia [29] conducted an experiment to study the effectiveness of welded connections against tied connections of conventional stirrups. The experimental program consisted of testing 6 beams reinforced with rectilinear stirrups in the transverse direction under two-points loading, where 3 are tied and 3 are welded to longitudinal steel. The spacing of the three beams of each connection type were 100 mm, 150 mm and 200 mm. For all three spacings considered, the beams reinforced with welded stirrups resulted in higher shear capacities, and first crack was observed at a higher load. Furthermore, it was observed that beams containing welded stirrups exhibited better behavior in the control of cracks and confinement of concrete. Figure 24 shows the maximum recorded shear values of the tested beams.

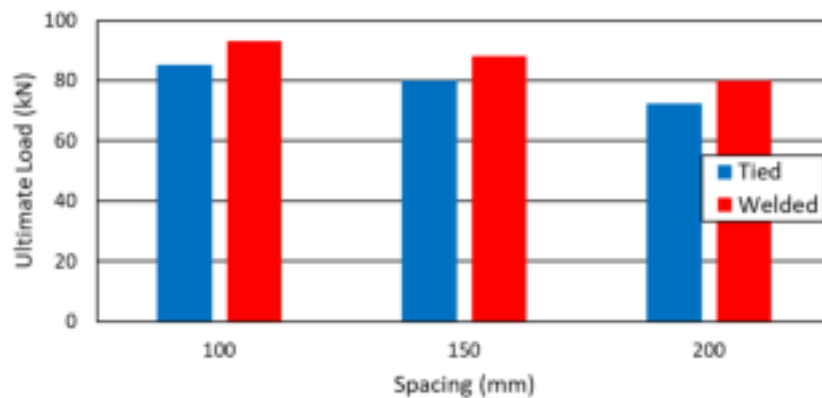


Figure 24: Maximum shear recorded in Deivanai and Sathia study [29].

In another study, Al-Nasra and Asha [30] used what they called “swimmer bars” as an alternative shear reinforcement to conventional stirrups. Swimmer bars are small inclined bars at an angle of approximately 40 degrees, with the ends bent horizontally parallel to the top and bottom flexural steel reinforcement. In total, swimmer bars were connected using 3 types of connections which are welded, bolted with a U-link, and bolted with a threaded bar. Figure 25 shows the steel cages of the beams reinforced with swimmer bars. The beams were subjected to a two-point loading scheme that was applied manually at increments of 20 kN. It was observed that beams reinforced with swimmer bars that are welded exhibited the highest load and deflection values, with about 20% increase in load carrying capacity, and 30% increase in levels of deflection than conventionally reinforced beam.



(a) Bolted swimmer bars using threaded bar.



(b) Bolted swimmer bars using U-link.



(c) Welded swimmer bars.

Figure 25: Beams reinforced with swimmer bars in the transverse direction [30].

4.2. Shear Performance of Beams Reinforced with WWF

With regard to research conducted on WWF reinforced beams in shear, Xuan et al. [4] in 1988 proposed the use of WWF as shear reinforcement in pretensioned concrete T-beams. The experimental program consisted of testing six T-beams by using WWF and different methods of shear reinforcement. Figure 26 shows the different reinforcement configurations of this study along with the tensile test results. To compare the results rationally, all beams had approximately the same transverse steel reinforcement ratio. In addition to the five types of transverse reinforcement considered, one beam was tested with no shear reinforcement. The tested beams were monitored for shear crack initiation, shear crack pattern, crack width, and ultimate shear strength. Results of the study demonstrated that crack widths were the same for all types of shear reinforcement. Beams reinforced with WWF as shear reinforcement exhibited similar effectiveness to those reinforced with conventional stirrups in terms of crack width control, shear strength and ductility. Figure 27 shows the load-deflection relationships for the beams with various types of transverse reinforcement.

Pincheira et al. [31] expanded the research of Xuan et al. by testing six beams with same reinforcement pattern but under cyclic loading in addition to three beams that were tested under static loading. The loading followed a sine function of frequency of 1 Hz that was reduced to 0.5 Hz at higher loading levels. The beams were unloaded every 10,000 cycles. The results showed that the beams tested under static loading experienced similar results to Xuan et al. Further, the WWF reinforced beams were not as effective as conventional stirrups under cyclic loading, as observed in Figure 28. Beams tested under cyclic loading exhibited much lower ultimate loads in comparison to beams tested under static loading.

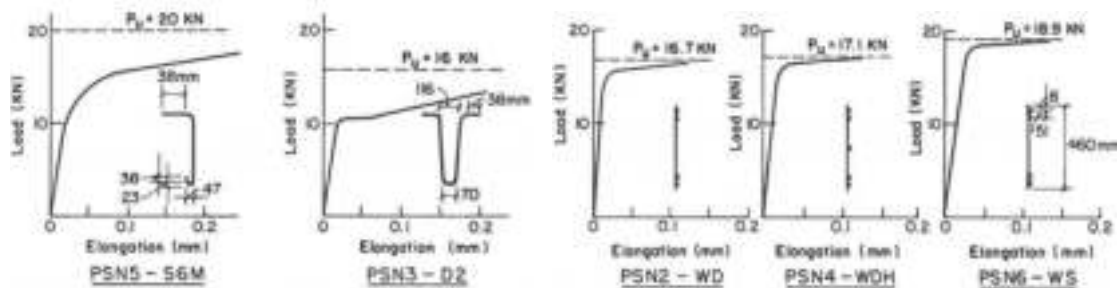


Figure 26: load-elongation relationships for stirrups and WWF [4].

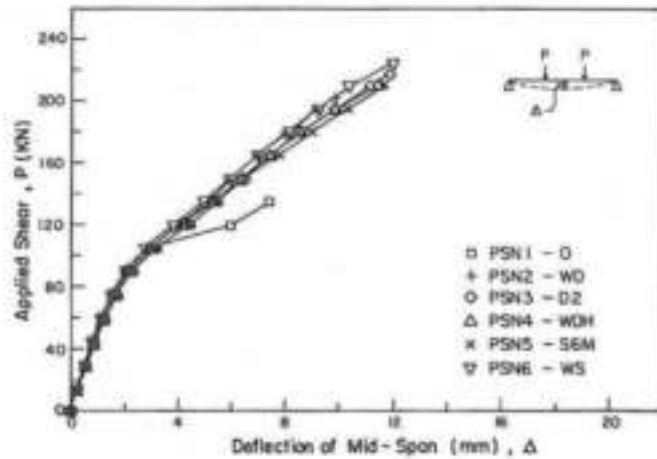


Figure 27: Results of Xuan et al. study [4].

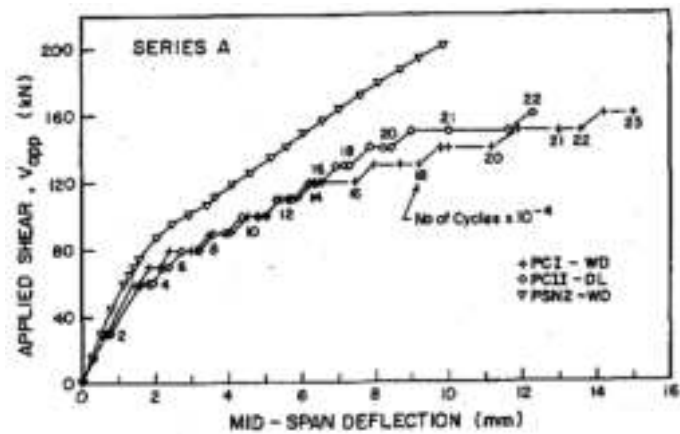


Figure 28: Results of Pincheira et al. study [31].

The use of WWF as shear reinforcement was further investigated by Griezic et al. [3]. The study consisted of testing four beams in which two were reinforced with cold-rolled grade 500 WWF cage and two were reinforced using hot-rolled conventional grade 400 steel stirrups. Figure 29 shows the results of the stress-strain curve of the two different types of shear reinforcement. The four beams were over-reinforced with No. 30 longitudinal bars to ensure a shear failure. Beams that were compared with each other were designed with similar transverse steel reinforcement ratios. The experimental results were compared with theoretical results, the Modified Compression Field Theory (MCFT) and the ACI318M-89. It was concluded that WWF exhibited large strains and sufficient ductility when used in concrete beams. Moreover, predictions of results were more accurate by the MCFT than the ACI318 code. Lastly,

it was observed that inclined shear crack widths were smaller in the beams reinforced with WWF when compared to beams reinforced with conventional stirrup, suggesting a better crack control, as shown in Figure 30.

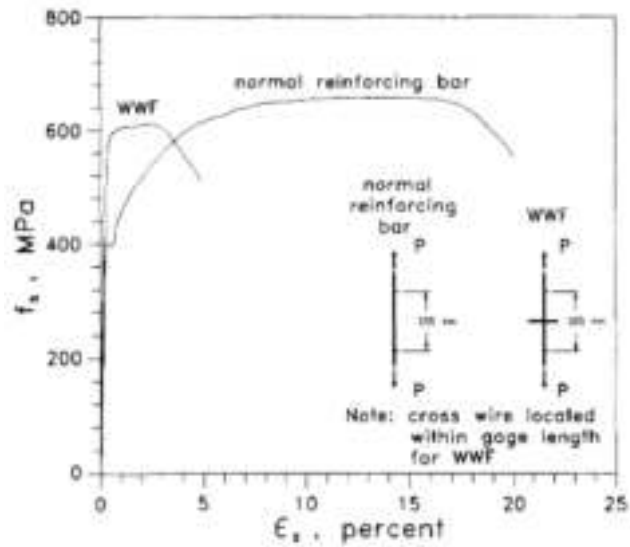


Figure 29: Cold-drawn WWF versus Rebar stress-strain curve [3].

Beam	Test results		ACI 318M-89 predictions		MCFT predictions			
	V_{max} at d , kN	Failure mode	V_s at d , kN	Failure mode	V_{max}/V_{ACI}	V_s at d , kN	Failure mode	V_{max}/V_{MCFT}
A500	332	Flexure	200	Shear	1.66	330	Flexure	1.01
A400	334	Flexure	212	Shear	1.58	316	Flexure	1.06
B500	291	Flexure	162	Shear	1.80	267	Flexure	1.09
B400	272	Flexure	169	Shear	1.61	266	Flexure	1.02

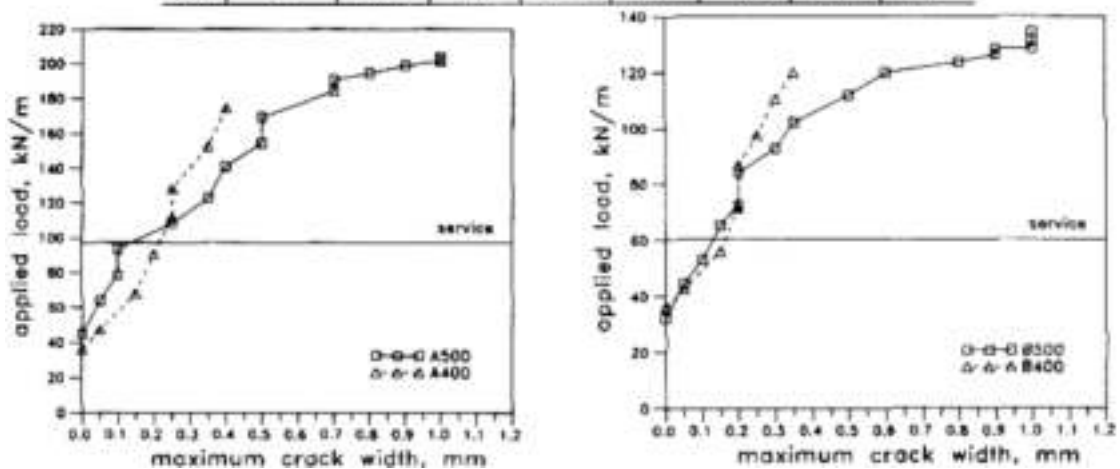


Figure 30: Summary of results of the work of Griezic et al. [3].

Using a different approach, Ladi and Mohite [32] studied the behavior of RC beams retrofitted with WWF mesh bonded to the exterior surface. The WWF mesh is jacketed to the concrete beam by a 20mm thick layer of mortar. A total of 25 beams were casted in which 19 beams were tested in flexure and 6 beams in shear. The results of the study showed that WWF can effectively be used to enhance existing RC beams in flexure and shear. Furthermore, beams retrofitted with WWF experienced lower deflection than the control beams. No de-bonding of the WWF mesh was observed during testing, even at failure. Figure 31 shows the WWF jacketing to the beams.



Figure 31: process of beam jacketing [32].

A study conducted by Yüksel [33] to assess the existing seismic code considered the use of WWF as reinforcement in a shear wall subjected to cyclic loading. The shear wall was designed and tested as cantilever under a reversed-cyclic lateral loading, and monitored through five LVDTs mounted to measure the lateral displacements over the wall height during testing. The maximum recorded displacement was at the top of the 2-meter wall and had a value of 27.4 mm, corresponding to a maximum load of 108 kN. At the end of the test the failure exhibited consisted of large crack openings at the wall base causing reinforcement buckling, as shown in Figure 32.



Figure 32: Buckling of vertical wires of WWF cage [33].

4.3. Flexural Performance of Beams Reinforced with WWF

Ajin and Gokulram [34] conducted experiments to study the effect of WWF on the flexural behavior of RC beams. The experiments included six simply supported beam specimens tested under two-point loadings. This paper studied the load-deflection behavior, shear and flexure strength, and mode of failures of the beams. It was also noticed that replacing conventional shear reinforcement with WWF cages showed no appreciable effect on the flexural strength, as shown in Figure 33. Both WWF reinforced beams and conventional stirrup reinforced beams showed modes of failure that were similar, consisting mainly of flexural cracks with no crushing of the concrete, as can be seen in Figure 34.

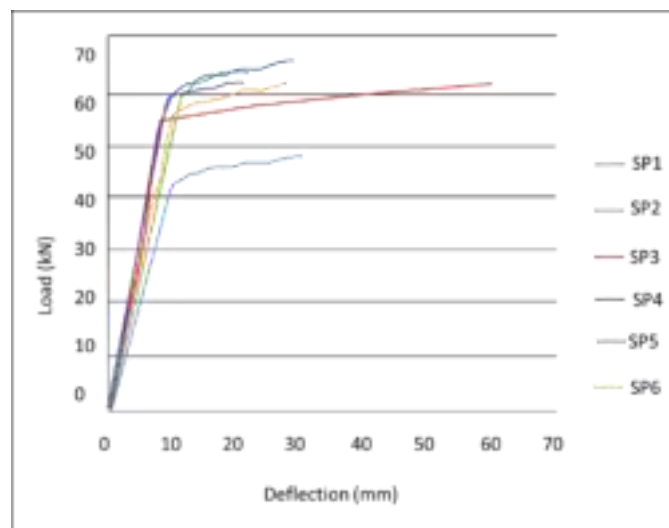


Figure 33: Load-Deflection graph of all tested specimens [34].



Figure 34: Mode of failures witnessed in Ajin and Gokulram's study [34].

Another study on the flexural behavior of beams transversely reinforced with WWF was conducted by Nithin and Kumar [35]. The comparisons were made between beams with no WWF, one layer of WWF and two layers of WWF. Figure 35 shows the reinforcement configuration of different specimens. Conclusions were drawn based on the analysis of the ductility, crack widths and propagations, and the flexure behavior of the tested beams. It was found that an increase of about 20% in the ultimate load was obtained by adding one layer of WWF. The addition of another layer of WWF only increased the strength of the beam by an additional 6%, indicating ineffectiveness of multi-layer of WWF reinforcement. Both one layer and two layers reinforced beams showed an enhancement in the ductility of the beams as well as an increase in deflections. It was also observed that the crack widths were reduced by the addition of WWF meshes.



Figure 35: Different WWF reinforcement configurations [35].

4.4. Axial Compression Performance of Columns Reinforced with WWF

In 2001, Lambert-Aikhionbare and Tabsh [36] conducted experiments to study the effect of using WWF as a confining element in RC columns, as an alternative to conventional rectilinear ties. The WWF sheet bundles were fixed parallel to the column cross-section at a desired spacing, as shown in Figure 36. Four different percentages of volumetric steel were considered as the results show in Figure 37. It was concluded from this study that a volumetric ratio of 4% yielded the best utilization of WWF as a confining element. Furthermore, it was observed that for the same volumetric ratio of transverse steel, the use of WWF provided higher strength in axial compression than conventional rectilinear ties, corresponding to about 17 to 43 % increase in strength.

Later on, Tabsh [37] focused his study on the stress-strain relation of high strength concrete columns confined by the WWF. A model of the results was developed and compared with previous models as well as the experimental results. It was found that the effectiveness of WWF increases after the spall off of the concrete cover. It was also found that the proposed model was the closest to experimental results. Figure 38 shows the proposed model in comparison with the previous models and the experimental results.

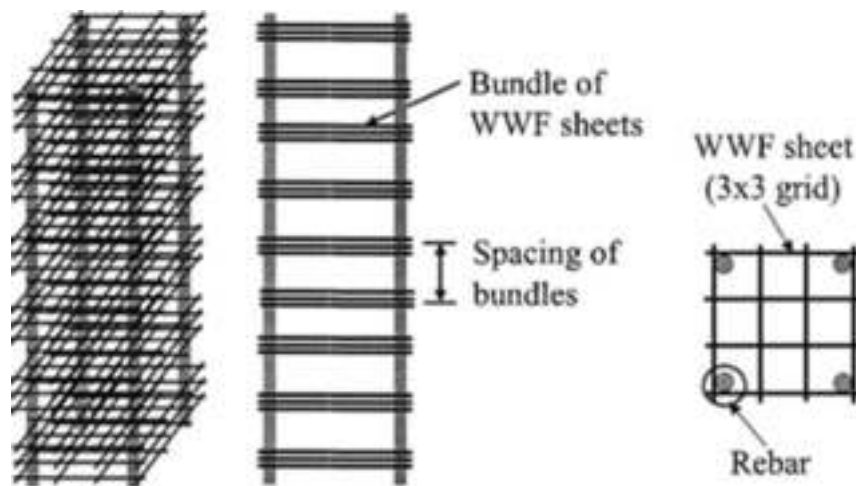


Figure 36: Reinforcement configuration of columns [36].

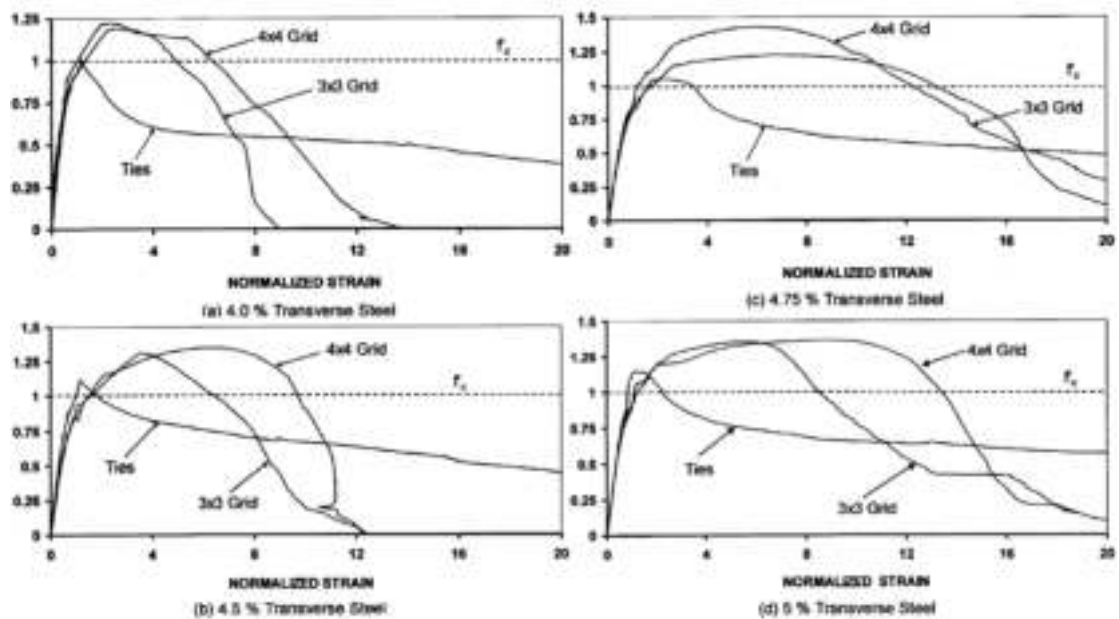


Figure 37: summary of results of study by Lambert-Aikhionbare and Tabsh [36].

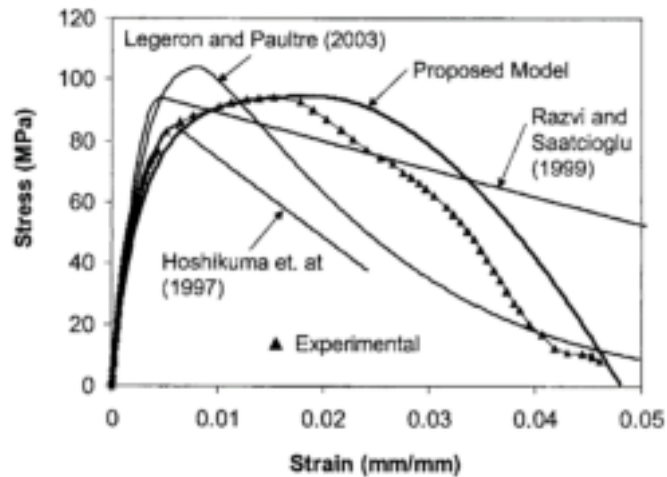


Figure 38: Previous models, proposed model and experimental results [37].

Similar to Tabsh's experiment[2], Kusuma et al. [38] performed a study to investigate the enhancement in ductility and strength by confinement of concrete using WWF sheets in columns. The difference was instead of using bundles of WWF, one sheet of WWF was used per spacing. Over a study of twenty columns, it was concluded that the placement of WWF sheets in columns can enhance column's strength and ductility by a factor of up to 2.23, thus making it an excellent potential application for earthquake-resistant structures as recommended by Kusuma et al. Figure 39 summarizes the findings of this study. It was recommended to further investigate the effectiveness of WWF subjected to cyclic loading.

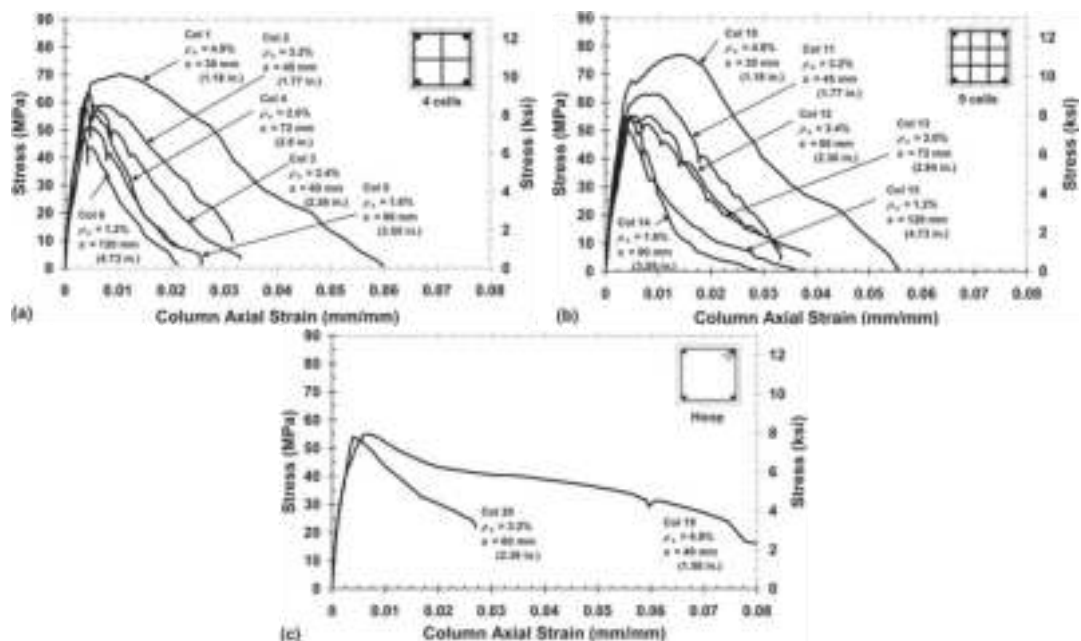


Figure 39: Summary of results presented by Kusuma [38].

4.5. Confinement Models and Reinforcing Methods

Since the proposed study is concerned in the effect of core confinement, a few papers on the subject are considered herein. The effect of confinement is expected to be achieved by using WWF cage and will result in improvement of the beam's strength and ductility. This improvement is expected in the shear strength provided by the concrete contribution rather than the shear strength provided by transverse steel. In 1988, Mander et al. [39] proposed a stress-strain model to account for the effect of core confinement of concrete by transverse reinforcement, subjected to uniaxial compressive loading. The reinforcing steel can be of any type, where the stress-strain relation of confined concrete can be computed using a single equation. Furthermore, the model allows for cyclic loading and includes the effect of strain rate. Figure 40 summarizes the equations used in the proposed model.

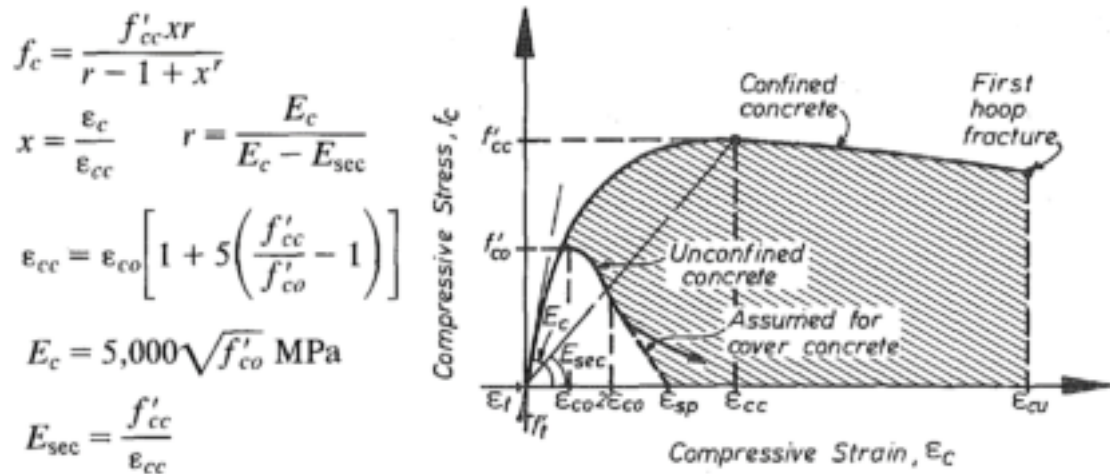


Figure 40: Confinement model proposed by Mander et al. [39].

Later in 1997, Hoshikuma et al. [40] developed a stress-strain model to capture the effect of confinement in concrete cores. There are four boundary conditions that must be met in developing the stress-strain model:

1. initial condition where $f_c = 0$ at $\epsilon_c = 0$
2. initial stiffness condition $df_c/d\epsilon_c = E_c$ at $\epsilon_c = 0$
3. peak condition $f_c = f_{cc}$ at $\epsilon_c = \epsilon_{cc}$
4. peak stiffness condition $df_c/d\epsilon_c = 0$ at $\epsilon_c = \epsilon_{cc}$

Hoshikuma et al. suggested that while previous researchers were able to approximate the behavior of confined concrete accurately, they were not considering

the third boundary condition. In the proposed model, the third boundary condition is accounted for, and is predicted by two equations, a parabolic function for the rising part and a linear function for the descending part as shown in Figure 41.

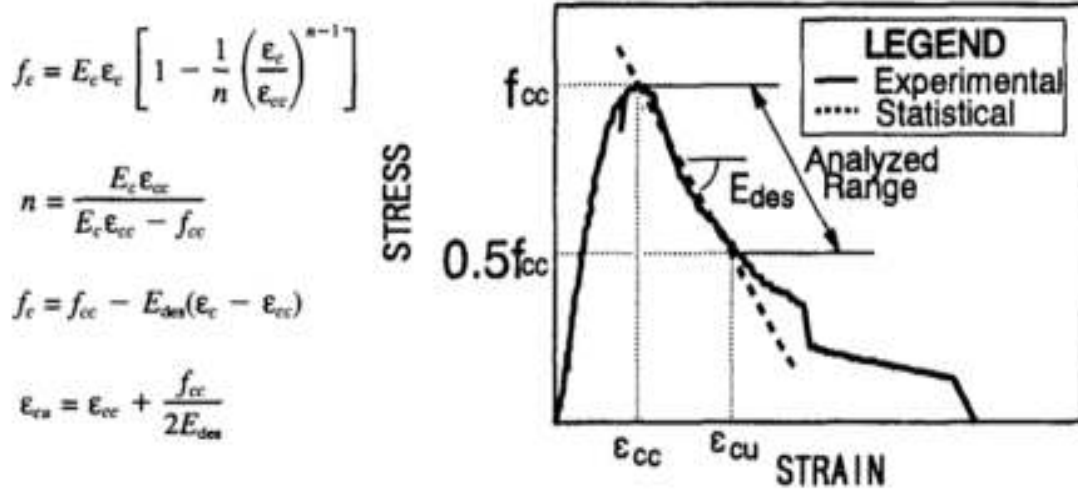


Figure 41: Confinement model proposed by Hoshikuma et al. [40].

Another model is proposed by Legeron and Paultre [41], based on strain compatibility and transverse force equilibrium. The model is particularly effective in predicting the confinement effect of concrete cores reinforced transversely by high-yield-strength steel. The model is split into a pre-peak part and a post-peak part and is predicted by the equations presented in Figure 42. The resulting model was verified against 200 circular columns and square columns, that were tested experimentally. The results of the predicted versus experimental confined strength of concrete is presented in Figure 43.

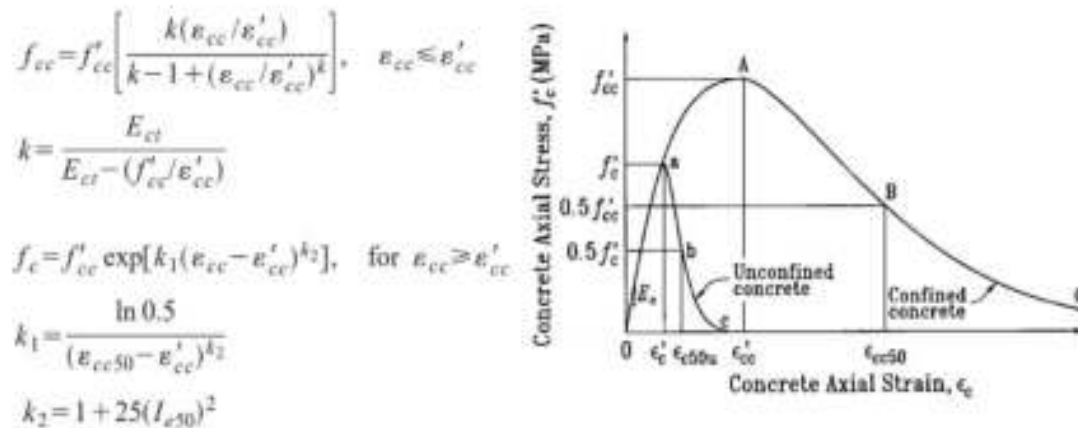


Figure 42: Confinement model proposed by Legeron and Paultre [41].

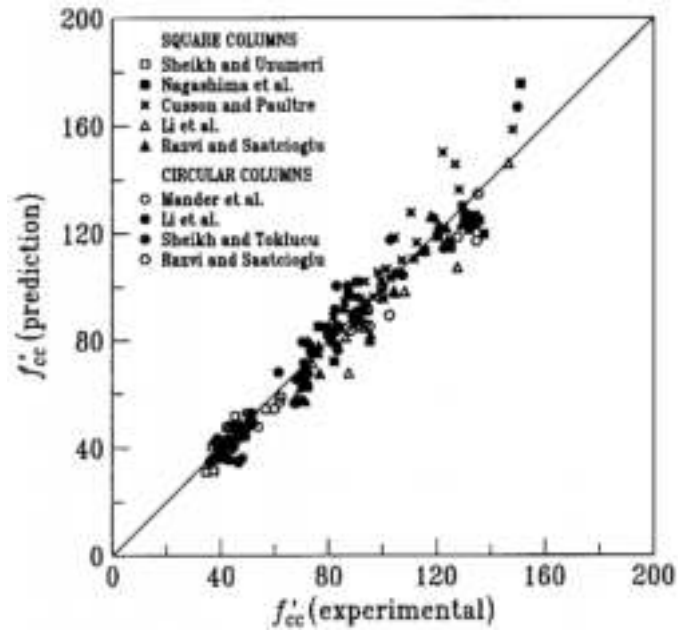


Figure 43: Predicted versus experimental comparison using proposed model [41].

A study by Han and Shin [42] was conducted to investigate the effect of confinement in columns and was compared with previous existing models. Figure 44 shows the different models that were considered during this study. The results showed enhancement of strength and ductility of confined columns by amounts that reaches up to 50%. Furthermore, it was noticed that the closest results were obtained from the modified Kent-Park model, which overestimated the results by around 15%.

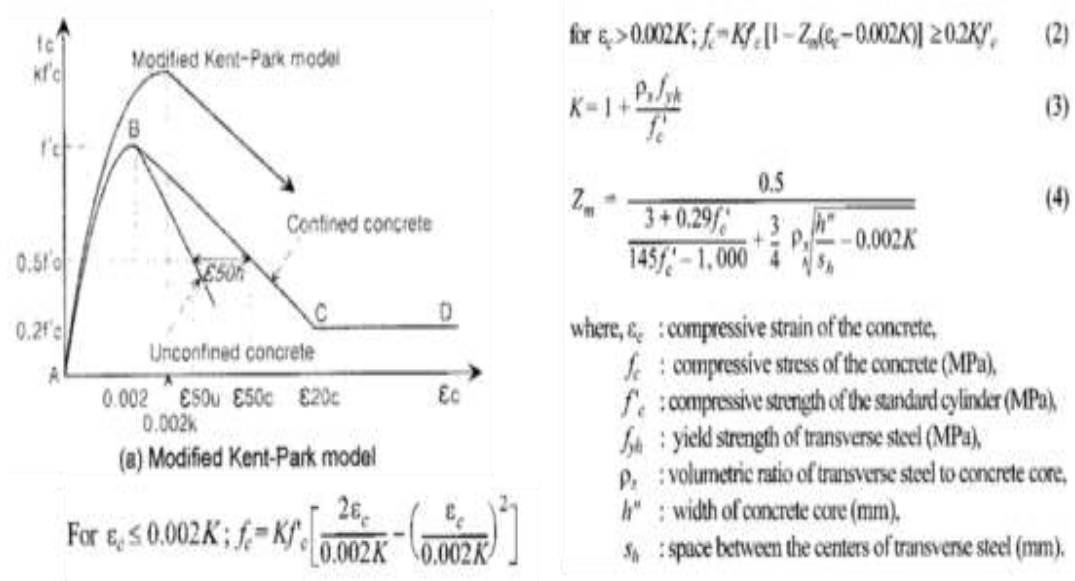


Figure 44: Previous models of concrete confinement [42].

Delalibera and Giongo [43] performed an experimental study on the effect of confinement in beams. In their study, square shaped stirrups were added at the compression zone between the normal stirrups to induce the effect of confinement. Figure 45 provides a visual aid of the reinforcement of the beams. From the results, significant improvement in ductility can be seen upon adding a confining element. It can be also seen that the ultimate strength is also higher for the beams that are confined, as shown in Figure 46.

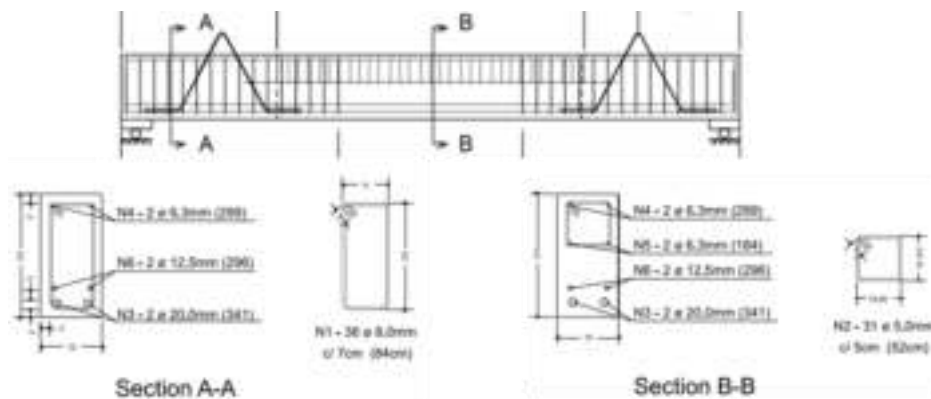


Figure 45: Detailing of sections [43].

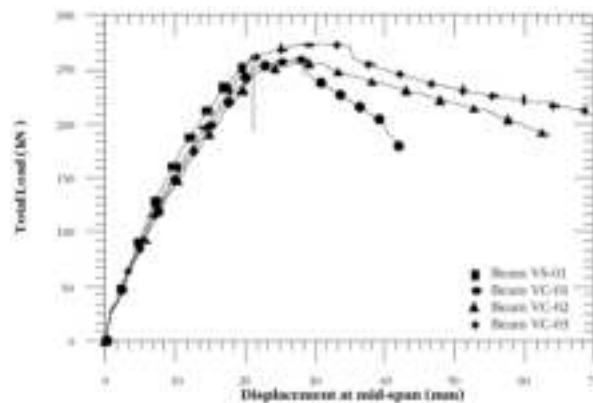


Figure 46: Experimental results of study by Delalibera and Giongo [43].

In an attempt to study the confining effect on concrete experimentally, Jaafar [44] conducted an experiment to study the use of using spiral links as shear reinforcement. He conducted his experiment on beams with different spiral reinforcing configurations. The analysis of the beam was performed using the modified compression field theory and non-linear finite element analysis. From the results of the experiment, it was concluded that the use of spirals contributed to the increase of

ultimate shear capacity. Furthermore, it was observed that the ductility of the beams was enhanced due to the confinement of the concrete core. While that is a great outcome, it was noticed that current design methods are inadequate for this unconventional method of reinforcement. The expected modelled results were incompatible with the experimental results as can be seen by Figure 47. Improving on this paper can help in modelling the confinement effect and understanding beams under confinement.

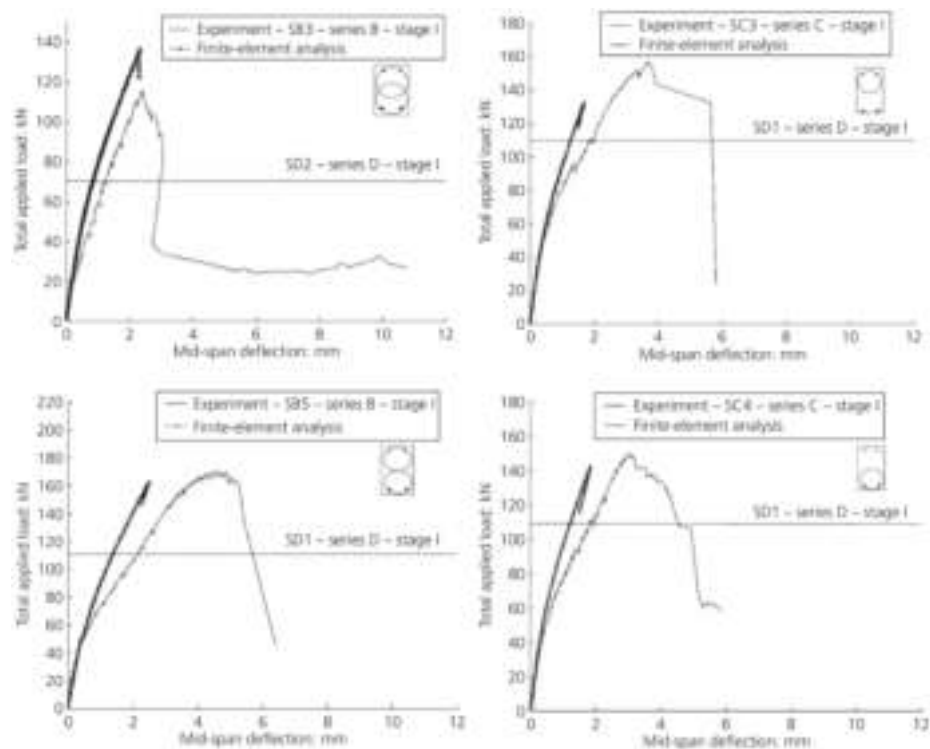


Figure 47: Experimental results versus modelled results of Jaafar’s study [44].

4.6. Final Remarks on the Literature Review

While some of the previous research included herein addressed the topic of WWF as shear reinforcement, none of the published work considered the use of a closed cage made of WWF, which is essential for concrete confinement in the core. Further, no comprehensive study was found that considered the effects of the shear span-to-depth ratio, concrete compressive strength, transverse steel ratio, wire diameters, and grid openings on the shear strength and ductility. Also, few of the published research included companion computational efforts based on international structural design codes. The current study fills the gap in research needs in those areas and beyond.

Chapter 5. Experimental Program

In this chapter, the experimental plan of the study is outlined and discussed, in addition to the specimen detailing and design, test setup and instrumentations used, mechanical properties of the materials used, and fabrications of the specimens.

5.1. Details of Beam Specimens

A total of 23 RC beams are considered in this study to examine the effectiveness of using WWF steel as a replacement of stirrups. This study is focused on investigating the shear behavior of the RC beams reinforced with this type of reinforcement.

5.1.1. Experimental plan. A well-developed experimental program is conceived to achieve the objectives of the study. The proposed research plan is composed of 23 half-scale RC beams that are tested in the materials and structures laboratory at AUS. The considered variables in the experiments are the shear span-to-total depth ratios ($a/h=2.5$ and 3.0), compressive strength of concrete ($f'_c=30$ and 35 MPa), WWF grid spacing ($s=25, 50$ & 100 mm), WWF wire diameter ($D=4, 6$ & 8 mm), and the transverse steel area per unit length of member ($A_v/s=0.502, 1.006$ and 1.12). The wire diameters and grid spacing are selected based on the available WWF in the UAE market. All beams have the same rectangular cross-sectional dimensions of 200 mm width by 300 mm depth, with 25 mm clear concrete cover on the transverse steel reinforcement. Based on the considered shear span-to-depth ratios, available UTM base length and the constant cross-sectional dimensions, beams having a shear span-to-total depth ratio of 2.5 are tested over 1700 mm long span, while beams with shear span-to-total depth ratios of 3.0 are over 1850 mm long span. All beams will have a 100 mm overhang from both sides to provide stability for the beam during testing. Furthermore, the experimental program is based on requiring the beams to fail in shear; therefore, all specimens were highly reinforced in flexure by high strength steels 7-wire strands without prestressing. Another advantage of the strands over rebars is that they do not provide high dowel action, which could influence the shear strength. In this study, the control (stirrup reinforced) beams are designed following three different approaches, as presented in Figure 48, in order to justify the stirrup replacement with welded wire mesh. Note that the nomenclature presented for the stirrup reinforced beam will be different than that of the WWF reinforced beam, and will be carried out throughout the paper.

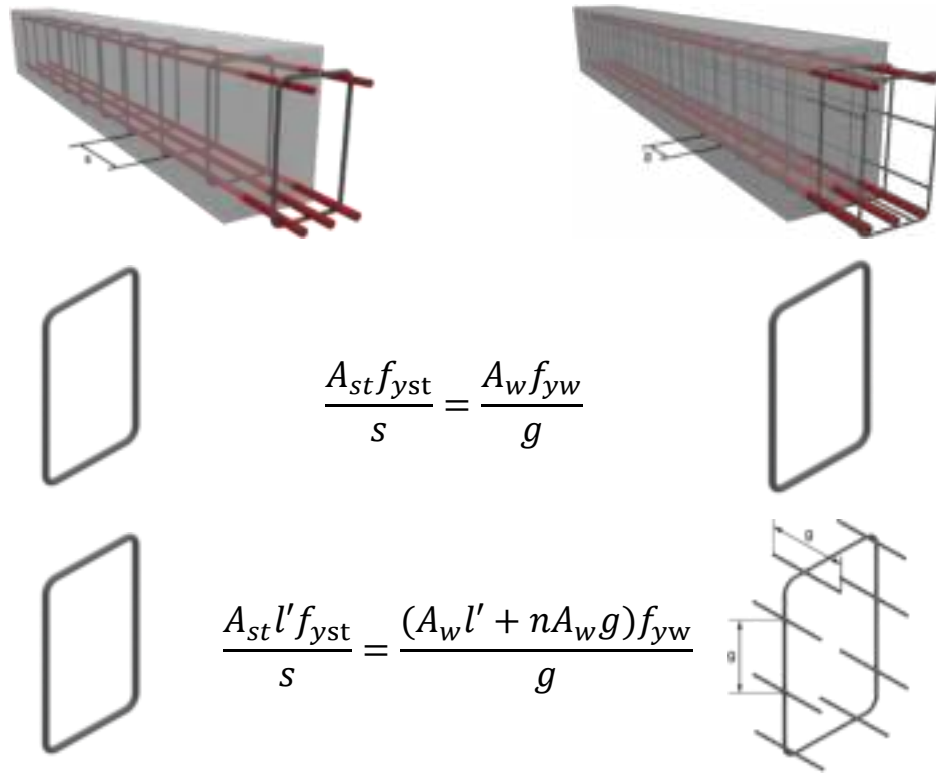


Figure 48: Summary of design approaches.

The relationship between the amount of steel in the WWF and stirrups in the control beams is as follows:

- (1) the total volume of the wires (vertical and horizontal wires) in the WWF reinforced beams times the yield strength of the wires matches the total volume of the stirrups (vertical) in the control beams times the yield strength of the stirrups (refer to Equation 26),
- (2) the volume of just the transverse reinforcement in the WWF beams (vertical wires) times the yield strength of the wires equals to the volume of the stirrups in the control beams times the yield strength of the stirrups (volume of steel is calculated using Equation 27), and
- (3) no transverse shear reinforcement in the control beams.

$$\frac{A_{st}f_{yst}}{s} = \frac{A_w f_{yw}}{g} \quad (26)$$

where:

A_{st} = total cross-sectional area of vertical stirrups reinforcement (mm^2),

f_{yst} = yield strength of stirrups (MPa),

s = spacing of stirrups (mm),

A_{sw} = total cross-sectional area of vertical WWF wire reinforcement (mm²),

f_{yw} = yield strength of WWF wire (MPa), and

g = grid opening of WWF (mm).

For example, to find out the spacing of No.8 stirrup with $f_y= 460$ MPa that has an equivalent area of vertical steel as a No.4 wire at 25mm WWF with $f_y= 500$ MPa, we substitute the values in the expression, where the only unknown is the spacing of the stirrups:

$$\frac{12.6 * 500}{25} = \frac{50.3 * 460}{s} \rightarrow s = 92$$

$$\frac{A_{st}l'f_{yst}}{s} = \frac{(A_wl'+nA_wg)f_{yw}}{g} \quad (27)$$

where:

n = number of cross-wires = $\frac{l'}{s}$

l' = length of transverse wires = $2(b' + h')$ (mm)

b' = width of steel cage (mm),

h' = height of steel cage (mm), and

For example, to find out the spacing of No.10 stirrup with $f_y= 460$ MPa that has an equivalent volume of steel as a No.6 wire at 50mm WWF with $f_y= 450$ MPa in a 2-meter steel cage with 150 mm width and 250 mm height, we substitute the values in the expression, where the only unknown is the spacing of the stirrups:

$$\left(\frac{78.5 * 800 * 460}{s}\right) = \left(\frac{\left(28.3 * 800 + \frac{800}{50} * 28.3 * 50\right) * 450}{50}\right) \rightarrow s = 70.9 \text{ mm}$$

The experimental program consists of 3 groups based on the shear span-to-depth ratio and concrete compressive strength, as presented in Figure 49. The first group represents specimens with $a/h=2.5$ and $f'_c=35$ MPa, the second contains beams with $a/h=3$ and $f'_c=35$ MPa, and the last group comprises beams with $a/h=3$ and $f'_c=30$ MP. The beams with a/h ratio equal to 2.5 correspond to shear span to effective beam depth ratio a/d equal to 2.85-3.10. Furthermore, the beams with a/h ratio equal to 3.0 correspond to shear span to effective beam depth ratio a/d equal to 3.52-3.69. Groups 1 and 2 each contains 8 beams while group 3 contains 7 beams, for a total of 23 beams.

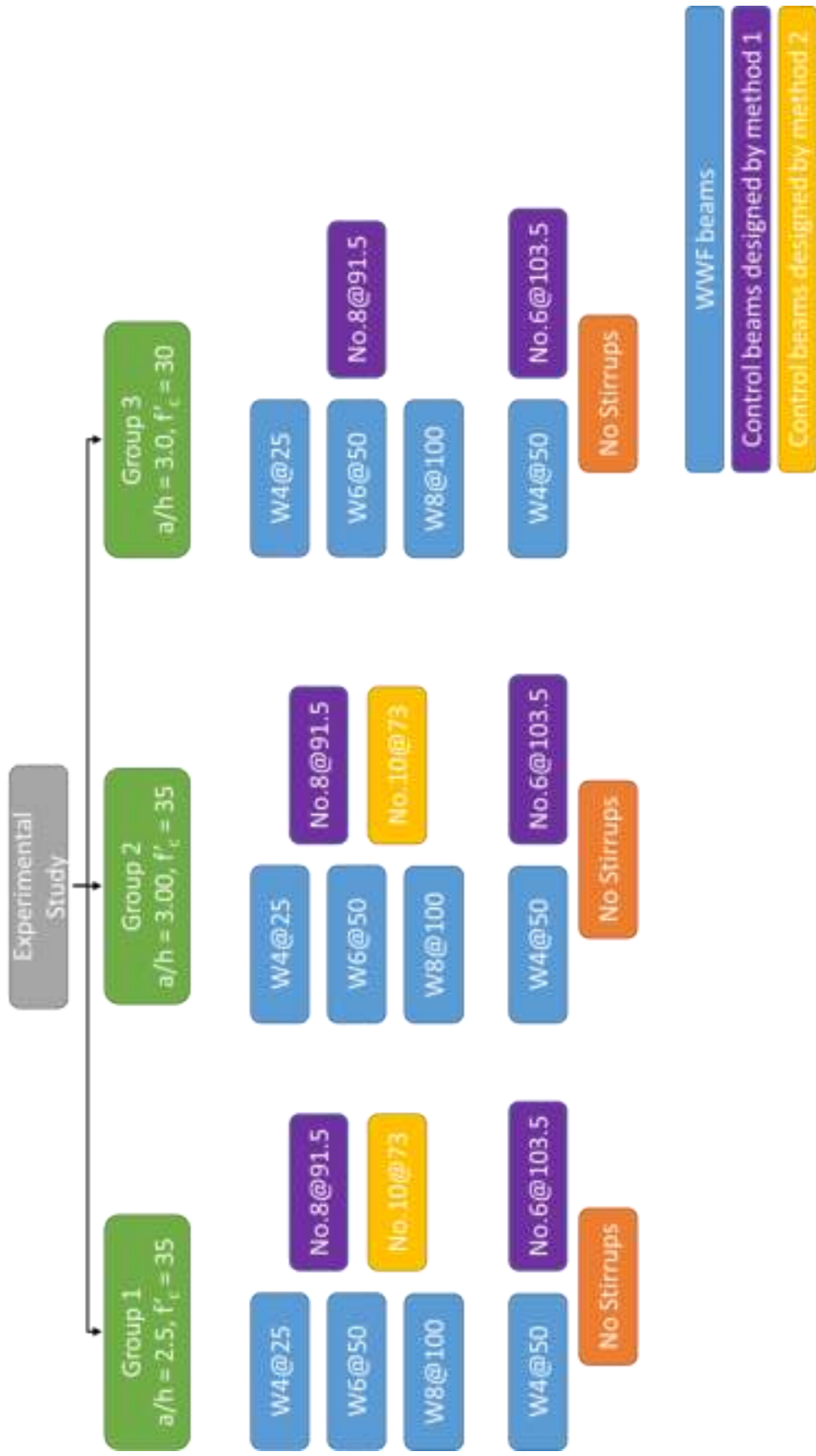


Figure 49: Experimental study.

In this study, a special identification scheme composed of 5 variables is developed to recognize the characteristics of each specimen, (reinforcement type)-(diameter)-(spacing)-(a/h)-(f'_c). This scheme starts by referring to the type of transverse reinforcement, letter “W” for WWF, letter “S” for stirrups, and “N” for no stirrups or WWF. This is followed by a number representing the diameter of the wire or stirrup in units of mm. After that, a number that refers to the spacing of the transverse reinforcement in mm. Next, “a/h” is shear span-to-total depth ratio. The last number in the specimen designation is the concrete compressive strength in the units of MPa. For example, W-6-50-3.5-30 refers to a beam that is transversely reinforced with WWF, having a wire diameter equal to 6 mm that is spaced at 50 mm, tested at a shear span-to-depth ratio of 3.5, with f'_c equal to 30 MPa. The detailing of the beams is shown in Figure 50 to Figure 52.

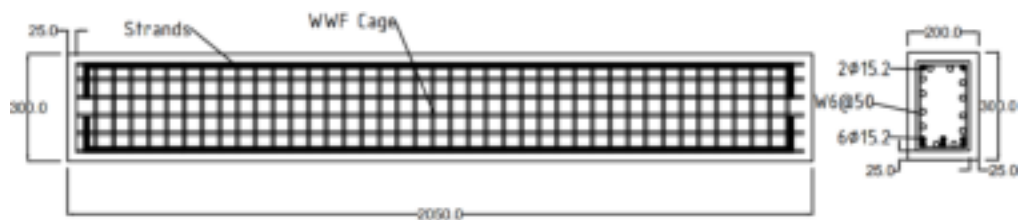


Figure 50: Sample beam detailing containing WWF (W-6-50-2.5-35).

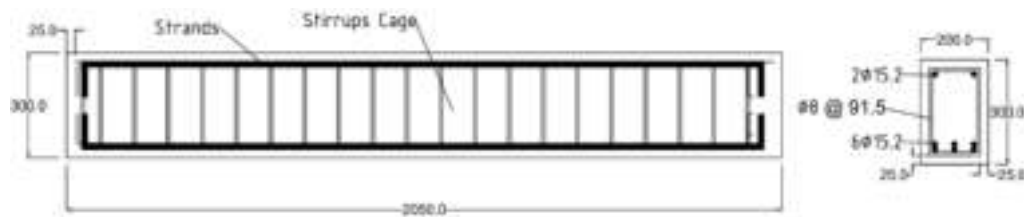


Figure 51: Sample beam detailing containing stirrups (S-8-91.5-2.5-35).



Figure 52: Sample beam detailing with no shear reinforcement (N-2.5-35).

5.1.2. Test setup and instrumentation. The beam specimens are tested using the 2500kN UTM available at the American University of Sharjah's Materials and Structures lab, shown in Figure 53. They are simply supported on chairs made from structural steel with some allowance for lateral movement through steel rollers placed inside halved cylinders, shown in Figure 54. The overhang length of the beams beyond the two supports is equal to 100 mm. The beams are subjected to one-point displacement-controlled loading at a rate of 1.0 mm per minute. Two LVDTs are attached to the beams at 40-degree angles from the horizontal axis to measure the average width of the diagonal cracks between the load and near support, and another LVDT was placed vertically just below the loading point to measure the beam deflection. The diagonal LVDTs are placed on the beam within the critical region of high moment and shear. Five strain gauges are placed on the transverse steel at different locations to monitor the strain in the transverse steel. The strain gauges are attached to the transverse steel in the critical region within 600 mm from the point of load application. Figure 55 shows a typical test setup schematic diagram.



Figure 53: UTM available at the AUS's Materials and Structures lab.



Figure 54: Beam support used made from structural steel chair and steel roller.

The test readings were captured at the specified time increment on each of the specimen. The results include the applied load, average crack widths, vertical deflection and transverse steel strains. Relationships from the obtained data are presented in the form of: (1) load-deflection graphs, (2) load-strain in longitudinal steel relationships, and (3) load-crack widths plots. These relationships are then used to discuss the shear strength, ductility, stiffness, crack propagation of tested specimens. Through comparisons of test results conclusions and practical recommendations are drawn.

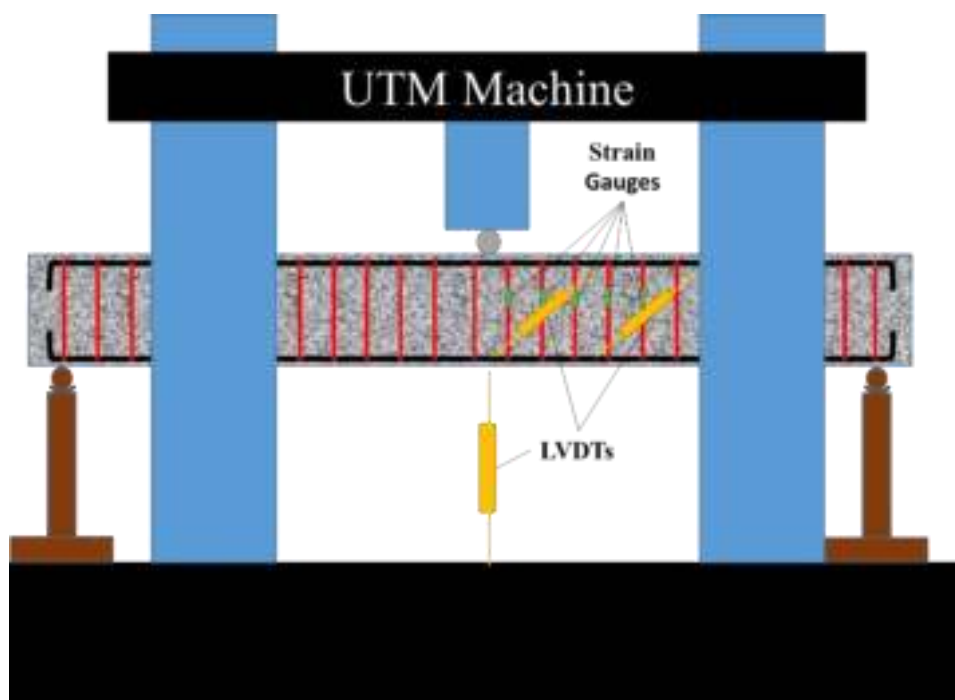


Figure 55: Typical test set-up and instrumentations.

5.2. Material

In this section, the mechanical properties of concrete and steel used in the specimens are obtained through compressive and tensile tests, respectively, in accordance to relevant ASTM standards.

5.2.1. Concrete. The beams were divided into 3 groups and casted over 3 days, in which two groups (designated Group 1 and 2) were designed to achieve a compressive strength equal to 35 MPa and the third group (Group 3) was intended to achieve a compressive strength of 30 MPa at the day of testing. A total of five 150mm-cubes per batch were obtained, for a total of 15 cubes. In addition, six 150 mm diameter by 300 mm length cylinders per batch were acquired, for a total of 18 cylinders. The cubes and cylinders were crushed on the days of the beam tests to determine the concrete properties for use later in the analytical part of the study. Test procedures for the cylinders and cubes followed the ASTM standard [45, 46] at a loading rate equal to 0.25 MPa/second and 0.3 MPa/second, respectively. Figure 56 shows the crushing machine used available in the AUS's asphalt lab. To obtain practical results, the cubes and cylinders were subjected to similar curing conditions as the beams. The cubes findings were used to verify the results of the cylindrical specimens. The details on the properties of the aggregates are shown in Table 2 and Table 3.



Figure 56: Crushing machine used available in the AUS's asphalt lab.

Table 2: Fineness modulus of fine aggregate.

	Dune Sand	Washed Sand	Combined Dune and Washed Sand
F.M	3.56	4.90	4.23

Table 3: Coarse aggregate properties.

Aggregate Size	Size (mm)	Bulk S.G	Apparent S.G	Absorption (%)	Moisture (%)	Abrasion Loss (%)	Crushing Value (%)
Coarse	10	2.6	2.68	1.4	0.9	23	18

5.2.1.1. High f_c . The concrete mix proportions of the higher strength concrete used in the study are presented in Table 4. The cylinders were capped at their ends with 10 mm neoprene sheets and a strain gauge was placed vertically at their mid-height. The compressive strength of the cubes and cylinders belonging to Groups 1 and 2 are presented in Table 5. Group 1 represents beams numbered 1 to 8, and Group 2 represents beams numbered 9 through 16. It was found that the average f_c is equal to 36.55 MPa for Group 1 and 35.91 MPa for Group 2. The slight difference in compressive strength between the two groups is due to the fact that the specimens in Group 2 were tested earlier than those in Group 1. Figure 57 and Figure 58 show the stress-strain relation up to the maximum stress obtained for the tested cylinders. All tested specimens exhibited uniform straining around the cylinder surface and a sample is shown in Figure 59. The strain corresponding to maximum stress ranged between 0.0014 and 0.0017 for Group 1 and 0.0023 and 0.0033 for Group 2.

Table 4: Mix proportions for high strength concrete used in the study.

Target strength (MPa)	10 mm Coarse Aggregate (kg/m ³)	Fine Aggregate (kg/m ³)		Cement (kg/m ³)	Water (kg/m ³)	Admixture (kg/m ³)	Total weight (kg/m ³)
		Dune	Washed				
35	700	440	730	380	170	4	2424

Table 5: Summary of results of high f'_c specimens.

Sample ID	Group 1		Group 2	
	Cubes	Cylinders	Cubes	Cylinders
Sample 1	45.00	39.43	54.00	35.73
Sample 2	42.00	35.69	36.00	35.62
Sample 3	41.00	36.78	49.00	35.73
Sample 4	46.00	37.10	45.00	36.43
Sample 5	48.00	36.98	35.00	35.81
Sample 6	-	33.34	-	36.16
Average Strength	44.40	36.55	43.80	35.91
SD of Strength	2.58	1.82	7.36	0.29
Average Cylinder/Cube Strength	0.82		0.82	

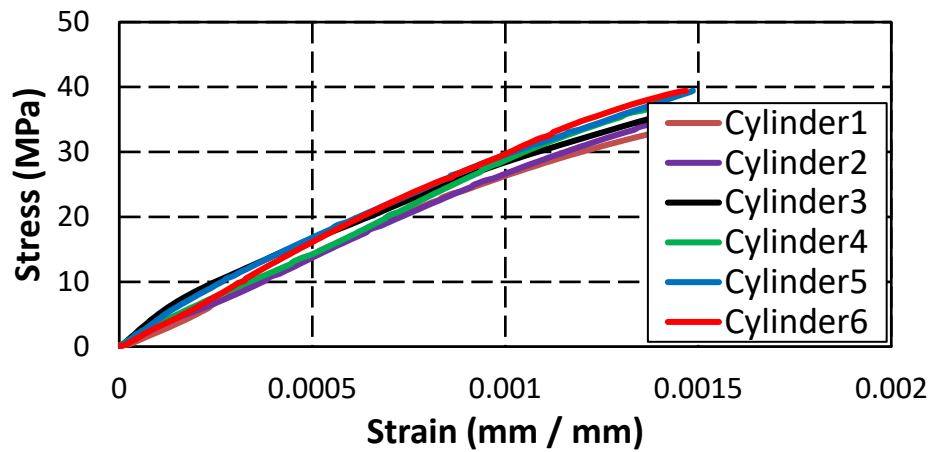


Figure 57: Stress-Strain relations of cylinders belonging to Group 1.

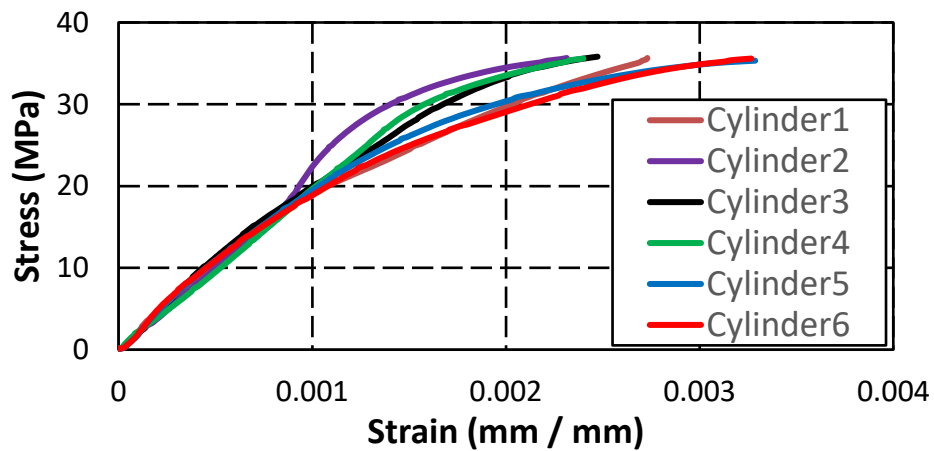


Figure 58: Stress-Strain relations of cylinders belonging to Groups 2.



Figure 59: Typical cubes and cylinders failures of high f'_c specimens.

5.2.1.2. Low f'_c . The concrete mix proportions of the lower strength concrete used in the research are presented in Table 6. The compressive strength of the cubes and cylinders belonging to group 3 are presented in Table 7. Group 3 represents beams numbered 17 to 23 in the experimental program. Figure 60 shows the stress-strain relationship obtained for the tested cylinders. It was found that the average f'_c in this group is equal to 30.81 MPa. The strain corresponding to maximum stress ranged between 0.0012 and 0.0019. Typical mode of failure can be seen in Figure 61.

Table 6: Mix proportions for low strength concrete used in the study

Target strength (MPa)	10 mm Coarse Aggregate (kg/m ³)	Fine Aggregate (kg/m ³)		Cement (kg/m ³)	Water (kg/m ³)	Admixture (kg/m ³)	Total weight (kg/m ³)
		Dune	Washed				
30	700	730	440	330	160	3.5	2364

5.2.2. Steel. There are three types of reinforcing steel that are used in this study, the WWF, normal strength deformed bars and high strength steel 7-wire strands. Figure 62 shows the three types of steel used in this study. The WWF is shaped as closed steel cage and utilized as replacement of conventional stirrups. The deformed bars are employed in the control beams as stirrups placed vertically to the centerline of the beams. The strands are used to reinforce the beams in the longitudinal direction in order to preclude flexural failure without inducing excessive dowel action. For each

Table 7: Summary of results of low f'_c specimens.

Sample ID	Group 3	
	Cubes	Cylinders
Sample 1	34.00	29.63
Sample 2	33.00	31.45
Sample 3	39.00	31.08
Sample 4	38.00	31.58
Sample 5	40.00	29.48
Sample 6	-	31.62
Average Strength	36.80	30.81
SD of Strength	2.79	0.90
Average Cylinder/Cube Strength	0.84	

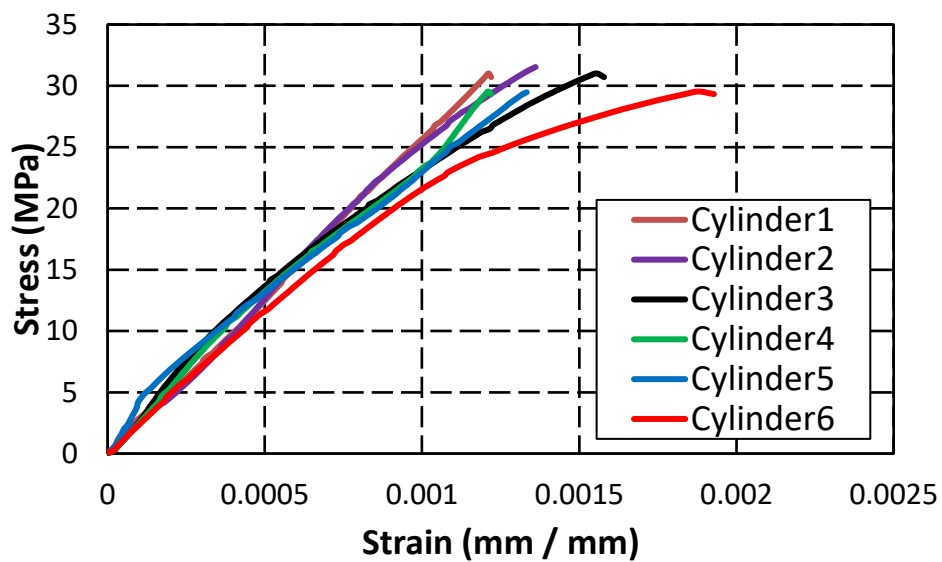


Figure 60: Stress-Strain relations of cylinders belonging to Group 3.



Figure 61: Typical cubes and cylinders failures of Group 3.

type and size of the steel, 3 samples were tested in tension to determine the stress-strain relationship and record the modulus of elasticity, yield strength and ultimate capacity. All tests were performed in accordance with ASTM standards [45, 46], using a universal testing machine shown in Figure 63, where the loading rate for all coupon tests was 1 mm/min. Figure 64 shows a schematic diagram of the tested coupons.



Figure 62: Types of steel used in this study.



Figure 63: UTM machine used for testing the steel bars.

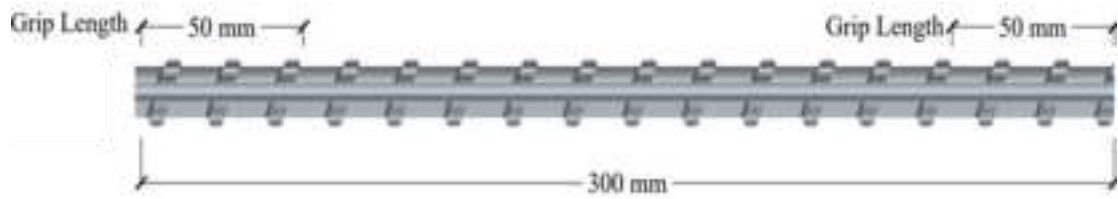


Figure 64: Test setup of steel coupons.

5.2.2.1. WWF. In this study, the WWF sizes that were available in the UAE market were considered, and they were 4 mm diameter at 25 mm and 50 mm spacing, 6 mm diameter at 50 mm, and 8 mm diameter at 100. The steel used in the study was galvanized and smooth-surfaced. For each wire size, 3 samples were taken from 3 different sheets to capture variability in results. Table 8 summarizes the results and Figure 66 shows the stress-strain curves of the tested coupons. The test results clearly indicated that 6 mm diameter mesh has markedly lower strength than the 4 mm and 8 mm meshes. Therefore, the nominal yield strength of the 6 mm diameter wire is assumed to be 450 MPa, and the 4 mm and 8 mm diameter wires are presumed to have a 500 MPa yield strength. Test results showed that the 4 mm wire had a much smaller ductility compared with the 6- and 8-mm wires. The average modulus of elasticity varied within a narrow range, 198-200 GPa. ASTM 1064/A 1064M-09, Standard Specification for Steel Wire and Welded Wire Reinforcement [16], requires the yield strength to be determined at an extension under load of 0.5 % of gage length, i.e. $\epsilon_y = 0.005$ mm/mm. The average yielding strength of the 4 mm, 6 mm, and 8 mm wires were 590 MPa, 509 MPa, and 574 MPa, respectively, and ultimate strength of 635 MPa, 555 MPa, and 660 MPa, respectively. A sample of the fractured wires following the tests is shown in Figure 65.



Figure 65: Tested wire specimens.

Table 8: Mechanical properties of WWF steel wire

Diam. Sample	4 mm			6 mm			8 mm		
	f_y (MPa)	ϵ_y (μ)	E (GPa)	f_y (MPa)	ϵ_y (μ)	E (GPa)	f_y (MPa)	ϵ_y (μ)	E (GPa)
1	564	5000	195	491	5000	198	578	5000	200
2	603	5000	199	519	5000	199	572	5000	199
3	604	5000	200	518	5000	200	571	5000	200
Average	590	5000	198	509	5000	199	574	5000	200
SD	18.6	-	2.16	13.0	-	0.82	3.09	-	0.471

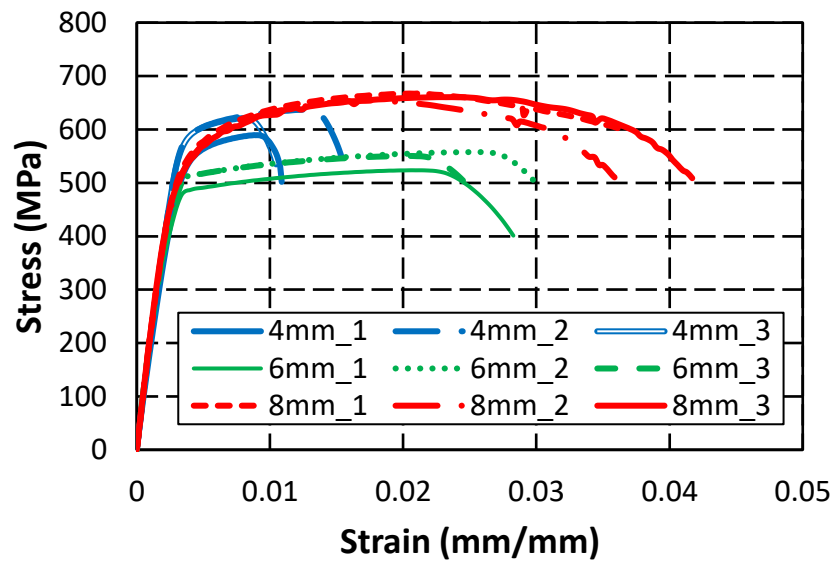


Figure 66: Stress versus strain curve for WWF coupons.

5.2.2.2. Stirrups. In order to match the steel ratio of the WWF cages, three sizes of closed steel stirrups were used in the control beams. The rebars that were utilized in the stirrups had diameters equal to 6 mm, 8 mm, and 10 mm. For each bar size, 3 samples were tested and averaged. Due to its unavailability in the market as straight bars, the deformed 6mm diameter stirrups were obtained from a welded wire fabric. The resulting yield strength and modulus of elasticity are summarized in Table 9 and Figure 67. The average modulus of elasticity varied within a narrow range, 195-205 GPa, with an average value of 199.2 GPa. Although there is variation in the actual yield stress within the different size of rebars, the findings indicate a nominal yield strength equal to 460 MPa (BS 4449), which is commonly used in the UAE. The average tested yield strength for the three considered sizes ranged between 556 and 577

MPa. The corresponding average yield strain is taken equal to the yield stress divided by the modulus of elasticity of the steel. An average value of the yield strain for the stirrups equal to 0.002828 will be considered in the study for the 6, 8 and 10 mm diameter stirrups. A sample of the tested stirrups specimens is shown in Figure 68.

Table 9: Mechanical properties of deformed bars steel test.

Diam. Sample	6 mm			8 mm			10 mm		
	f_y (MPa)	ϵ_y (μ)	E (GPa)	f_y (MPa)	ϵ_y (μ)	E (GPa)	f_y (MPa)	ϵ_y (μ)	E (GPa)
1	534	2738	195	538	2690	200	560	2814	199
2	553	2821	196	556	2780	200	577	2885	200
3	582	2839	205	577	2914	198	595	2975	200
Average	556.3	2799	198.7	557	2795	199.3	577.3	2891	199.7
SD	19.74	47.14	4.50	15.94	0.00	0.94	14.29	47.14	0.47

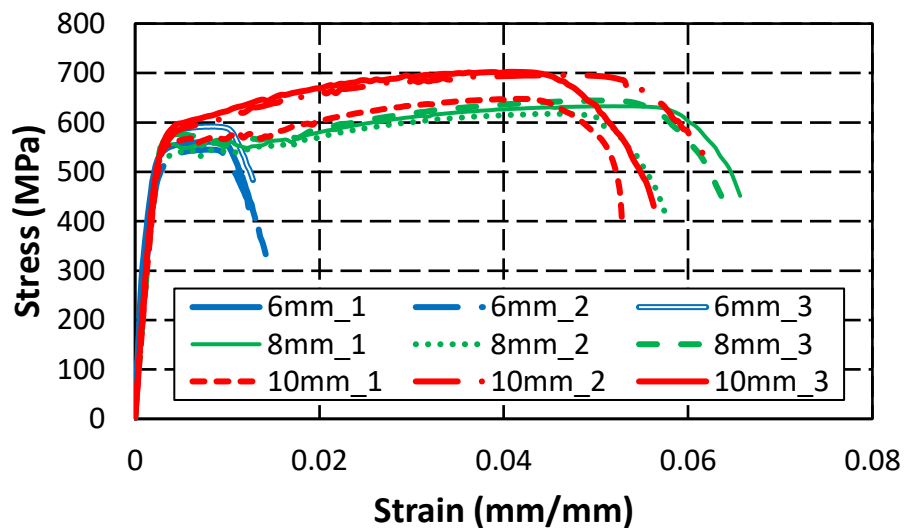


Figure 67: Stress versus strain curve for deformed bars.



Figure 68: Tested stirrups samples.

5.2.2.3. Strands. Lastly, the 15.2 mm 7-wires strands were tested to determine the mechanical properties of the steel. The cross-sectional area is 140 mm². Note that these strands were used to reinforce the beams in flexure. According to the beams' designs, the yield of the strands is never to be reached, nevertheless the mechanical properties of the strands are reported in Table 10 and Figure 69. To determine the yield strength of the steel strands, the 0.2% offset method was used. The yield strength of the strands used had a nominal value of 1680 MPa and an average actual value of 1711 MPa. The ultimate strength of the strands averaged approximately 1906 MPa, corresponding to an ultimate strain ranging between 0.03 to 0.055. Figure 70 shows a sample of the tested strands.

Table 10: Summary of strands steel test.

Sample \ d _b	15.2 mm Diam. Strand		
	f _y (MPa)	ε _y (μ)	E (GPa)
1	1694	9200	195
2	1735	9400	198
3	1703	9200	196
Average	1711	9267	196.3
SD	17.59	94.28	1.25

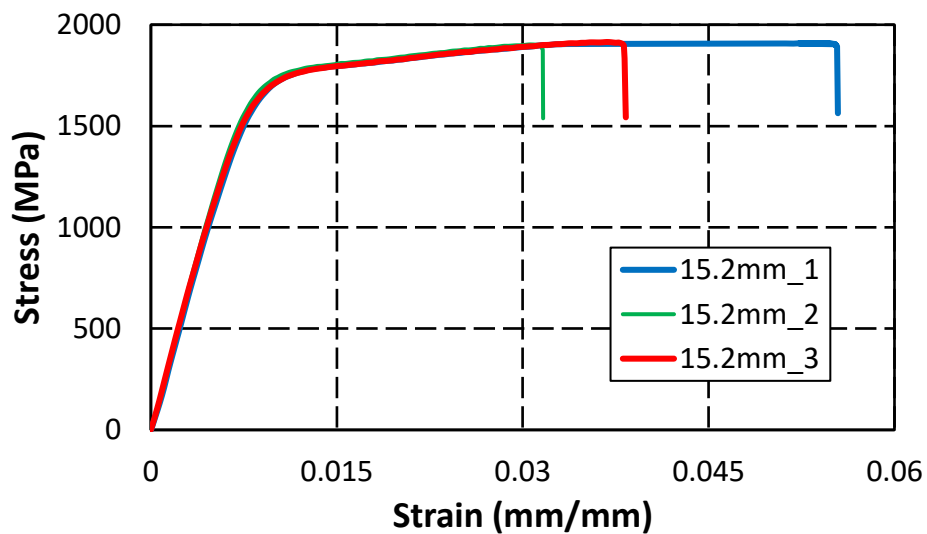


Figure 69: Stress versus strain curve for strands.



Figure 70: Tested strands samples.

5.3. Laboratory Work

In this section, the stages followed in constructing the beam specimens are discussed. The work is divided into tasks that are performed in part at the AUS Materials and Structures laboratory, and in part at the Emirates Stones precast concrete factory in Sharjah.

5.3.1. Bending bench. The biggest challenge of this study is to prepare the reinforcement made up of WWF because a mechanism is needed to bend a 2 m long sheet in the shape of a steel cage. In a previous senior design project, the device shown in Figure 71 was used, but the resulting steel cage was not uniform leading to deviations in the clear concrete cover on reinforcement. Therefore, another mechanism that is inspired by an apparatus in the manufacturing lab at AUS, shown in Figure 72, is developed. Using a table bench, heavy duty hinges, structural steel angles, and steel pipes, a WWF sheet bending equipment is constructed at the AUS Materials and Structures laboratory, as shown in Figure 73. Figure 74 shows the process of manufacturing the bending bench. Holes are then drilled through the apparatus to allow fixing the WWF steel cage to it using bolts and nuts. The final product is demonstrated in action in Figure 75.

5.3.2. Specimen fabrication. The process of preparing the test specimens was split into two parts. The first part that consists of constructing the steel cages from

WWF sheets is performed at AUS Materials and Structures laboratory. The other part that includes making the formwork, erecting the control beams with stirrups, placement of flexural steel, attaching strain gauges to the steel cages, concrete casting and curing is performed at the Emirates Stones precast concrete plant in Sharjah. Once cured, the beams, cubes and cylinders were transported by a truck to the AUS Materials and Structures laboratory. The sequence of this work is summarized in Figure 76 through Figure 80.



Figure 71: Preparing the WWF cages using the old method.



Figure 72: A metal brake machine used to bend thin metal sheets.



Figure 73: Parts used in the assembly.



Figure 74: Manufacturing process.



Figure 75: Preparing the WWF cages using the new method.



Figure 76: Preparing WWF steel cages using bending bench.



Figure 77: Attaching strain gauges to steel cages.



Figure 78: Formwork prepared on top of the vibrating bench.



Figure 79: Casting of beams, cubes and cylinders specimens.



Figure 80: Curing of demolded specimens.

5.3.3. Finishing of specimens. Following their arrival at AUS, the beams were painted on one side with a double layer of white paint to make it easier to track cracks during testing. Gridlines were also drawn on the face of the beam to identify the location the cracks. Figure 81 displays the process of painting and gridline drawing. A typical finished beam ready for placement in the UTM is shown in Figure 82. A beam ready for testing is presented in Figure 83.



Figure 81: Painting and constructing gridlines process.



Figure 82: Typical finished beam.



Figure 83: Typical testing setup.

Chapter 6. Experimental Results

In this chapter, results of the experimental testing program are presented in the form of load-deflection, load-strain, and load-crack width relationships. Such findings are obtained from the UTM, strain gauge and LVDT records. Analysis of the results will follow in the next chapter.

6.1. Introduction

The experimental work consists of 3 groups of beams that are tested to study the shear behavior of concrete beams transversely reinforced with WWF, in place of stirrups. All beams are heavily reinforced for flexure with 15.2 mm diameter strands, without prestressing, to preclude flexural failure. This type of longitudinal reinforcement is selected in place of conventional rebars in order to reduce the area of steel since longitudinal steel can contribute to shear strength by dowel action. Each group consists of 4 beams reinforced with WWF cages that are compared to 2 control beams reinforced with conventional rebar cages and 1 beam with no shear reinforcement used to quantify the concrete shear strength contribution. The transverse reinforcement (i.e. stirrups) in the 2 control beams is designed based on an equivalent transverse (i.e. vertical) steel reinforcement ratio criteria with consideration of the difference in nominal yield strength between the WWF and stirrups, as shown below. This equivalency is carried out in order to ensure fair comparison between the two different reinforcement schemes with regard to vertical steel. In addition, Groups 1 and 2 have an additional control beam, in which the number of stirrups is based on the total volume of steel of both the vertical and horizontal wires in the corresponding WWF cage, as presented below. This equivalency is carried out in order to ensure fair comparison between the total steel in the WWF and stirrups, with consideration of the differences in yield strength.

In order to capture the full response of the beams beyond the ultimate strength, a displacement-controlled loading is adopted by the UTM at a rate of 1 mm/minute. For the transversely reinforced beams, the duration each test varied roughly between 10-35 min. In this study, the failure criterion is defined as a drop of 30% of ultimate load on the descending part of the load-deflection curve. Beam deflection of each beam specimen is monitored at the location where the load is applied. All specimens were monitored for average crack widths in regions located in the vicinity of high moment

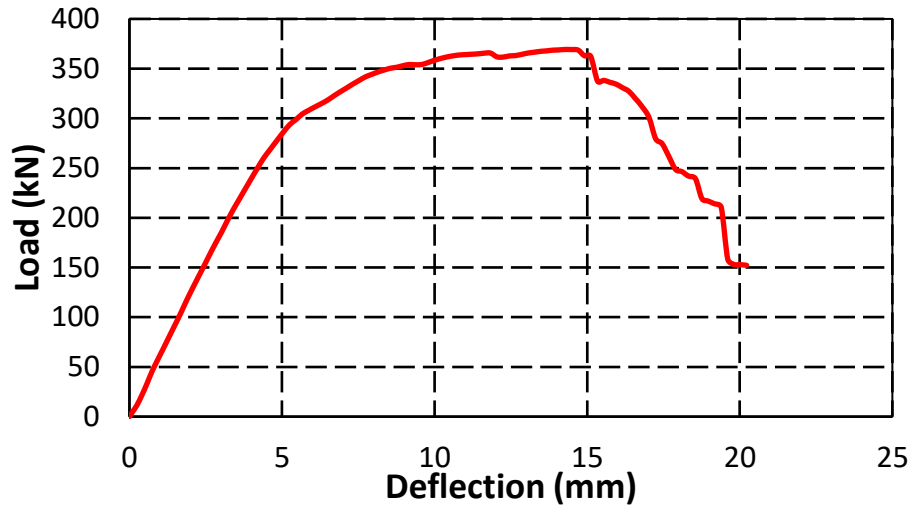
and low shear (lowest shear resistance area), using LVDTs inclined at 40 degrees. In addition, strain gauges were installed on the transverse steel at 75 mm, 225 mm, 375 mm, 525 mm, and 675 mm from the loading point to monitor the strain in the reinforcement and check the potential of yielding. Table 11 summarizes the beam identification and details of the tested specimens. The load versus deflection, load versus strain, and load versus average crack width curves for the specimens are presented here, and will be analyzed in detail in the next chapter with regards to ultimate shear strength, stiffness, ductility and residual strength.

Table 11: Beams details and identification scheme.

Group Detail	Serial Number	Beam ID.	Reinforcement Type	Diameter (mm)	Spacing (mm)
Group 1 L=1700mm a/h=2.5 f _c =35MPa	1	W-4-25-2.5-35	WWF	4	25
	2	W-6-50-2.5-35	WWF	6	50
	3	W-8-100-2.5-35	WWF	8	100
	4	S-8-91.5-2.5-35	Stirrup	8	91.5
	5	W-4-50-2.5-35	WWF	4	50
	6	S-6-103.5-2.5-35	Stirrup	6	103.5
	7	S-10-73-2.5-35	Stirrup	10	73
	8	N-2.5-35	None	N. A.	N. A.
Group 2 L=1850mm a/h=3.0 f _c =35MPa	9	W-4-25-3.0-35	WWF	4	25
	10	W-6-50-3.0-35	WWF	6	50
	11	W-8-100-3.0-35	WWF	8	100
	12	S-8-91.5-3.0-35	Stirrup	8	91.5
	13	W-4-50-3.0-35	WWF	4	50
	14	S-6-103.5-3.0-35	Stirrup	6	103.5
	15	S-10-73-3.0-35	Stirrup	10	73
	16	N-3.0-35	None	N. A.	N. A.
Group 3 L=1850mm a/h=3.0 f _c =30MPa	17	W-4-25-3.0-30	WWF	4	25
	18	W-6-50-3.0-30	WWF	6	50
	19	W-8-100-3.0-30	WWF	8	100
	20	S-8-91.5-3.0-30	Stirrup	8	91.5
	21	W-4-50-3.0-30	WWF	4	50
	22	S-6-103.5-3.0-30	Stirrup	6	103.5
	23	N-3.0-30	None	N. A.	N. A.

6.2. Load-Deflection Relationships

In this section, load versus deflection curves are reported in Figure 84 to Figure 106, along with photos of each specimen at the pre-cracking stage, post-cracking stage and ultimate stage. The first glance at the performance of the WWF reinforced beams against the conventionally stirrup reinforced beams show promising potential for the usage of WWF. Similar ultimate strength behavior, failure modes, and crack patterns were witnessed between WWF beams and stirrups beams. It is worth mentioning that despite all efforts to ensure shear failures in the tested specimens, there were 2 beams that exhibited shear-flexure failure through crushing of the concrete accompanied with inclined shear cracks, and they are “W-6-50-2.5-35” and “S-10-73-3.0-35”. Note that one of these beams have been heavily reinforced in shear, and they correspond to replacing both vertical and horizontal wires present in WWF cage with equivalent conventional stirrups. Nevertheless, the findings of the shear ultimate capacity of all beams were consistent where specimens with higher compressive strength or reinforcing ratios yielded higher ultimate capacities. As anticipated, all specimens exhibited a constant stiffness up until yielding is reached. It was then followed by a reduction in stiffness where the load carrying capacity stayed constant or decreased slightly but the deflection of the beams continued to increase till the ultimate level was reached where the load carrying capacity started to decline rapidly. It is also observed that beams reinforced with rectilinear stirrups shows double peaks in the load-deflection curves, opposing a single peak in the WWF reinforced beams; however, few WWF beams exhibited a double peak behavior. In some cases, the second peak would be higher and in others it would be lower. The cracking pattern of almost all specimens was similar, where small vertical flexure cracks initiated which then propagated into inclined shear cracks as the load increased. Naturally, specimens with lower reinforcement ratio experienced first crack at lower load than specimens with higher reinforcement. Beams with no shear reinforcement exhibited a change of stiffness while the load is applied, where a change is noticed in the slope of the ascending part of the load-deflection curve. An extensive study on the performance of WWF beams against the stirrups beam, effect of shear span-to-depth ratios, effect of compressive strength, effect of mesh opening, etc. will be presented in the next chapter.



(a) Load-deflection output



(b) Pre-cracking stage

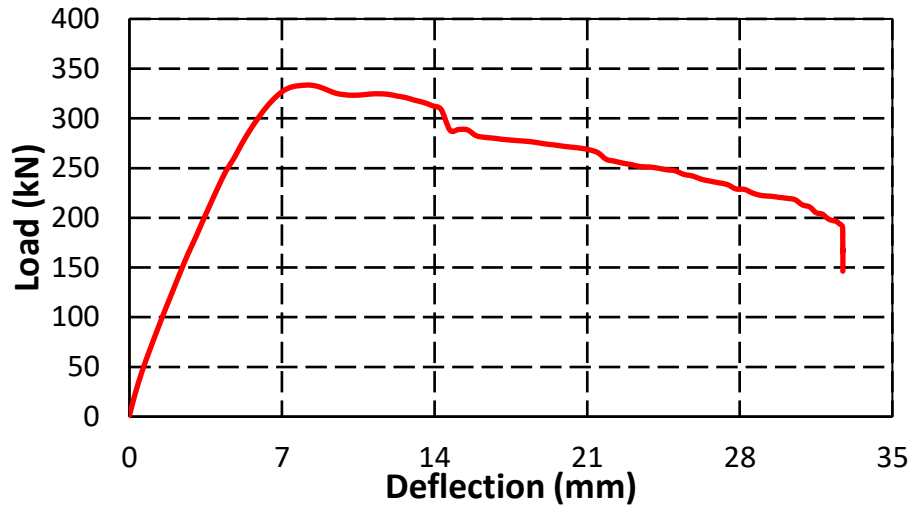


(c) Post-cracking stage



(d) At ultimate stage

Figure 84: Experimental details of beam W-4-25-2.5-35



(a) Load-deflection output



(b) Pre-cracking stage

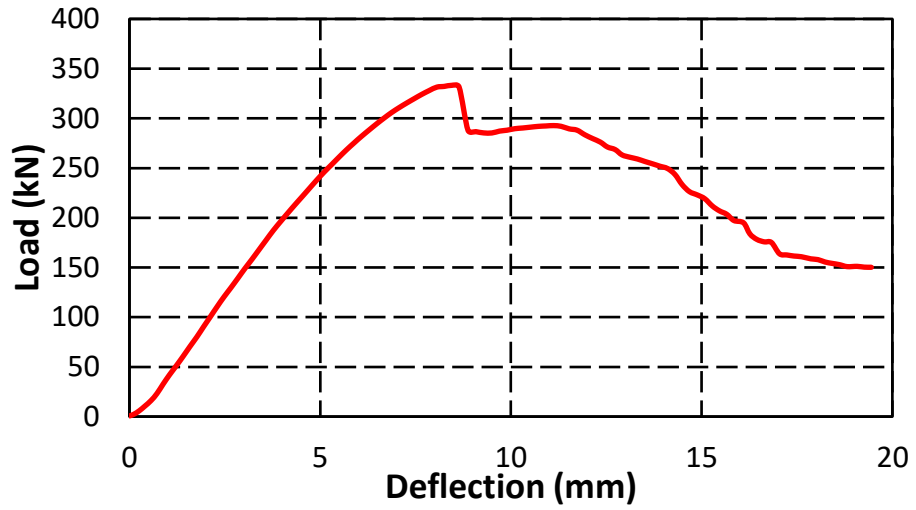


(c) Post-cracking stage



(d) At ultimate stage

Figure 85: Experimental details of beam W-6-50-2.5-35



(a) Load-deflection output



(b) Pre-cracking stage

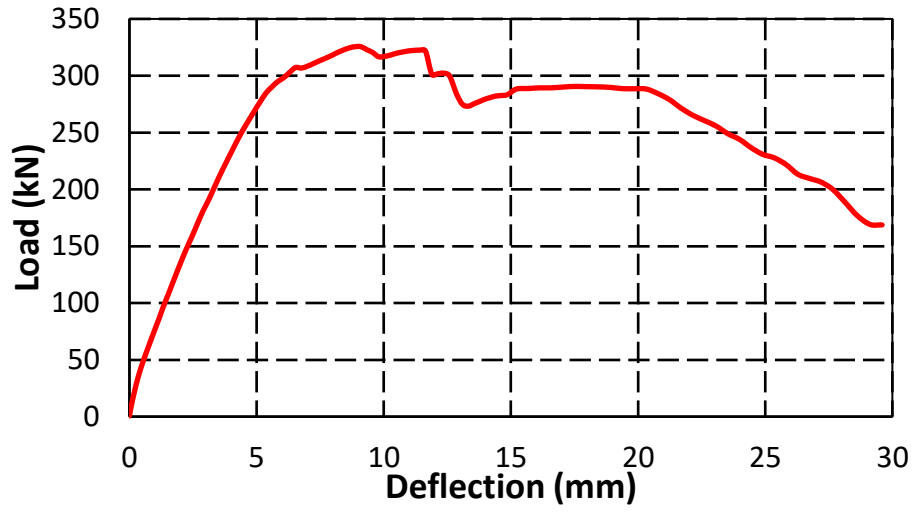


(c) Post-cracking stage



(d) At ultimate stage

Figure 86: Experimental details of beam W-8-100-2.5-35



(a) Load versus deflection curve



(b) Pre-cracking stage

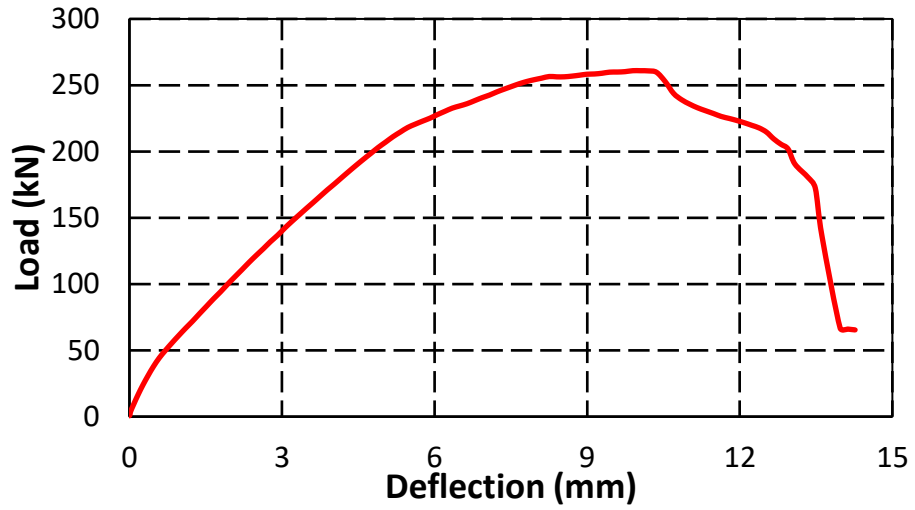


(c) Post-cracking stage



(d) At ultimate stage

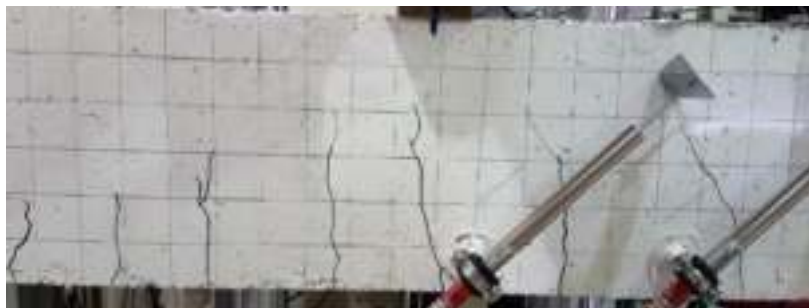
Figure 87: Experimental details of beam S-8-91.5-2.5-35



(a) Load versus deflection curve



(b) Pre-cracking stage

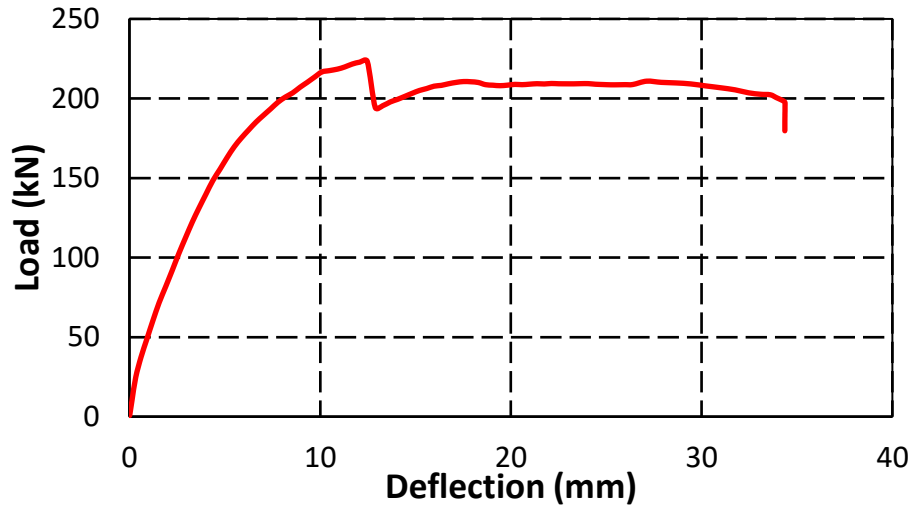


(c) Post-cracking stage



(d) At ultimate stage

Figure 88: Experimental details of beam W-4-50-2.5-35



(a) Load versus deflection curve



(b) Pre-cracking stage

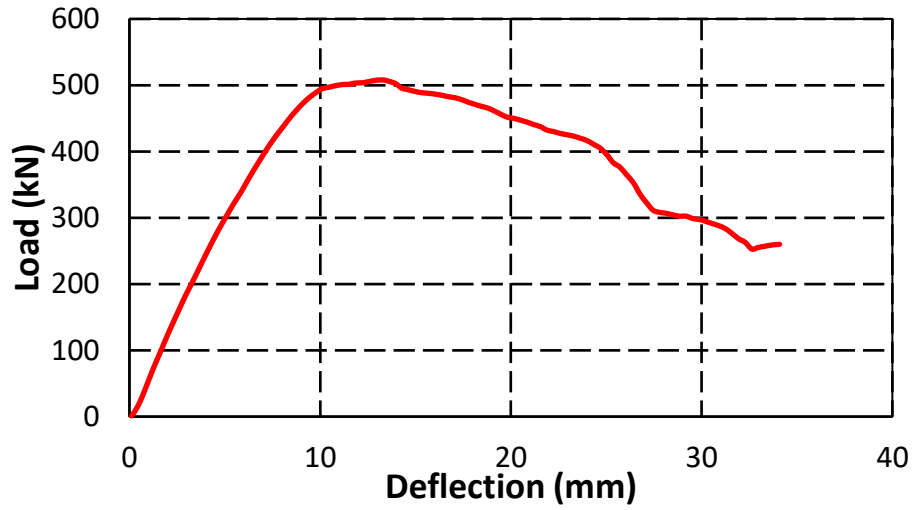


(c) Post-cracking stage



(d) At ultimate stage

Figure 89: Experimental details of beam S-6-103.5-2.5-35



(a) Load versus deflection curve



(b) Pre-cracking stage

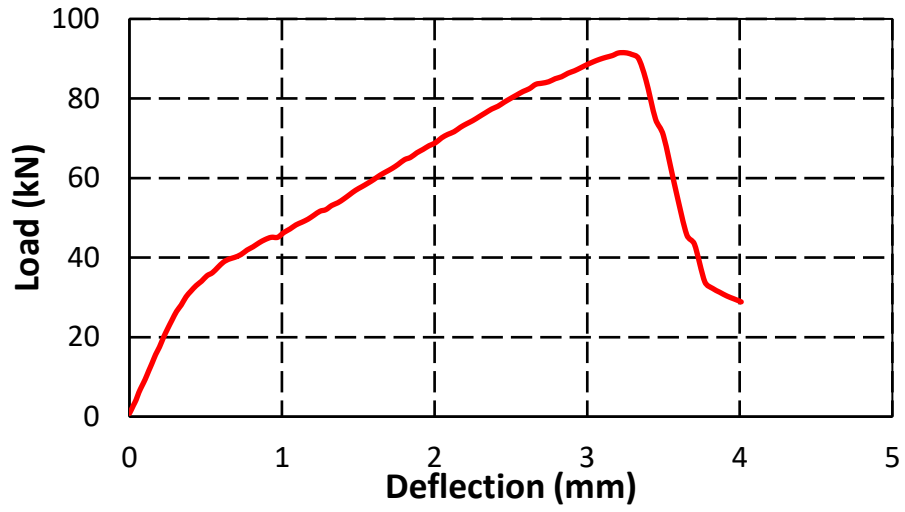


(c) Post-cracking stage



(d) At ultimate stage

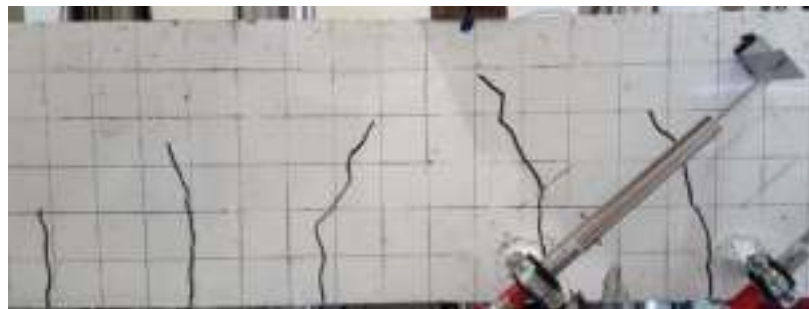
Figure 90: Experimental details of beam S-10-73-2.5-35



(a) Load versus deflection curve



(b) Pre-cracking stage

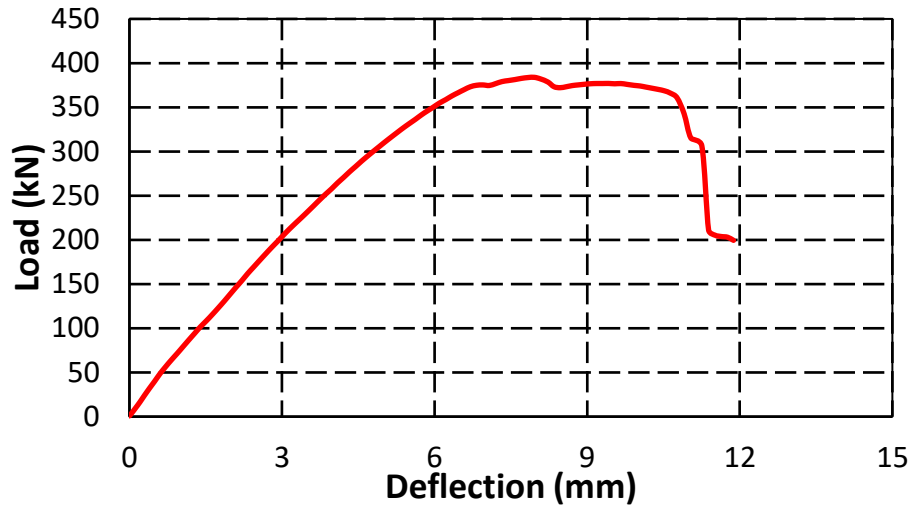


(c) Post-cracking stage



(d) At ultimate stage

Figure 91: Experimental details of beam N-2.5-35



(a) Load versus deflection curve



(b) Pre-cracking stage

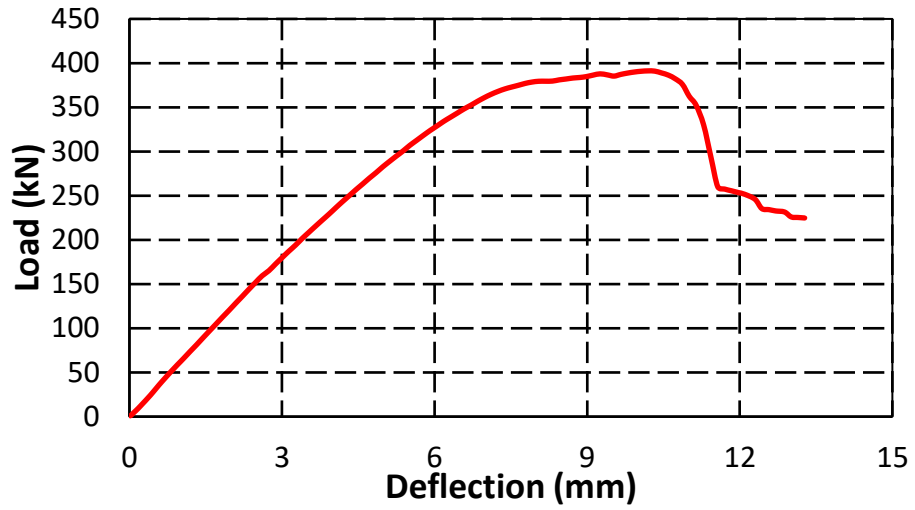


(c) Post-cracking stage



(d) At ultimate stage

Figure 92: Experimental details of beam W-4-25-3.0-35



(a) Load versus deflection curve



(b) Pre-cracking stage

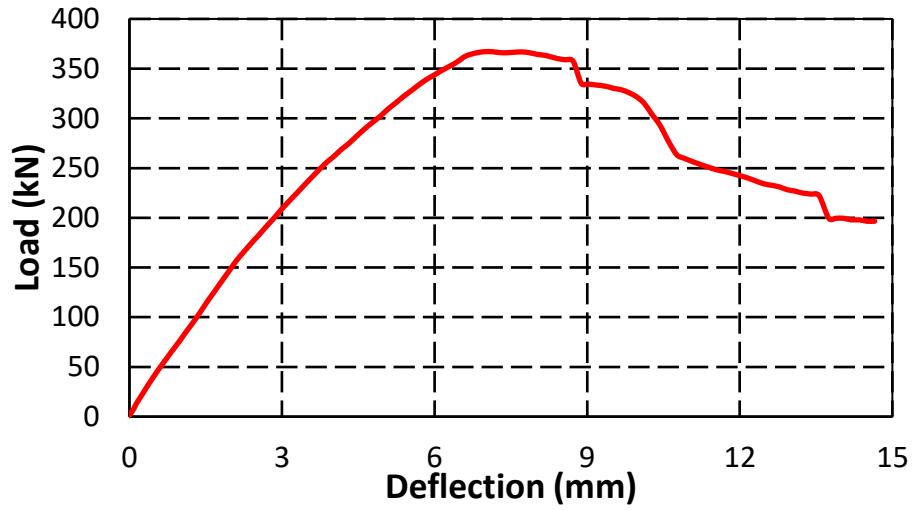


(c) Post-cracking stage



(d) At ultimate stage

Figure 93: Experimental details of beam W-6-50-3.0-35



(a) Load versus deflection curve



(b) Pre-cracking stage

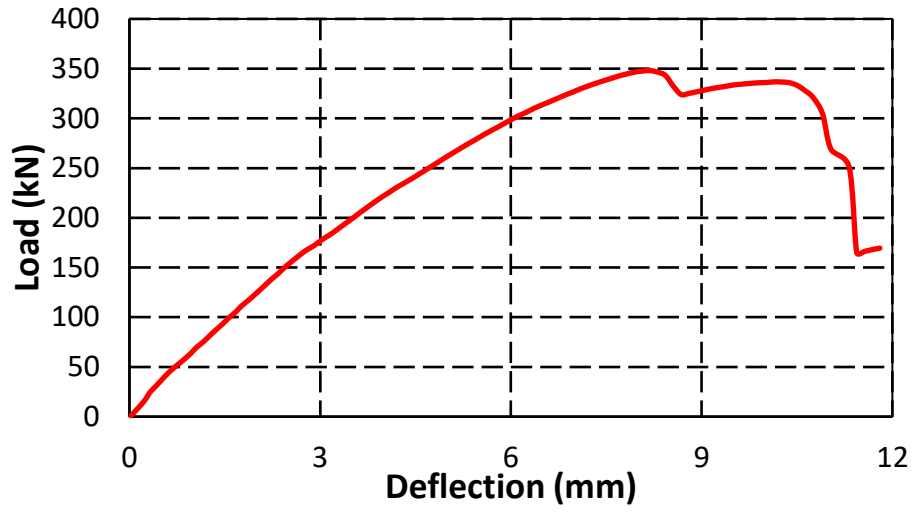


(c) Post-cracking stage



(d) At ultimate stage

Figure 94: Experimental details of beam W-8-100-3.0-35



(a) Load versus deflection curve



(b) Pre-cracking stage

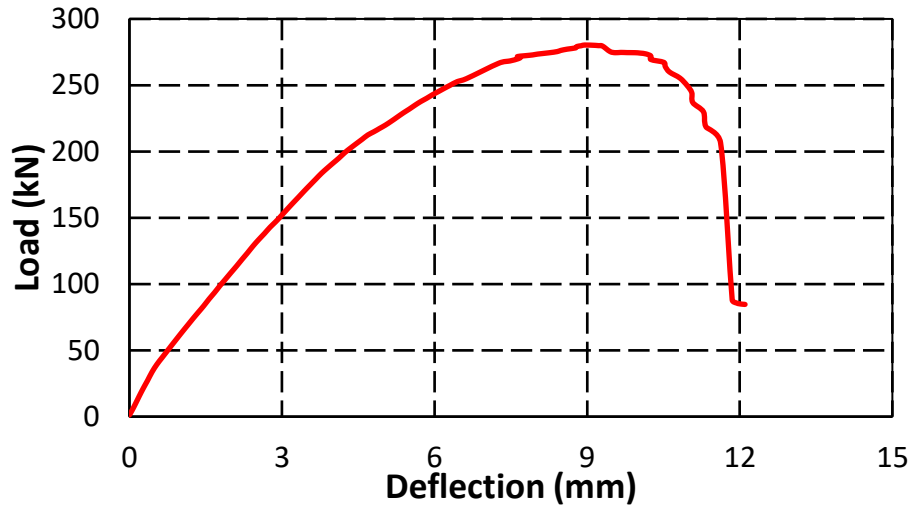


(c) Post-cracking stage



(d) At ultimate stage

Figure 95: Experimental details of beam S-8-91.5-3.0-35



(a) Load versus deflection curve



(b) Pre-cracking stage

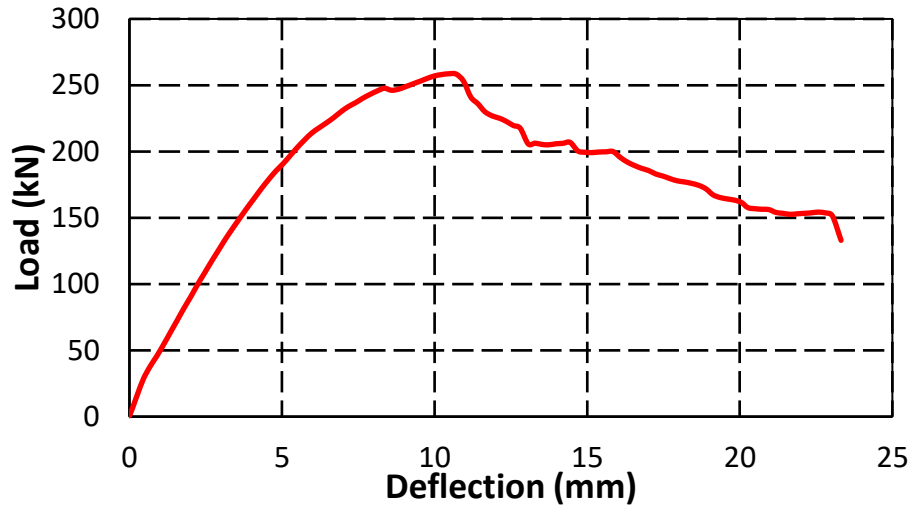


(c) Post-cracking stage



(d) At ultimate stage

Figure 96: Experimental details of beam W-4-50-3.0-35



(a) Load versus deflection curve



(b) Pre-cracking stage

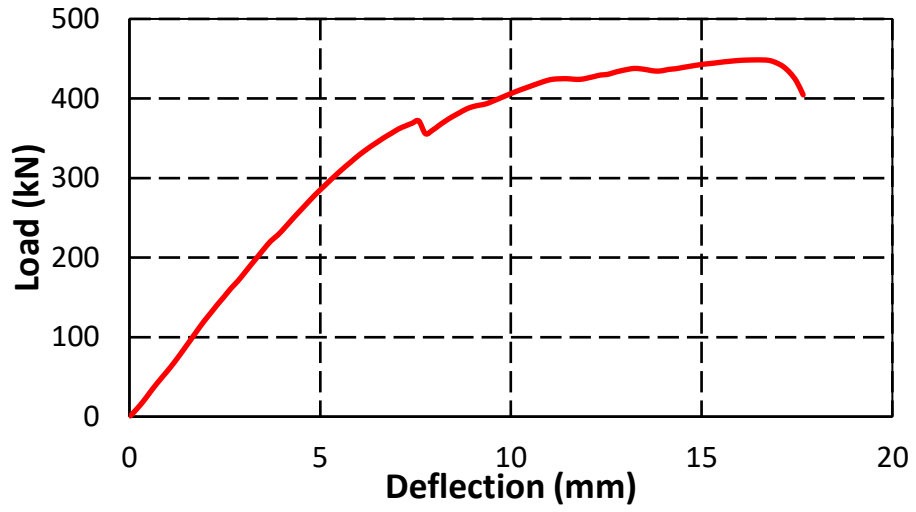


(c) Post-cracking stage



(d) At ultimate stage

Figure 97: Experimental details of beam S-6-103.5-3.0-35



(a) Load versus deflection curve



(b) Pre-cracking stage

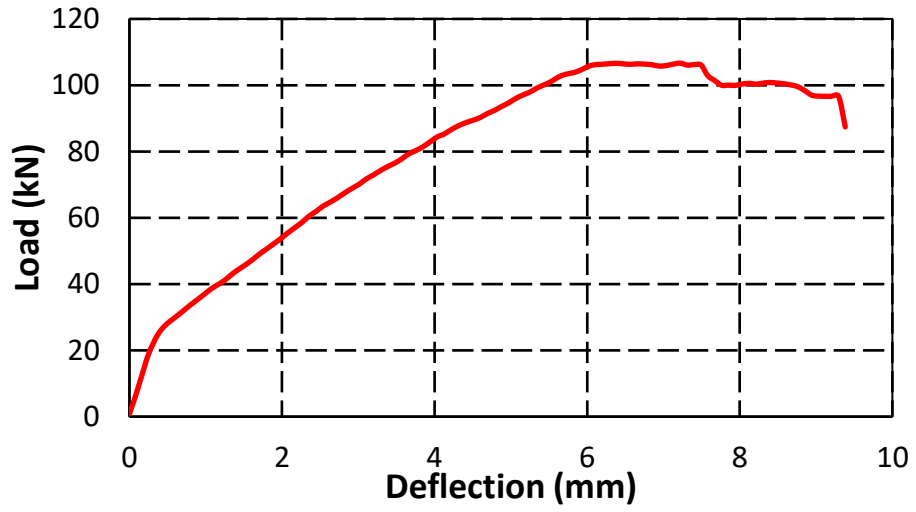


(c) Post-cracking stage



(d) At ultimate stage

Figure 98: Experimental details of beam S-10-73-3.0-35



(a) Load versus deflection curve



(b) Pre-cracking stage

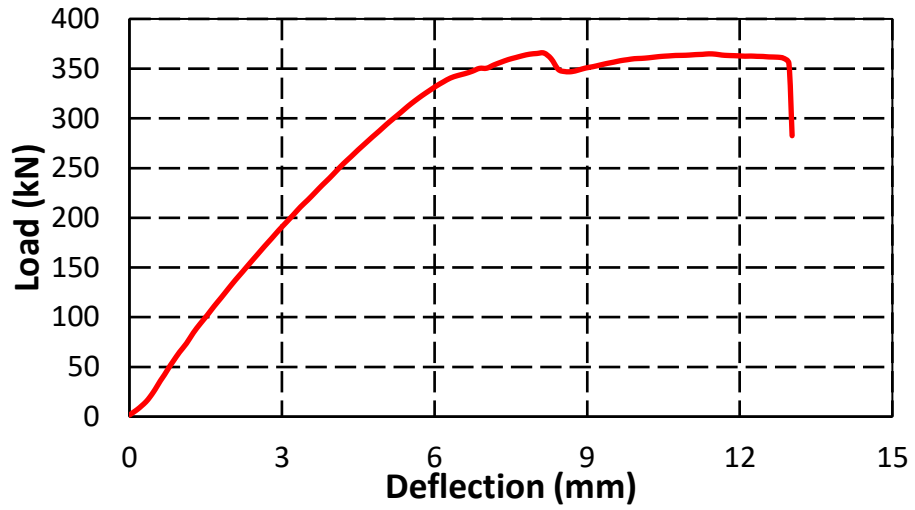


(c) Post-cracking stage



(d) At ultimate stage

Figure 99: Experimental details of beam N-3.0-35



(a) Load versus deflection curve



(b) Pre-cracking stage

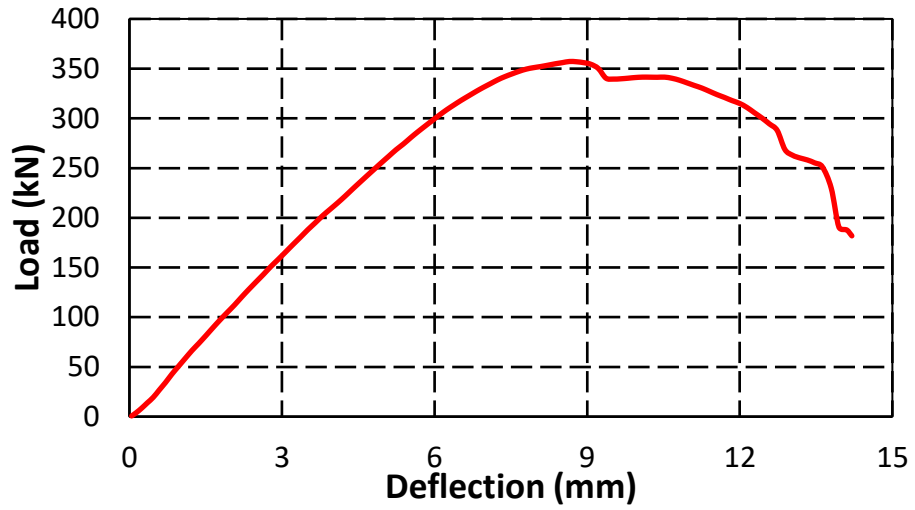


(c) Post-cracking stage



(d) At ultimate stage

Figure 100: Experimental details of beam W-4-25-3.0-30



(a) Load versus deflection curve



(b) Pre-cracking stage

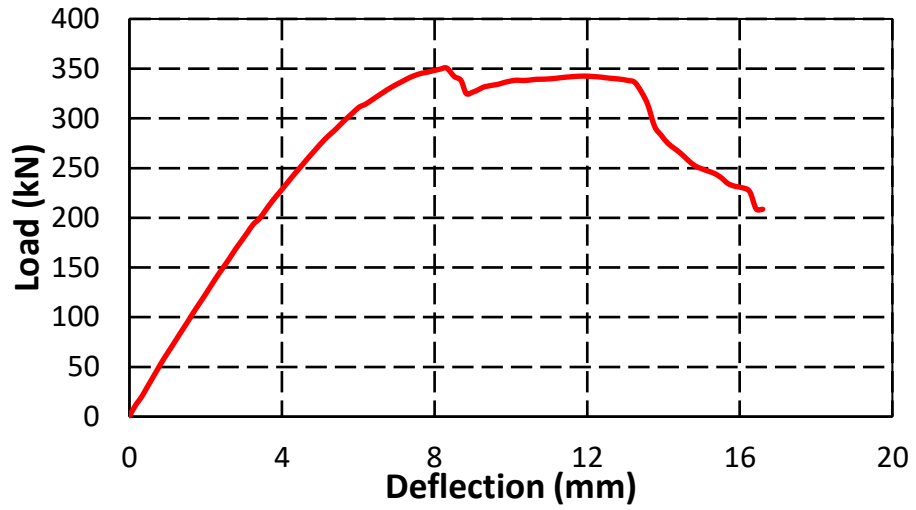


(c) Post-cracking stage



(d) At ultimate stage

Figure 101: Experimental details of beam W-6-50-3.0-30
106



(a) Load versus deflection curve



(b) Pre-cracking stage

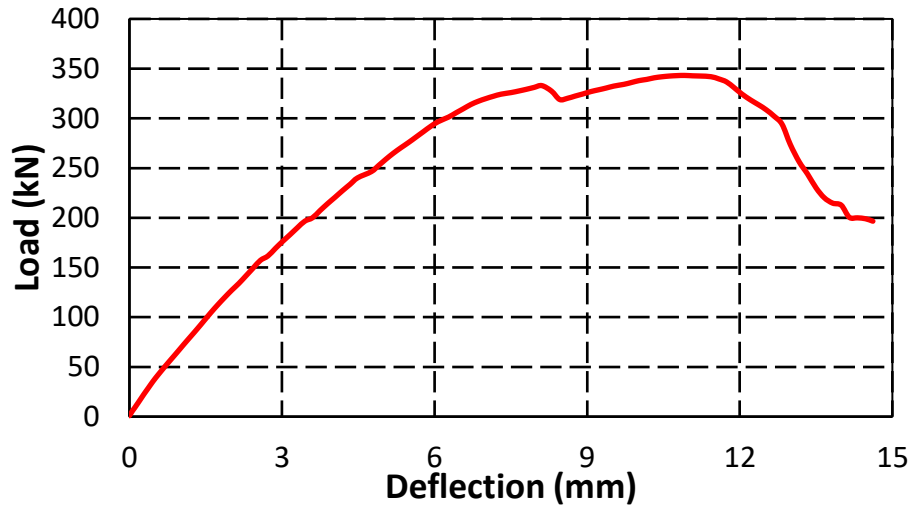


(c) Post-cracking stage



(d) At ultimate stage

Figure 102: Experimental details of beam W-8-100-3.0-30



(a) Load versus deflection curve



(b) Pre-cracking stage

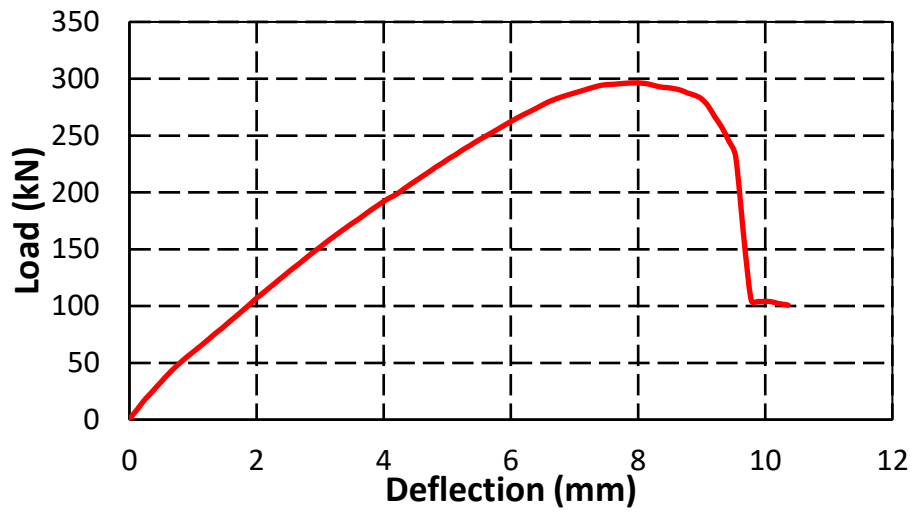


(c) Post-cracking stage



(d) At ultimate stage

Figure 103: Experimental details of beam S-8-91.5-3.0-30
108



(a) Load versus deflection curve



(b) Pre-cracking stage

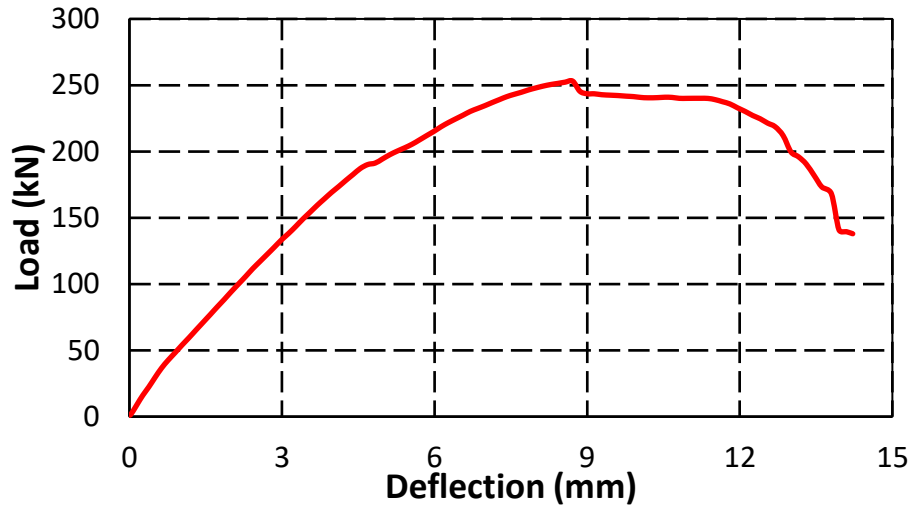


(c) Post-cracking stage



(d) At ultimate stage

Figure 104: Experimental details of beam W-4-50-3.0-30



(a) Load versus deflection curve



(b) Pre-cracking stage

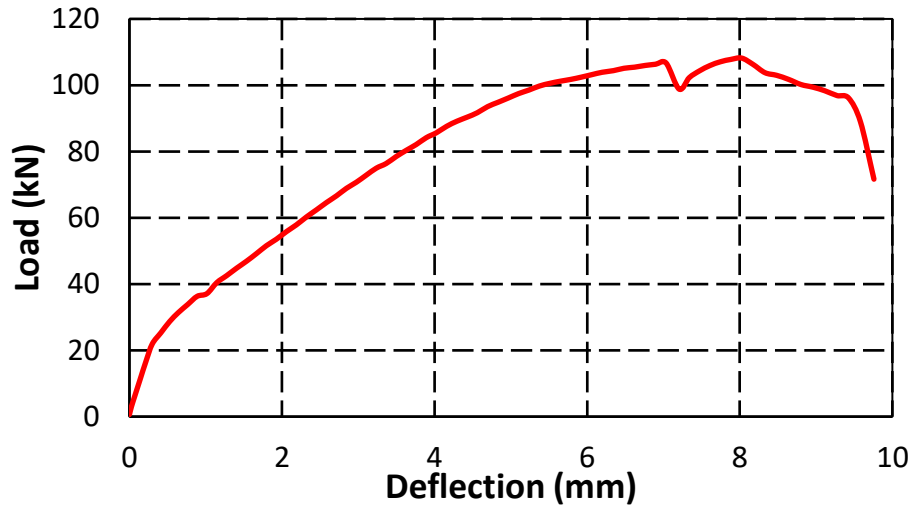


(c) Post-cracking stage



(d) At ultimate stage

Figure 105: Experimental details of beam S-6-103.5-3.0-30



(a) Load versus deflection curve



(b) Pre-cracking stage



(c) Post-cracking stage



(d) At ultimate stage

Figure 106: Experimental details of beam N-3.0-30

6.3. Shear Force

In order to determine the ultimate shear capacity of the tested specimens, the maximum load recorded by the UTM needs to be changed to shear using statics. Beams in Group 1 have a beam span equal to 1700 mm corresponding to shear span-to-depth ratio $a/h=2.5$ and beams in Groups 2 and 3 have a beam span equal to 1900 mm that corresponds to shear span-to-depth ratio $a/h=3.0$. The shear and moment diagrams of beams within Group 1 is shown in Figure 107, while the shear and moment diagrams of beams belonging to Groups 2 and 3 are presented in Figure 108. Following common practice, the self-weight of the beam (2.7-3.0 kN) is not considered in the analysis because it is negligibly small compared the ultimate load (91.5-508 kN). Table 12 summarizes the maximum recorded values of load and corresponding shear of each beam. The beams that have the sign “*” next to them correspond to the beams that failed in flexure instead of shear; therefore, the observed strength of these beams represent the minimum shear strength. Note that the ACI 318-14 code addresses the shear span to effective depth of the longitudinal steel reinforcement, a/d , instead of a/h . This ratio is different for the various cross-sections even within the Group since d depends not only on the clear concrete cover but also on the diameter of the transverse and longitudinal steel reinforcement. The ACI Committee 318 [5], identifies beams having shear span to effective depth ratios (a/d) less than 2 as deep beams. Another criterion for defining beams as deep is clear span-to-depth ratio (L/h) less than 4. Both criteria recognize the beams of this study as shallow beams. The choice of unequal spans for the beam specimens was not only based on achieving the specified a/d ratio, but also to force the beams into failing in shear within a desired region, between the load and nearby support, since it is not practical to instrument the whole beam. While this has worked well for most of the tested beams, there were 2 (out of the 23) beams that failed within the non-instrumented region possibly due to nonideal conditions concerning the inherent concrete material properties, concrete placement procedures, steel cage workmanship, vibrations, and non-homogeneity of concrete.

6.4. Load-Strains Relationships

The purpose of using strain gauges on the transverse reinforcement is to monitor the behavior of the steel and to determine if the transverse reinforcement reaches the yielding point or remains in the elastic region during the test. While shear provisions in

design codes assume that the transverse steel yields, recent research [47] claims the opposite. Five strain gauges were placed vertically on the transverse steel reinforcement of each beam. The first strain gauge is positioned within the region of high shear at 75 mm away from the location of the load, with the remaining ones at increments of 150 mm from each other. Hence, the location of strain gauges from the point where the load

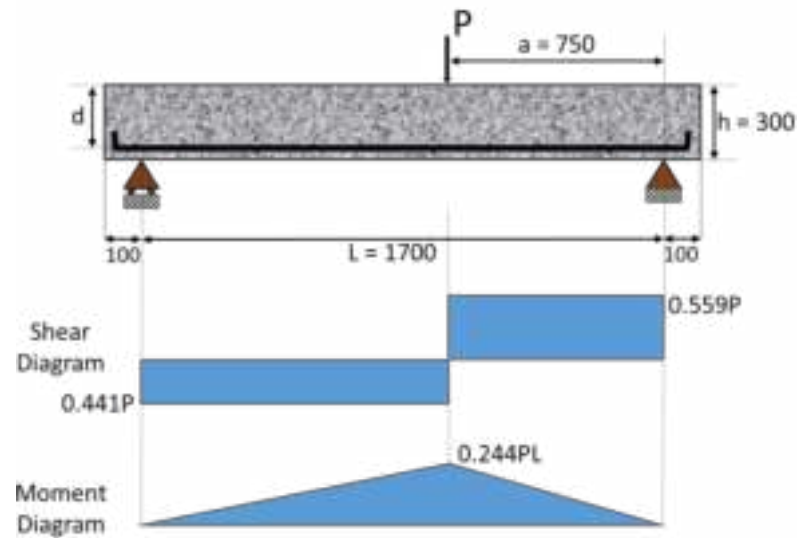


Figure 107: Shear-Moment diagram of beams with $a/h=2.5$.

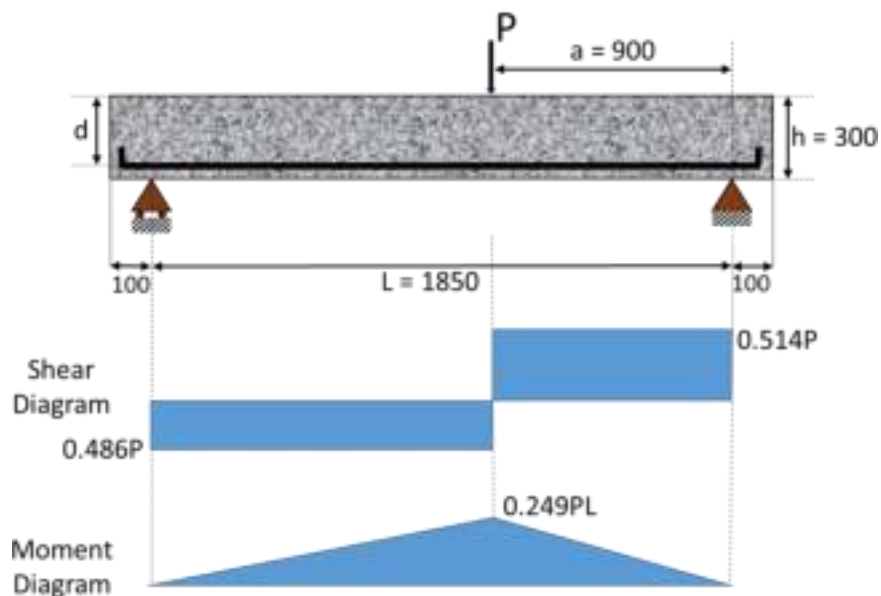


Figure 108: Shear-Moment diagram of beams with $a/h=3.0$.

Table 12: Maximum recorded values of load and shear.

Group	Beam ID.	a/d	Load (kN)	Shear (kN)
Group 1 $L = 1700\text{mm}$ $a/h = 2.5$ $f'_c = 35\text{MPa}$	W-4-25-2.5-35	2.93	369.29	206.37
	W-6-50-2.5-35	2.96	333.47	186.35
	W-8-100-2.5-35	2.98	333.21	186.21
	S-8-91.5-2.5-35	2.98	325.60	181.95
	W-4-50-2.5-35	2.85	260.97	145.84
	S-6-103.5-2.5-35*	2.87	223.35	124.81
	S-10-73-2.5-35	3.10	507.99	283.88
N-2.5-35	2.89	91.49	51.13	
Group 2 $L = 1850\text{mm}$ $a/h = 3.0$ $f'_c = 35\text{MPa}$	W-4-25-3.0-35	3.63	383.95	197.16
	W-6-50-3.0-35	3.66	391.24	200.91
	W-8-100-3.0-35	3.69	367.11	188.51
	S-8-91.5-3.0-35	3.69	348.10	178.75
	W-4-50-3.0-35	3.52	280.33	143.95
	S-6-103.5-3.0-35	3.55	258.66	132.82
	S-10-73-3.0-35*	3.72	448.52	230.32
N-3.0-35	3.37	106.66	54.77	
Group 3 $L = 1850\text{mm}$ $a/h = 3.0$ $f'_c = 30\text{MPa}$	W-4-25-3.0-30	3.63	365.69	187.79
	W-6-50-3.0-30	3.66	357.22	183.44
	W-8-100-3.0-30	3.69	350.58	180.03
	S-8-91.5-3.0-30	3.69	343.19	176.23
	W-4-50-3.0-30	3.52	296.40	152.20
	S-6-103.5-3.0-30	3.55	253.10	129.97
	N-3.0-30	3.44	108.20	55.56

* These beams failed in flexure.

is applied are 75 mm, 225 mm, 375 mm, 525 mm, and 675 mm, as shown in Figure 109. Since beams “N-2.5-35”, “N-3.0-35”, and “N-3.0-30” do not have any shear reinforcement, no strain gauges were used; therefore, no graphs on the subject are included for such specimens. Despite all efforts to protect the strain gauges during casting, demolding, curing, transportation, handling, and testing, few of the installed strain gauges were damaged or stopped recording during the tests. The unworkable strain gauges are omitted from the analysis. The relationship between load and strain in the transverse steel at various locations along the beams is plotted in Figure 110 to Figure 112. Note that the relevant ASTM standard on welded wire fabric [16] states

that the yield stress is the stress corresponding to a strain equal to 0.005 on the stress-strain. For stirrups, the strain corresponding to yield strength is taken 0.002828. In the load versus vertical steel strain diagrams, a vertical line representing the strain at yield is provided in order to examine whether the wires/stirrups have yielded during the test. Out of the 20 tested beams that contained transverse reinforcement, 11 beams had one or more wires/stirrups that reached the yielding point. Specifically, 6 out of the 8 stirrup reinforced beams had at least 1 instrumented stirrup reaching the yielding point, although the stirrups in the remaining 2 beams were very close to yielding. Further, 5 out of the 12 WWF reinforced beams had at least 1 instrumented vertical wire reaching the yielding point corresponding to 0.005 mm/mm strain. Careful examination of the strain gauge records of the WWF reinforced beams shows all but one of the beams had at least one wire reaching 90% of the yield strength. The results show that the yielding of the transverse reinforcement was reached around the ultimate load of the tested beams, but there was no consistency whether it was post peak or pre-peak. There was no noticeable trend regarding which wire or stirrup reached the yielding point with respect to the location of the load on the beam. For example, the wire that reached the yielded in beam “W-4-25-2.5-35” was at a distance of 225 mm from the point of applying the load, and before the ultimate load was reached. On the other hand, in beam “S-10-73-2.5-35” the stirrup placed at 525 from the point where the load is applied reached yielding, at the descending part of the graph post peak. The finding concerning the observation that not all transverse reinforcement reach yielding in beams failing in shear agrees with the recently published research of Russo et al. [47].

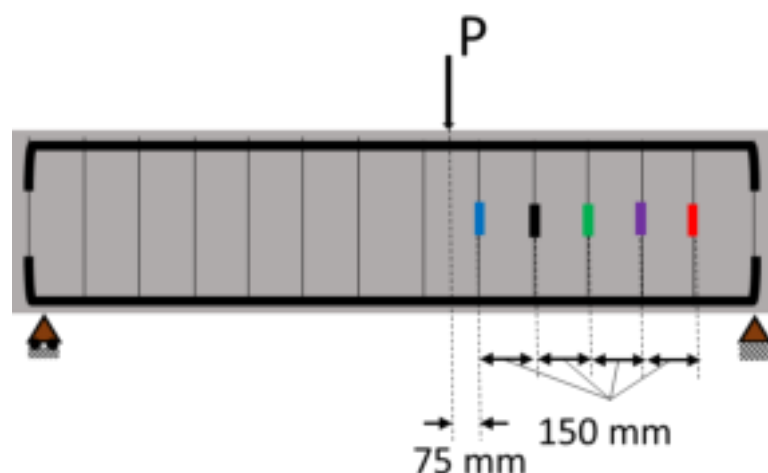


Figure 109: Placement of strain gauges.

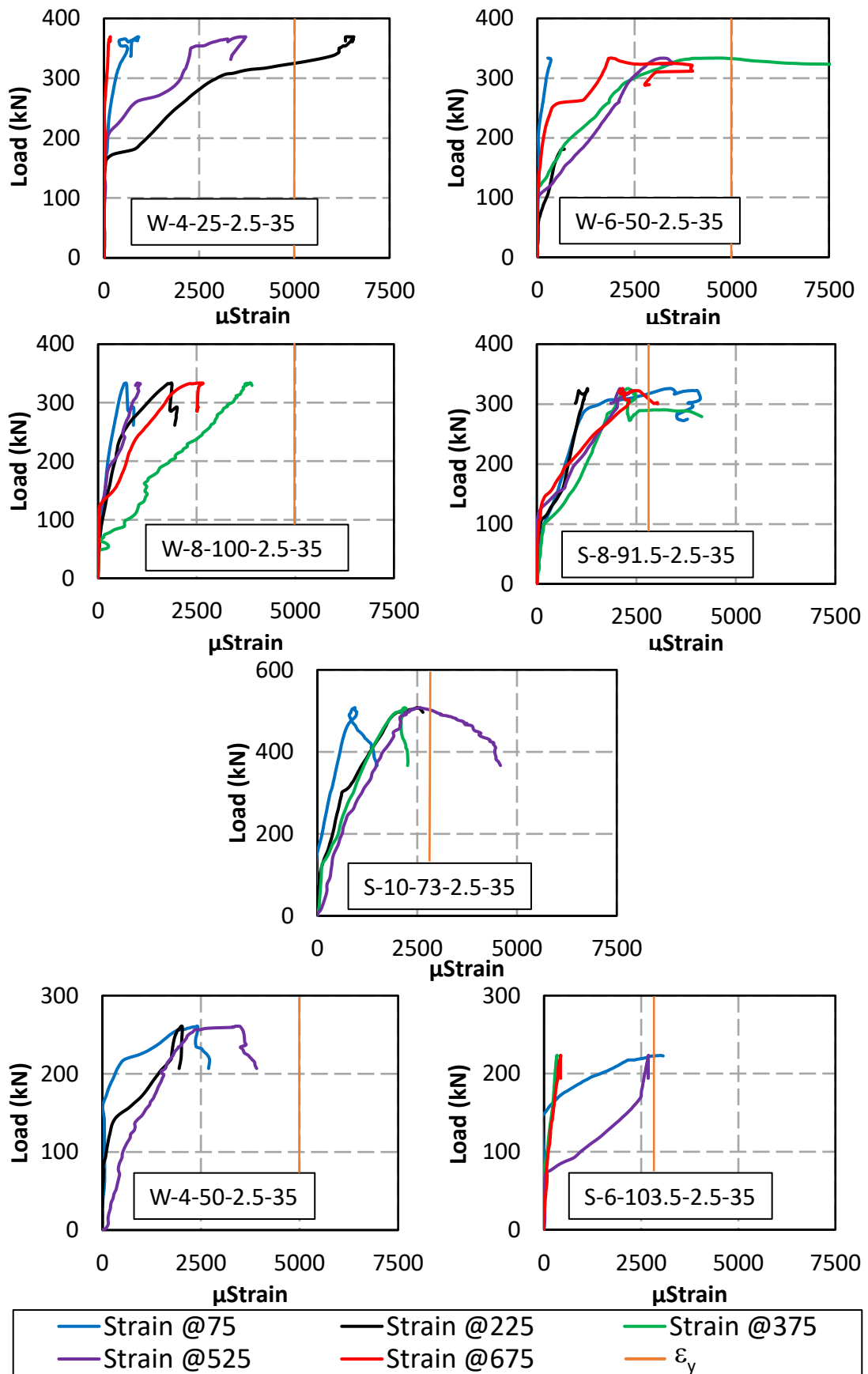


Figure 110: Load versus strain in transverse steel for beams of Group 1.

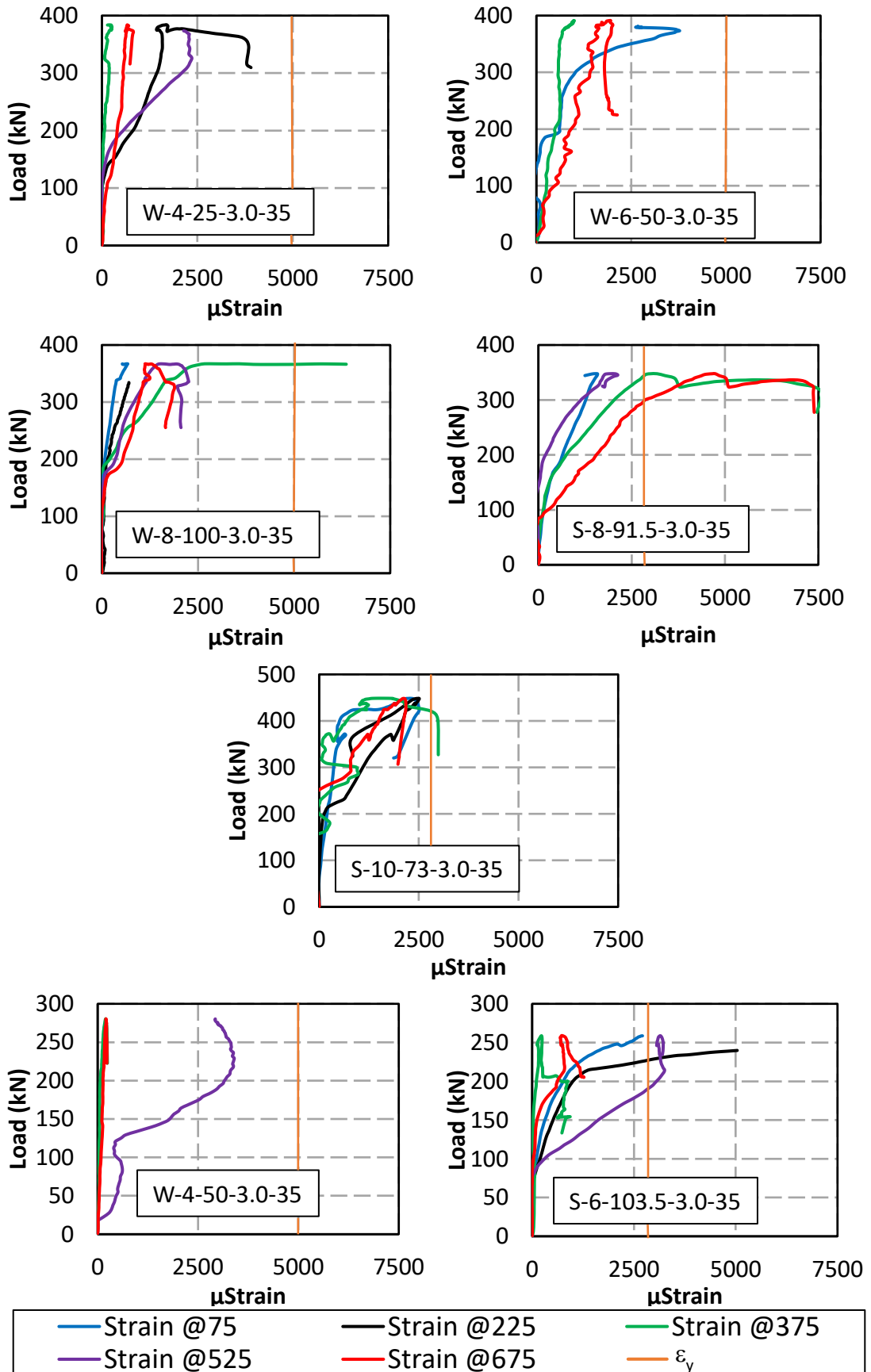


Figure 111: Load versus strain in transverse steel for beams of Group 2.

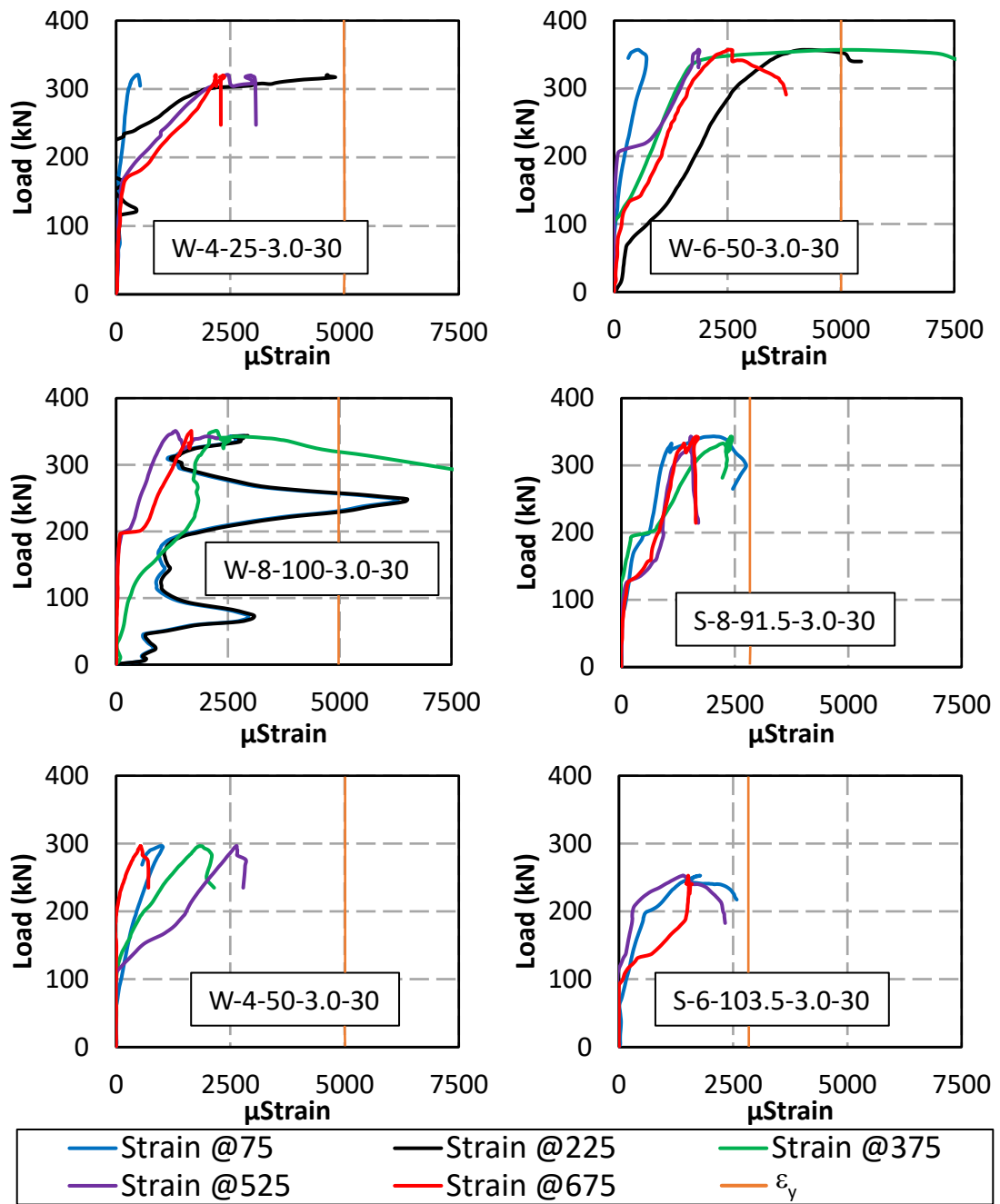


Figure 112: Load versus strain in transverse steel for beams of Group 3.

6.5. Load-Crack Width Relationships and Cracking Patterns

The average shear-crack width was measured using two LVDTs positioned on the concrete surface over a distance of 300 mm inclined at an angle of 40° as shown in Figure 113, where “LVDT1” refers to the LVDT closer to the point where the load is applied, and “LVDT2” refers to the one that is further. Since the actual location and inclination angle of the major shear cracks are very difficult to be determined prior to

the test, the LVDTs were often not exactly perpendicular to the shear cracks; hence the measured crack width only gives an idea about the crack size and opening and can be used for comparative purposes. Since the crack inclination and side-mounted LVDTs orientation are known, using simple trigonometric relationships one can determine the crack opening perpendicular to the crack, as shown in Figure 114. It is worth mentioning that some LVDTs fell off during testing because some of the cracks propagated towards the attached LVDT support mechanism.

The data obtained from the LVDTs indicates that the shear cracks start to form after some time from the start of the test, after development of the flexure cracks. Once the shear cracks started to appear, the average crack width begins to enlarge as the load increases. When the beam reaches its full capacity and the shear failure mechanism, represented by a diagonal tension failure, takes place, the measured average crack width between two points on the beam surface keeps widening as the beam gradually loses its resistance. The average crack width versus the applied load for some of the tested beams is shown in Figure 115 to Figure 117.

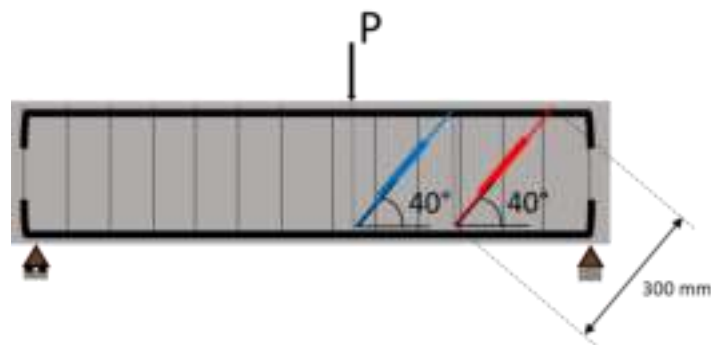


Figure 113: Placement of LVDTs.

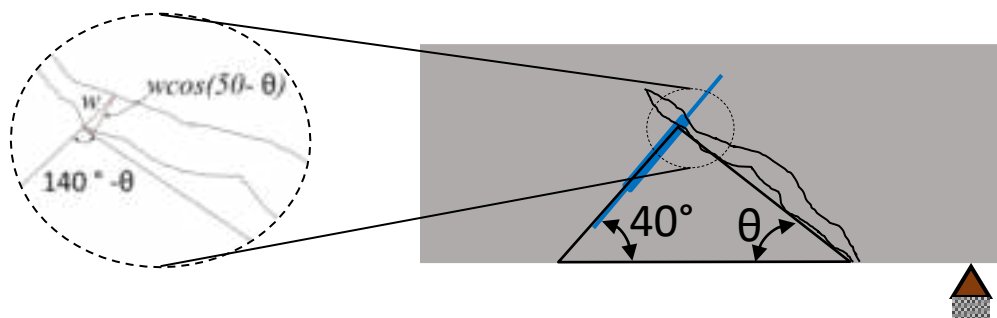


Figure 114: Adjustment of crack width.

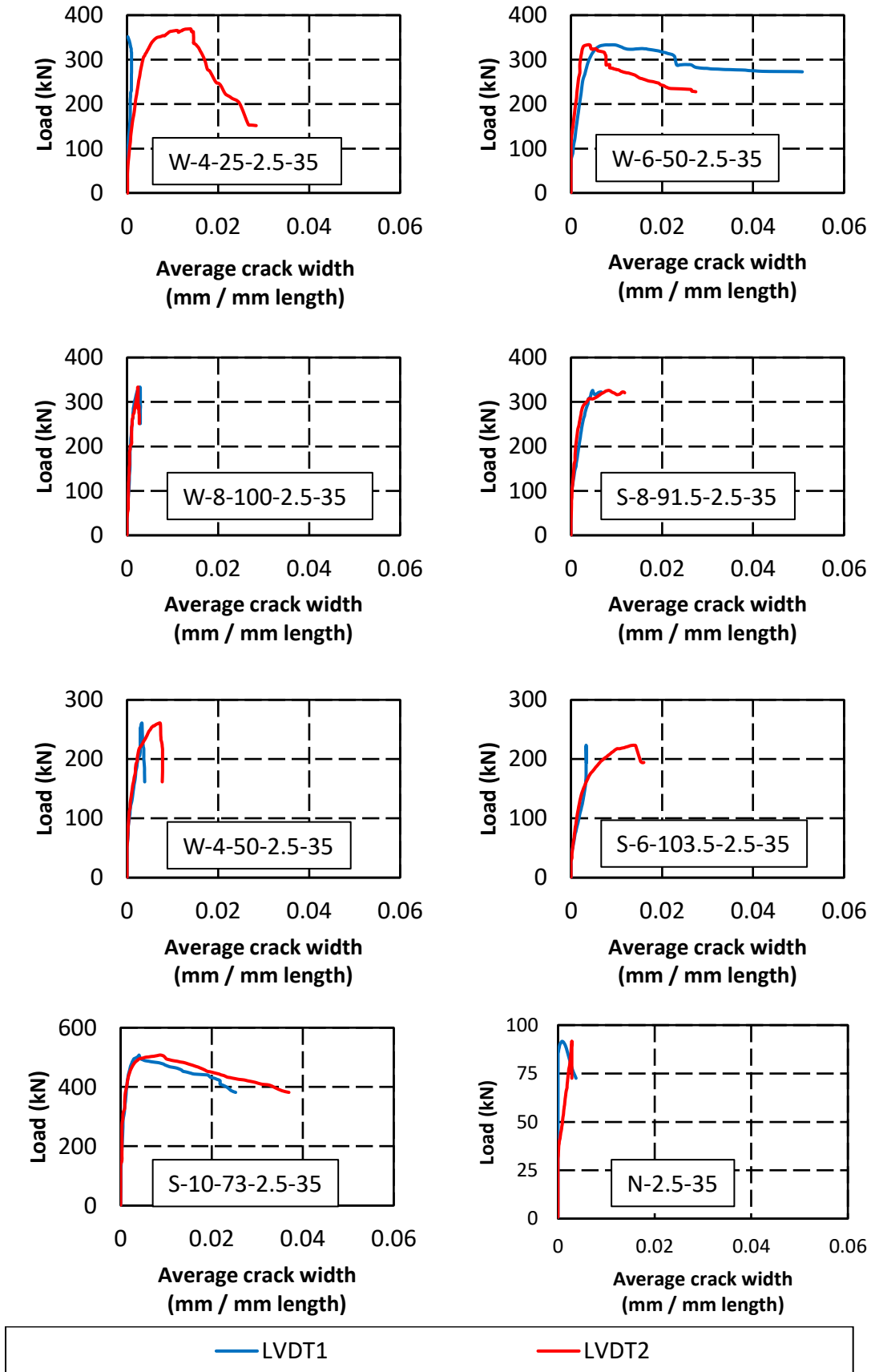


Figure 115: Load versus average crack width for beams of Group 1.

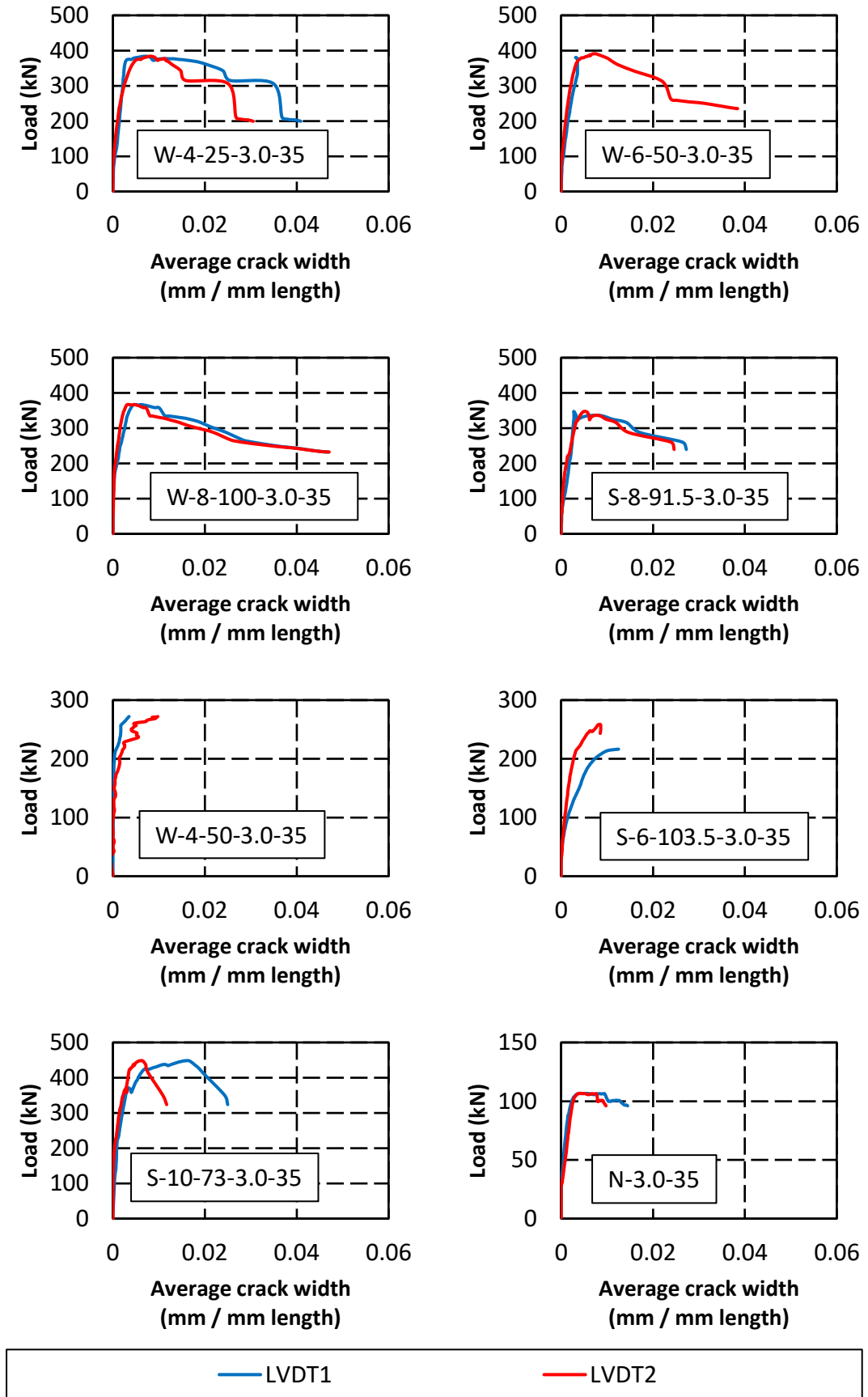


Figure 116: Load versus average crack width for beams of Group 2.

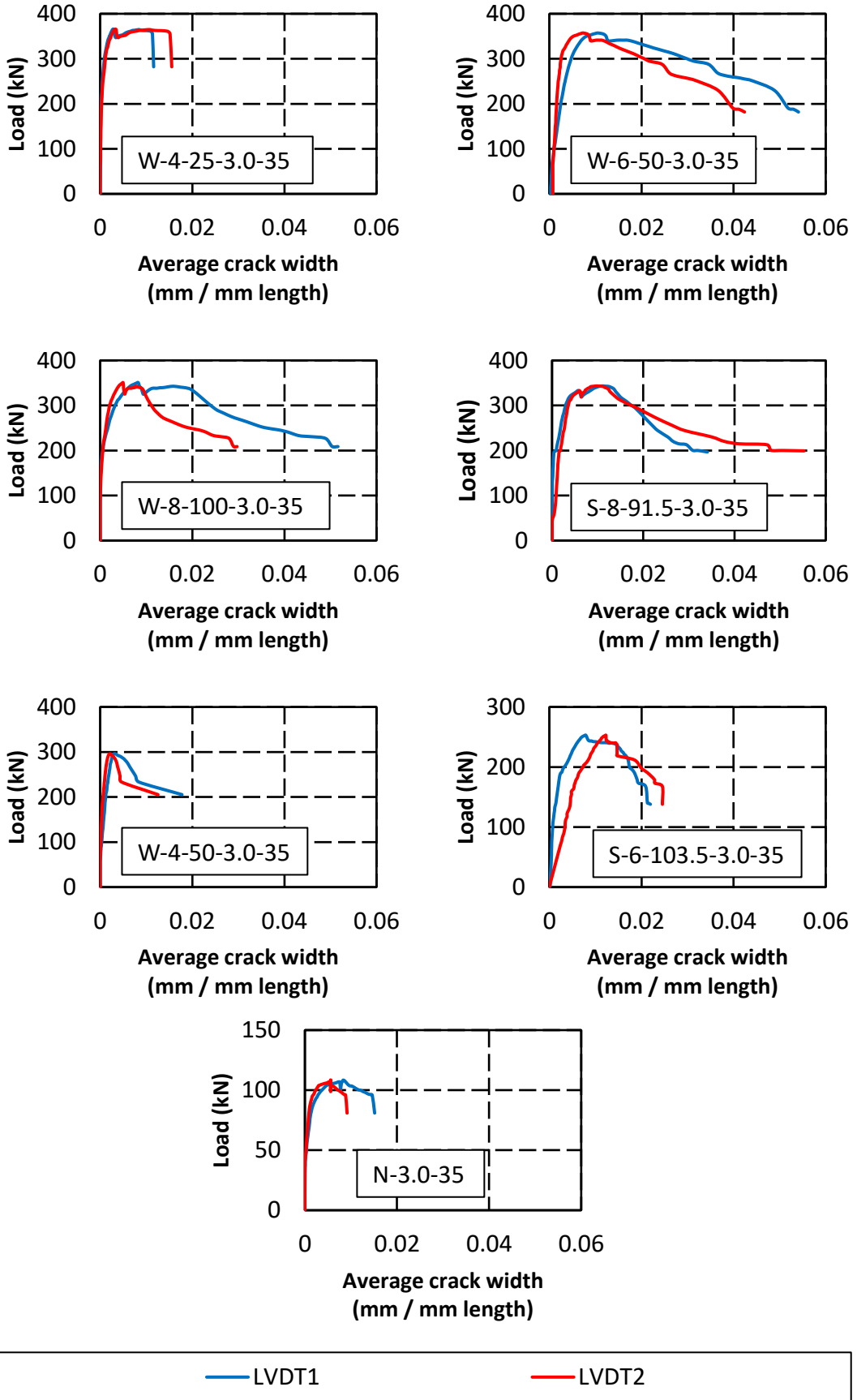


Figure 117: Load versus average crack width for beams of Group 3.

The angle of the major crack on the beam due to shear is approximated using the computer-aided design software AutoCAD. In this procedure, the photos of the beams are imported into the software as background images, and the angle of inclination are measured using available commands. The angle between the two lines was then calculated and reported in Figure 118 to Figure 120. The value of the angles was approximated to the nearest 0.5 degree, and reported in Table 13. In general, the recorded values of the angle are between 26.5 degrees and 48.5 degrees. The larger angles were observed in the beams that were loaded at a small shear span ($a/h=2.5$) than in the beams that were loaded at a large shear span ($a/h=3$). The inclination angle of the crack and the frequency of the cracks are independent of the type of reinforcement used. It is noticed; however, that for the beams that did not contain any transverse reinforcement there were fewer number of cracks and a major crack dominated the shear failure. While there is no consistent trend with regard to the crack width, on average the WWF reinforced beams recorded crack openings that are smaller than that of the stirrups reinforced beam. Note that while in design codes, crack width (from flexure) is considered at service load levels, the previous discussion considers the crack width at ultimate loads since crack width at service loads are difficult to measure.

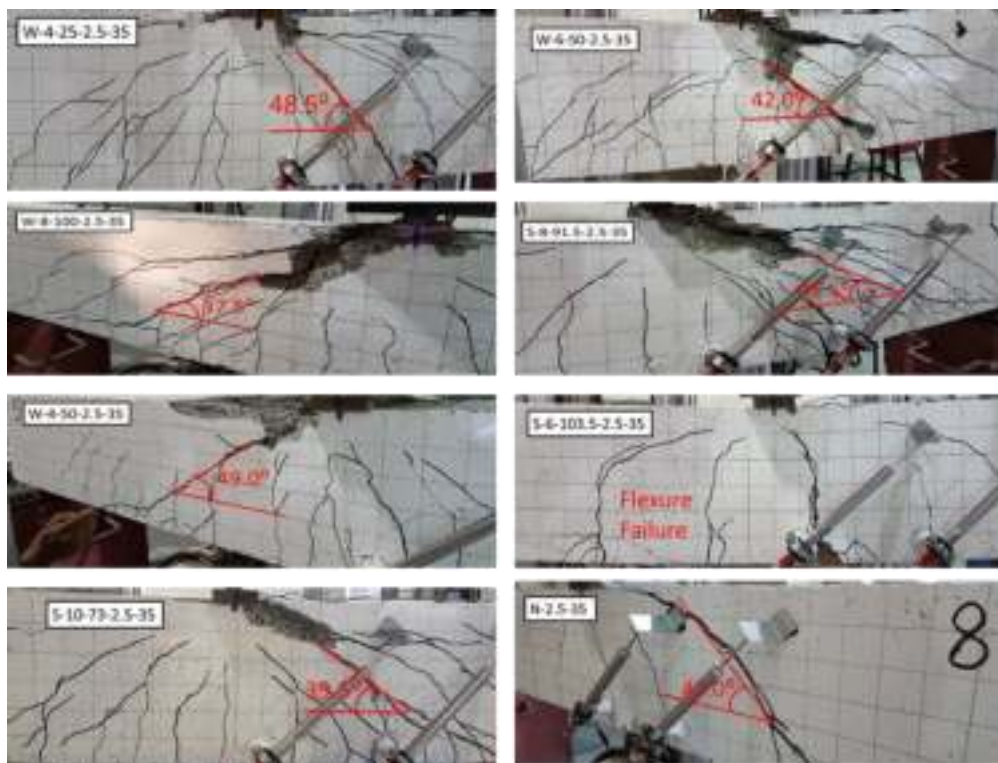


Figure 118: Crack inclination of beams belonging to Group 1.

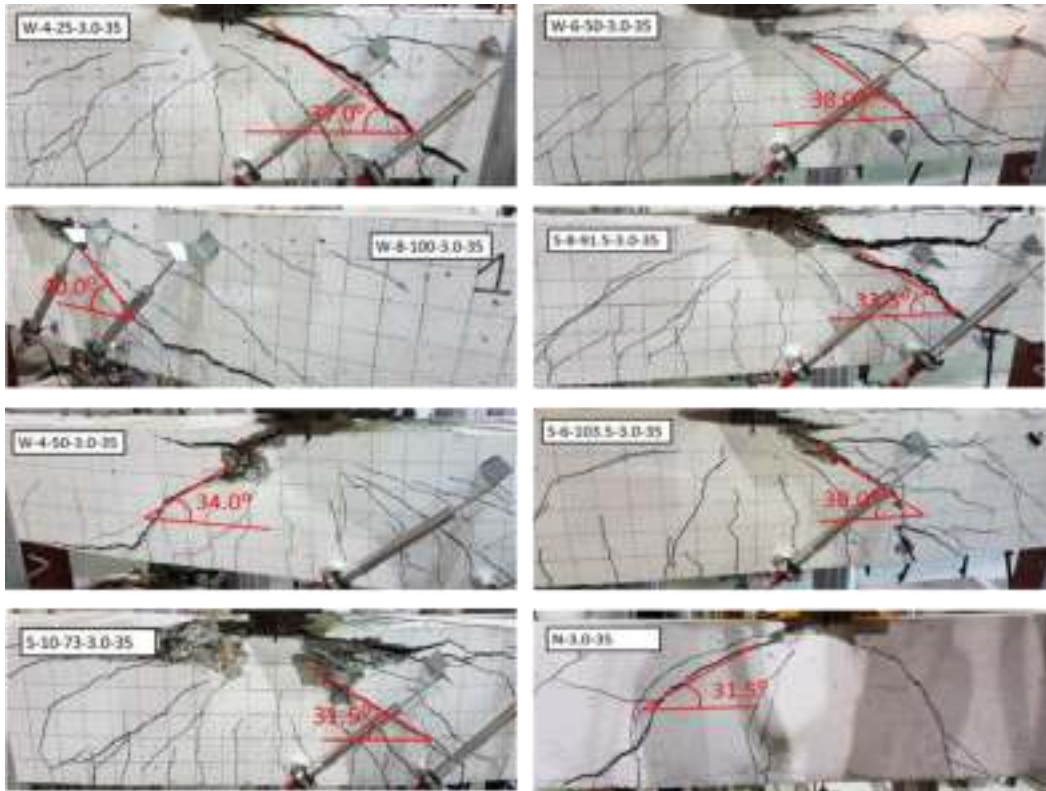


Figure 119: Crack inclination of beams belonging to Group 2.

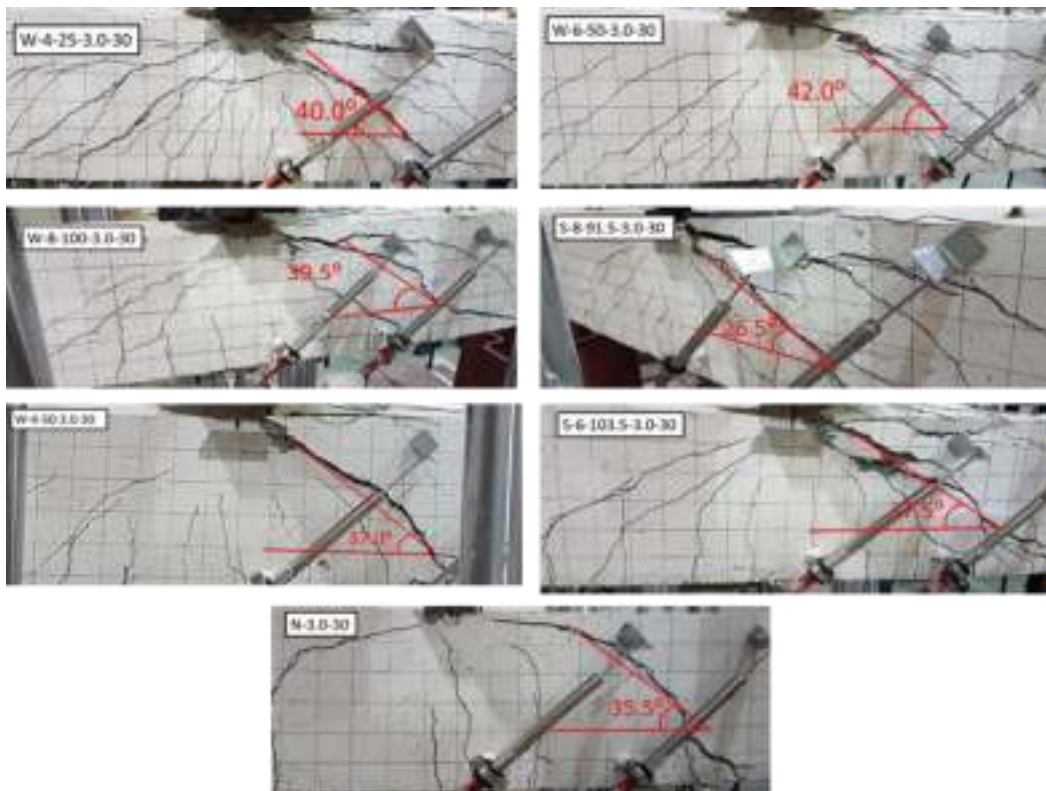


Figure 120: Crack inclination of beams belonging to Group 3.

Table 13: Summary of crack width and inclination of tested specimens.

Group	Beam ID.	Max. Shear (kN)	Adjusted Crack width at Max. shear (mm)	Major Crack Angle (Degree)
Group 1 $L = 1700\text{mm}$ $a/h = 2.5$ $f_c = 35\text{MPa}$	W-4-25-2.5-35	206.37	2.07	48.5
	W-6-50-2.5-35	186.35	1.72	42.0
	W-8-100-2.5-35	186.21	0.76	37.5
	S-8-91.5-2.5-35	181.95	1.93	41.0
	W-4-50-2.5-35	145.84	1.56	49.0
	S-6-103.5-2.5-35*	124.81	2.55	-
Group 2 $L = 1850\text{mm}$ $a/h = 3.0$ $f_c = 35\text{MPa}$	W-4-25-3.0-35	197.16	2.29	37.5
	W-6-50-3.0-35	200.91	1.53	38.0
	W-8-100-3.0-35	188.51	1.13	40.0
	S-8-91.5-3.0-35	178.75	1.15	33.5
	W-4-50-3.0-35	143.95	1.91	34.0
	S-6-103.5-3.0-35	132.82	3.08	39.0
Group 3 $L = 1850\text{mm}$ $a/h = 3.0$ $f_c = 30\text{MPa}$	W-4-25-3.0-30	187.79	0.90	40.0
	W-6-50-3.0-30	183.44	2.61	42.0
	W-8-100-3.0-30	180.03	1.95	39.5
	S-8-91.5-3.0-30	176.23	2.90	26.5
	W-4-50-3.0-30	152.20	0.80	37.0
	S-6-103.5-3.0-30	129.97	2.96	37.5

* This beam failed in flexure.

Chapter 7. Analysis of Results

In this chapter, the experimental results are compared with each other and with theoretical predictions. The important parameters that are considered in the analysis are the shear force-deflection relationships, elastic stiffness, average crack widths, shear strength, and ductility indices. Figure 121 shows the beams that are compared to each other within their groups. Comparison across groups is also conducted to study the effects of the concrete compressive strength and the shear span-to-depth ratio.

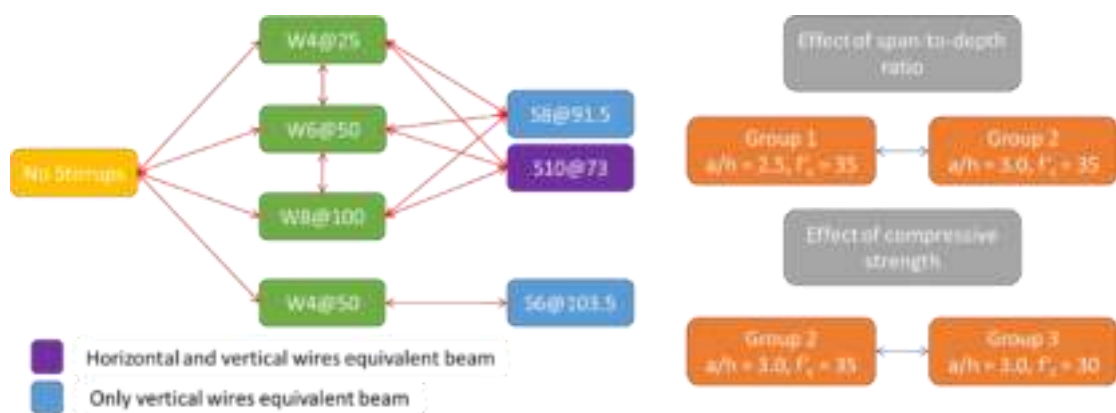


Figure 121: Summary of comparison network.

7.1. Shear Force-Deflection Relationships

The shear- deflection relationships of all tested specimens are compared in this section. The WWF and stirrups reinforced beams of each group are plotted together on the same graph for comparative purposes. Figure 122 and Figure 124 present the plots of shear force versus deflection of the WWF reinforced beams and the equivalent stirrups reinforced beams for each group and for all the considered vertical steel ratios.

Two different transverse reinforcement ratios are considered in each group, $A_{sf_{yst}}/s = A_{wf_{yw}}/g = 505 \text{ N/mm}$ and 251 N/mm on average. In addition, Groups 1 and 2 considers replacing both vertical and horizontal wires result which results in almost double the reinforcement of the stirrup reinforced beam when only vertical wires are replaced, where $A_{sf_{yst}}/s = 990 \text{ N/mm}$. To observe the benefits of using transverse reinforcement, beams with no shear reinforcement ($A_{sf_{yst}}/s = 0 \text{ N/mm}$) were tested and considered. In general, the curves obtained from the experiments consist of an

ascending part, somewhat horizontal portion leading to a peak, and then followed by descending branch. The results show that the elastic stiffness and post-elastic stiffness on the ascending part of the curve before the peak for the WWF reinforced beams are similar to those for the stirrups reinforced beams. Further, some specimens experienced single peaks while others double peaks, which could be due to sudden crack formation, abrupt increase in crack width, concrete crushing or steel yielding. No clear trend is observed among the tested beams containing transverse reinforcement with regard to post-peak residual shear strength.

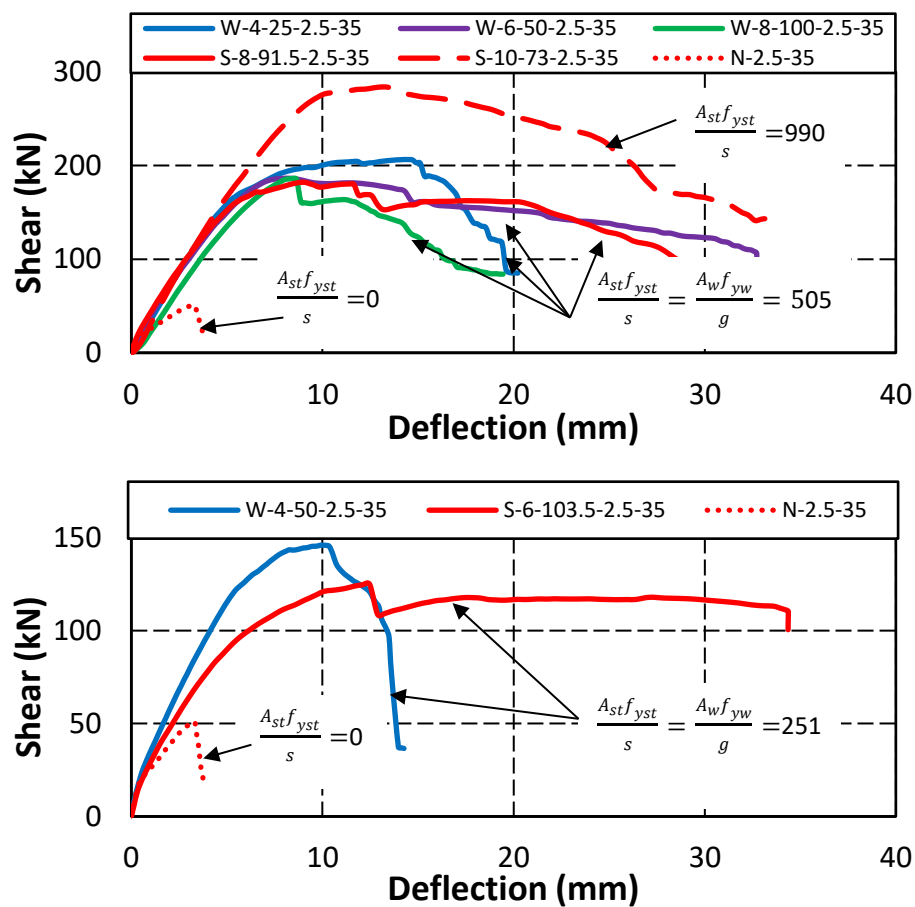
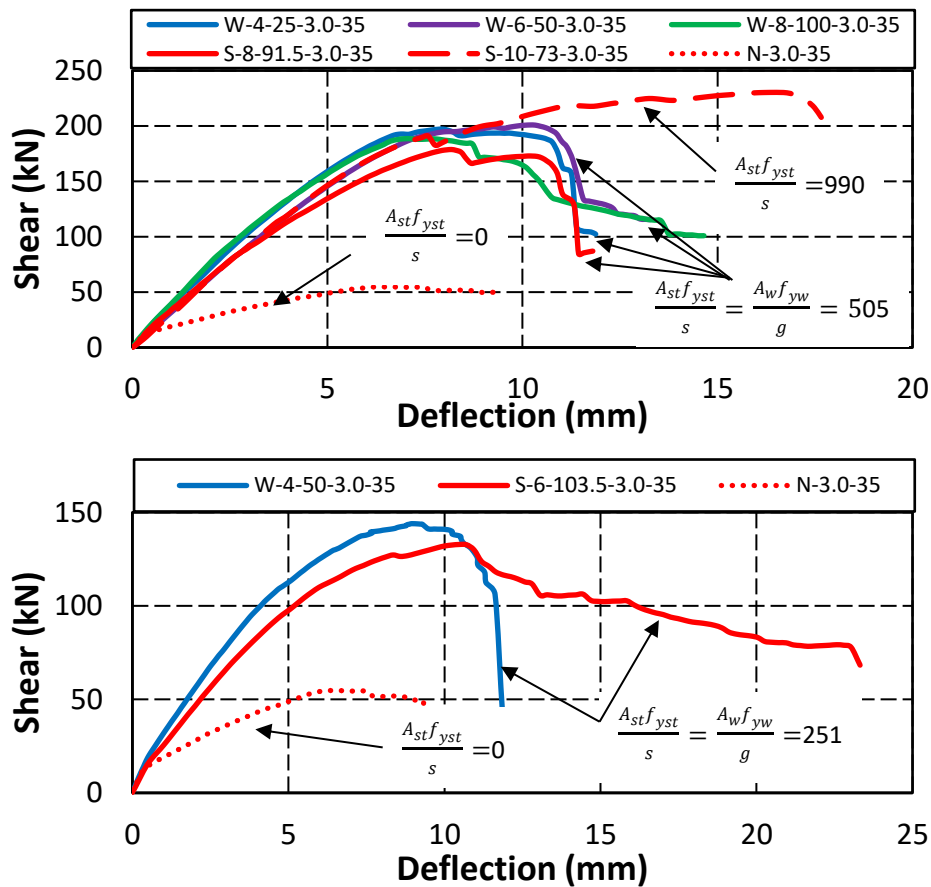


Figure 122: Shear-deflection graphs of beams belonging to Group 1.

As expected, the specimens that are reinforced with less transverse steel revealed generally lower strength than those reinforced with more transverse steel. Within Group 1, the shear strength of the 4mm-diameter mesh at 25mm spacing is 41.5% greater than that of the 4mm-diameter mesh at 50mm spacing. The corresponding increase in the equivalent heavily reinforced from the lightly reinforced

stirrup beams in Group 1 is 45.8%. Within Group 2, this increase is 37% for the beams with WWF and 34.6% for the beams with stirrups. The matching increase for the beams in Group 3 is 23.4% for the beams containing WWF and 35.5% for the beams containing stirrups. The results also showed that the ductility of the WWF and stirrup reinforced beams is comparable for the case of $A_{st}f_{yst}/s = A_wf_{yw}/g = 505$ N/mm; however, stirrup reinforced beams exhibited more ductility than WWF reinforced beams when $A_{st}f_{yst}/s = A_wf_{yw}/g = 251$ N/mm. While there is no increase observed in the elastic and post-elastic stiffness on the ascending part of the curve as a result of increasing the amount of steel, the stirrups reinforced beams that are designed based on replacing both vertical and horizontal wires exceed the WWF beams in every aspect. On average, beams reinforced with conventionally reinforced beams of $A_{st}f_{yst}/s = 990$ N/mm recorded higher loads than similar beams with $A_{st}f_{yst}/s = A_wf_{yw}/g = 505$ N/mm by about 56% for Group 1, and 29% for Group 2. It is worth noting that the beam “S-10-73-3.0-35” failed in flexure through crushing of concrete, hence the recorded strength corresponds to the minimum shear strength of that beam.



3

Figure 123: Shear-deflection graphs of beams belonging to Group 2.

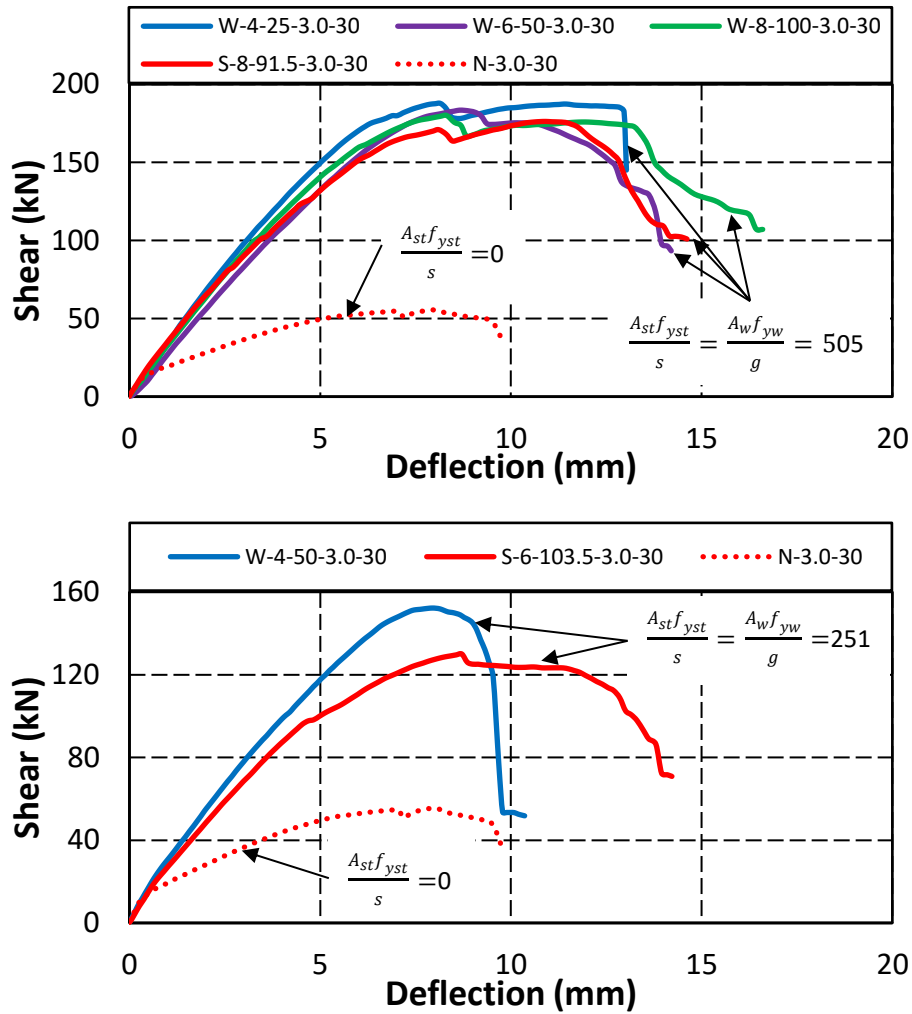


Figure 124: Shear-deflection graphs of beams belonging to Group 3.

Beams with no shear reinforcement reached ultimate loads and deflection that are significantly lower than beams that contain either type of reinforcement. This highlights the significant gains from using transverse reinforcement in concrete beams. Furthermore, the peak load of beams reinforced with WWF was reached at lower deflections than beams reinforced with conventional stirrups, with some exceptions. For example, beam W-4-25 from Group 1 reached the maximum shear load at a deflection of 14.27 mm which is higher than that of beam S-8-91.5 corresponding to a deflection of 8.87 mm. There is a noticeable difference between the deflection levels of beams that contain reinforcement and those which contained no transverse reinforcement at all. This highlights the gains of using steel as shear reinforcement in

concrete beams. Table 14 summarizes the shear strength of the WWF reinforced beams and equivalent stirrup reinforced beams.

Table 14: Shear Strength of all tested specimens

Group	Beam ID.	$A_{stf_{yst}/s}$ or $A_{wf_{yw}/g}$ (N/mm)	Shear strength (kN)	Deflection corresponding to shear strength (mm)
Group 1 $L = 1700\text{mm}$ $a/h = 2.5$ $f'_c = 35\text{MPa}$	W-4-25-2.5-35	505	206.37	14.27
	W-6-50-2.5-35	505	186.35	8.28
	W-8-100-2.5-35	505	186.21	8.45
	S-8-91.5-2.5-35	505	181.95	8.87
	W-4-50-2.5-35	251	145.84	9.90
	S-6-103.5-2.5-35*	251	124.81	12.47
	S-10-73-2.5-35	909	283.88	13.28
	N-2.5-35	0	51.13	3.25
Group 2 $L = 1850\text{mm}$ $a/h = 3.0$ $f'_c = 35\text{MPa}$	W-4-25-3.0-35	505	197.16	7.96
	W-6-50-3.0-35	505	200.91	10.19
	W-8-100-3.0-35	505	188.51	7.12
	S-8-91.5-3.0-35	505	178.75	8.18
	W-4-50-3.0-35	251	143.95	8.95
	S-6-103.5-3.0-35	251	132.82	10.47
	S-10-73-3.0-35*	909	230.32	16.43
	N-3.0-35	0	54.77	6.37
Group 3 $L = 1850\text{mm}$ $a/h = 3.0$ $f'_c = 30\text{MPa}$	W-4-25-3.0-30	505	187.79	8.15
	W-6-50-3.0-30	505	183.44	8.65
	W-8-100-3.0-30	505	180.03	8.32
	S-8-91.5-3.0-30	505	176.23	10.76
	W-4-50-3.0-30	251	152.20	7.93
	S-6-103.5-3.0-30	251	129.97	8.71
	N-3.0-30	0	55.56	8.02

* These two beams failed in flexure.

7.2. Shear Strength

The shear strength is the peak point on the shear force-deflection relationships obtained from the experiments. The shear strength of the WWF beams is compared

with that of the stirrup reinforced beams based on different criteria. When shear strength of the WWF reinforced beams is normalized with respect to the equivalent stirrup reinforced beams, one can directly observe the percentage increase or decrease in strength of the proposed transverse reinforcement relative to the conventional. Table 15 shows the normalized results with consideration of vertical wires only, whereas Table 16 shows the normalized results with consideration of both vertical and horizontal wires. As expected, the ratio of the shear strength of the WWF reinforced beam to that of the stirrup reinforced beams, denoted by $(V_{Exp})_{WWF}/(V_{Exp})_{Stir}$, is larger when the stirrup size and spacing are based on the vertical wires of the WWF than when stirrup size and spacing are based on both vertical and horizontal wires of the WWF (with correction for yield strength). These results are discussed further in detail in the following four sub-sections with respect to the effects of the grid size, amount of shear reinforcement, shear span-to-depth ratio, and concrete compressive strength.

7.2.1. Effect of grid size. Here, the transverse steel ratio is maintained constant and variations are performed on the wire size and grid openings. Figure 125 shows the normalized shear strength of WWF reinforced beams with respect to the strength of a stirrup reinforced beams based on an equivalent $A_{st}f_{yst}/s = (A_wf_{yw}/g)_v$, i.e. stirrups size and spacing corresponds to the vertical wires of the WWF. Close examination of the results reveals that all the WWF reinforced beams have higher strength than their stirrups reinforced counterparts, since all normalized data have values greater than 1.0. This shows the advantage of WWF as shear reinforcement in concrete beams compared to stirrups. The grid size has an impact on the shear strength because the beams containing WWF cages that consisted of smaller diameter wires at narrow spacing exhibited higher shear strength than corresponding ones containing larger diameter wires at wide spacing. This observation is visible in all groups, which supports the notion of better core confinement can be achieved from smaller mesh openings without using extra amount of steel. From Group 1, the WWF beam reinforced with a grid size of 25 mm reached an ultimate shear capacity of 206 kN, while the 50 mm and 100 mm grid size mesh both reached an ultimate shear capacity of 186 kN. This corresponds to a 11% enhancement in load carrying capacity gained by changing the size of the grid opening. Similar trends are similar in Group 3, and slightly off in Group 2 where beam reinforced with a mesh of 50 mm grid opening reached the highest shear capacity then

Table 15: Shear strength of beams with $A_{st}f_{yst}/s = (A_wf_{yw}/g)_v$.

Group Details	Beam ID.	A_vf_y/s (N/mm)	V_{Exp} (kN)	$\frac{(V_{Exp})_{WWF}}{(V_{Exp})_{Stir}}$
Group 1 $L = 1700\text{mm}$ $a/h = 2.5$ $f_c = 35\text{MPa}$	W-4-25-2.5-35	505	206.37	1.13
	W-6-50-2.5-35	505	186.35	1.02
	W-8-100-2.5-35	505	186.21	1.02
	S-8-91.5-2.5-35	505	181.95	-
	W-4-50-2.5-35	251	145.84	1.17
	S-6-103.5-2.5-35*	251	124.81	-
Group 2 $L = 1850\text{mm}$ $a/h = 3.0$ $f_c = 35\text{MPa}$	W-4-25-3.0-35	505	197.16	1.10
	W-6-50-3.0-35	505	200.91	1.12
	W-8-100-3.0-35	505	188.51	1.05
	S-8-91.5-3.0-35	505	178.75	-
	W-4-50-3.0-35	251	143.95	1.08
	S-6-103.5-3.0-35	251	132.82	-
Group 3 $L = 1850\text{mm}$ $a/h = 3.0$ $f_c = 30\text{MPa}$	W-4-25-3.0-30	505	187.79	1.07
	W-6-50-3.0-30	505	183.44	1.04
	W-8-100-3.0-30	505	180.03	1.02
	S-8-91.5-3.0-30	505	176.23	-
	W-4-50-3.0-30	251	152.20	1.17
	S-6-103.5-3.0-30	251	129.97	-

* Beam failed in flexure.

Table 16: Shear strength of beams with $A_{st}f_{yst}/s = (A_wf_{yw}/g)_{v+h}$.

Group Details	Beam ID.	A_vf_y/s (N/mm)	V_{Exp} (kN)	$\frac{(V_{Exp})_{WWF}}{(V_{Exp})_{Stir}}$
Group 1 $L = 1700\text{mm}$ $a/h = 2.5$ $f_c = 35\text{MPa}$	W-4-25-2.5-35	505	206.37	0.73
	W-6-50-2.5-35	505	186.35	0.66
	W-8-100-2.5-35	505	186.21	0.66
	S-10-73-2.5-35	990	283.88	-
Group 2 $L = 1850\text{mm}$ $a/h = 3.0$ $f_c = 35\text{MPa}$	W-4-25-3.0-35	505	197.16	0.86
	W-6-50-3.0-35	505	200.91	0.87
	W-8-100-3.0-35	505	188.51	0.82
	S-10-73-3.0-35*	990	230.32	-

* Beam failed in flexure.

the 25 mm grid opening mesh and lastly the 100 mm grid opening mesh. The values are 201 kN, 197 kN, and 188 kN respectively. The normalized shear strength of the 25mm mesh ranged 1.07-1.13, of the 50mm mesh ranged 1.02-1.12, and of the 100mm mesh ranged 1.02-1.05.

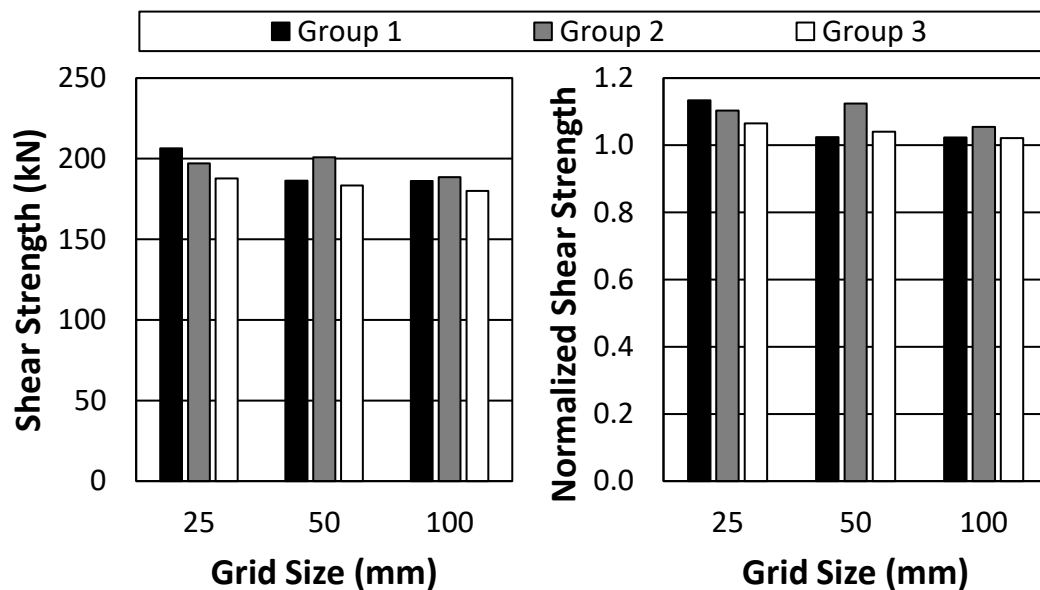


Figure 125: Effect of grid size on shear strength based on equivalent $(A_{st}f_{yst}/s)_v$.

Figure 126 shows the impact of the grid size on the normalized shear strength of WWF beams with respect to stirrup reinforced beams based on an equivalent total $A_{st}f_{yst}/s = (A_wf_{yw}/g)_{v+h}$ (i.e. stirrups size and spacing corresponds to both vertical and horizontal wires of the WWF). While the magnitude of the normalized shear strength ratios all fall below 1.0, the effect of the grid size is consistent with the previous finding; namely, beams reinforced with fine wire mesh have higher strength than beams reinforced with coarse wire mesh. The reduction in the normalized shear strength ratio well below 1.0 confirms the idea that shear forces in concrete beams are better carried by vertical than by horizontal reinforcement. Nevertheless, the WWF was capable of producing at least 66% shear strength of the equivalent beams containing stirrups having the same weight (after correction of the yield strength is applied). Note that although Figure 126 shows major differences between the results of beams in Group 1 ($a/h=2.5$) and Group 2 ($a/h=3.0$), this is because the control (stirrup reinforced) beam

in Group 2 failed unexpectedly in flexure; hence, the actual shear strength of that beam is higher. While the results indicate that the contribution of the horizontal wires of the WWF is not as critical to the shear capacity of the beams as the vertical wires, they do provide better confinement to the concrete within the core and their influence on flexural behavior is expected to be positive.

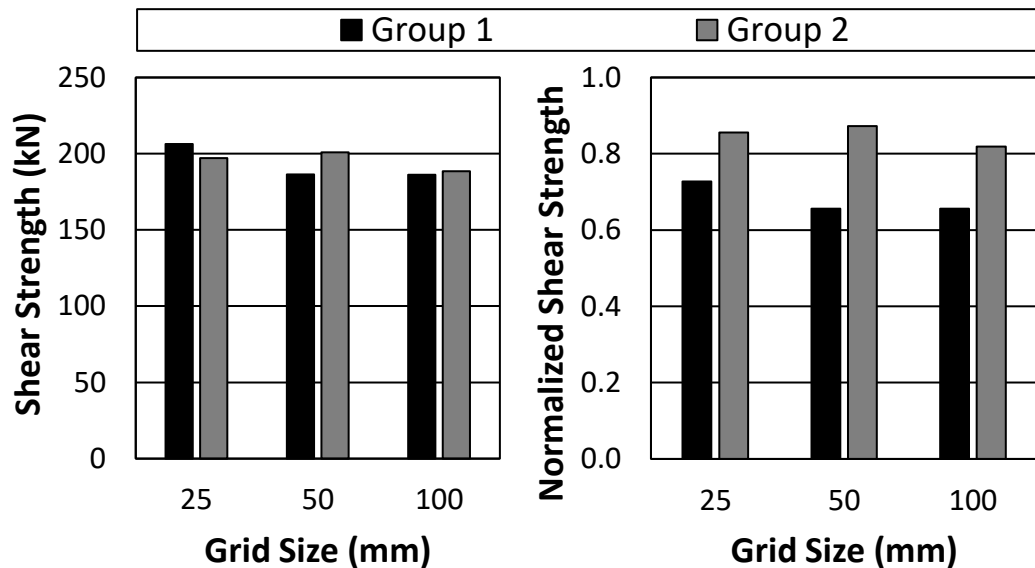


Figure 126: Effect of grid size on shear strength based on equivalent $(A_{stf_{yst}/s})_{v+h}$.

7.2.2. Effect of transverse steel reinforcement ratio. In Figure 127, beams reinforced with different transverse (i.e. vertical) steel reinforcement ratios are compared together. The comparison is conducted with and without normalization with their respective stirrups reinforced beams. The two different steel ratios are $(A_{wf_{yw}/g})_v = 505 \text{ N/mm}$ (denoted by W-4-25) and 251 N/mm (denoted by W-4-50), which are achieved through maintaining the wire diameter and doubling the grid size. The findings show that reducing the grid size by 50% (i.e. doubling $(A_{wf_{yw}/g})_v$) results in an average 34% increase in the shear strength for the WWF reinforced beams. The corresponding average shear strength increase in the stirrups reinforced beams is equal to 38%. Also, the WWF reinforced beams are able to perform better in shear than the beams reinforced with stirrups irrespective of the amount of $(A_{wf_{yw}/g})_v$, as the normalized values are greater than 1.0 for all groups. It can be noticed that beams that are reinforced with a smaller transverse steel ratio perform better than beams with higher transverse ratio. The average normalized shear strength for the WWF reinforced

beams with 4mm-diameter at 50mm spacing (i.e. $(A_w f_{yw}/g)_v = 505$ N/mm) mesh averaged 1.14 and for the WWF reinforced beams with 4mm-diameter spaced at 25mm (i.e. $(A_w f_{yw}/g)_v = 251$ N/mm) averaged 1.10.

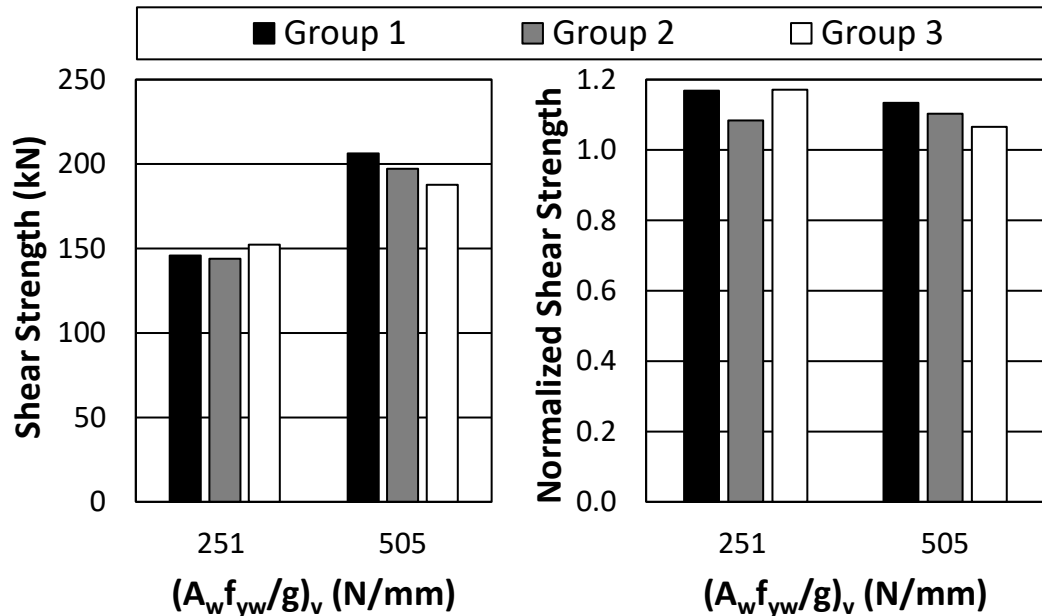


Figure 127: Effect of vertical steel reinforcement ratio on shear strength.

7.2.3. Effect of shear span-to-depth ratio. The behavior of the WWF reinforced beams is considered under different shear span to thickness ratio, shown in Figure 128. Note that beam W-4-50 belonging to Group 1 was omitted from the normalized analysis since the corresponding stirrup reinforced beam (S-6-103.5) failed in flexure instead of shear, hence reflects the minimum shear capacity. In the ACI 318 code, the shear span to effective steel reinforcement depth ratio (a/d) is used to judge whether a beam is deep or not. The test results show no consistent trend with regard to the effect of the shear span-to-depth ratio on shear strength; in some cases, beams loaded at $a/h = 2.5$ had higher strength than their corresponding counterparts that are loaded at $a/h = 3.0$ and in some other cases the opposite was observed. For example, the beam reinforced with 4mm diameter wires that are spaced at 25 mm reached a higher load when tested at $a/h = 2.5$ (206 kN) than when tested at $a/h = 3.0$ (197 kN), while the beam reinforced with 6mm diameter wires witnessed the opposite (189 kN at $a/h = 2.5$ and 201 kN at $a/h = 3.0$). This could be because the two considered shear span-to-depth ratios are close to each other or the shear-span is not an important

parameter in such tests. Nevertheless, the findings support the new concrete shear strength provisions in the ACI318-19 [6], which are independent of shear span.

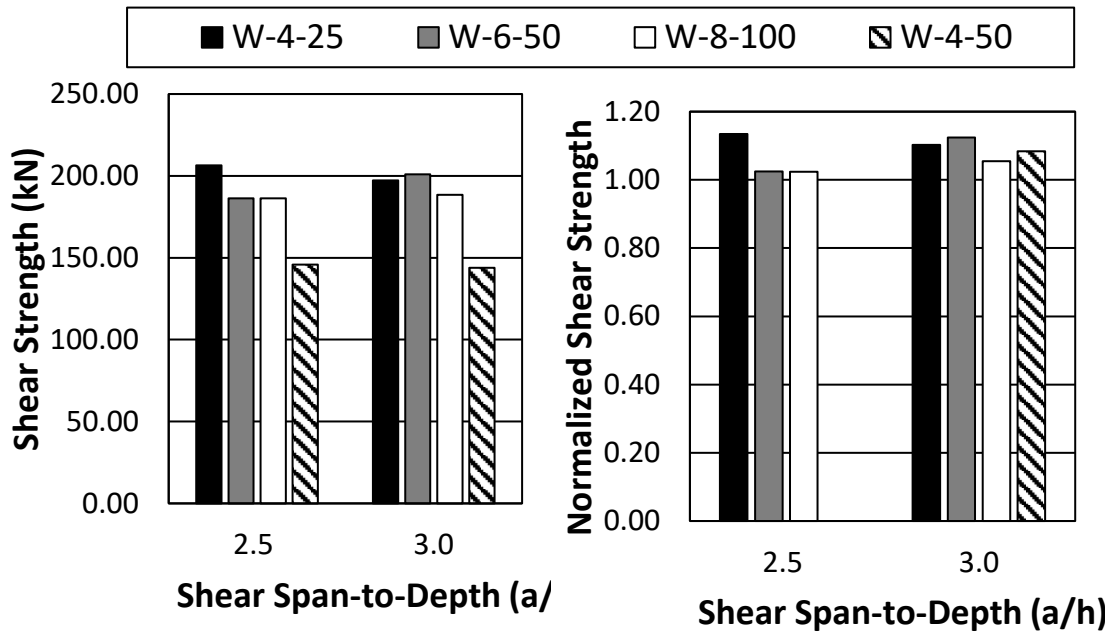


Figure 128: Effect of shear span-to-depth ratio on shear strength.

7.2.4. Effect of concrete compressive strength. The effect of the concrete compressive strength at the time of testing on the shear strength is addressed in Figure 129. In this study, two different f'_c are considered, 30 and 35 MPa. The small difference between the two values is because the concrete supplier could not furnish higher strength concrete than 35 MPa. Without normalizing with respect to the outcome of the stirrups reinforced beams, the WWF reinforced specimens that have lower concrete compressive strength demonstrated on average 6.0% lower shear capacity than those possessed higher concrete compressive strength, with the exception of the WWF beam reinforced with 4mm at 50mm spacing which showed unexpectedly 5.7% higher shear strength. This could be because the two considered concrete compressive strengths are close to each other and possibly due to non-ideal conditions concerning the inherent concrete material properties, concrete placement procedures, steel cage workmanship, vibrations, and non-homogeneity of the concrete material. When the shear strength of each WWF beam is normalized with respect to the corresponding control stirrup reinforced beams, the shear strength of the WWF reinforced beams with higher concrete

compressive strength ranged between 1.05 and 1.12 and with the lower concrete compressive strength ranged between 1.02 and 1.07. This shows that the performance of WWF is a little more effective in shear when higher strength concrete is used. For the 3 beams that have higher vertical steel reinforcement ratio of 505 N/mmm, the results showed that the WWF is more effective than stirrups in resisting shear when $f'_c = 35\text{MPa}$ than when $f'_c = 30\text{MPa}$ since the normalized shear strength ratio averaged 1.09 for the former and 1.04 for latter.

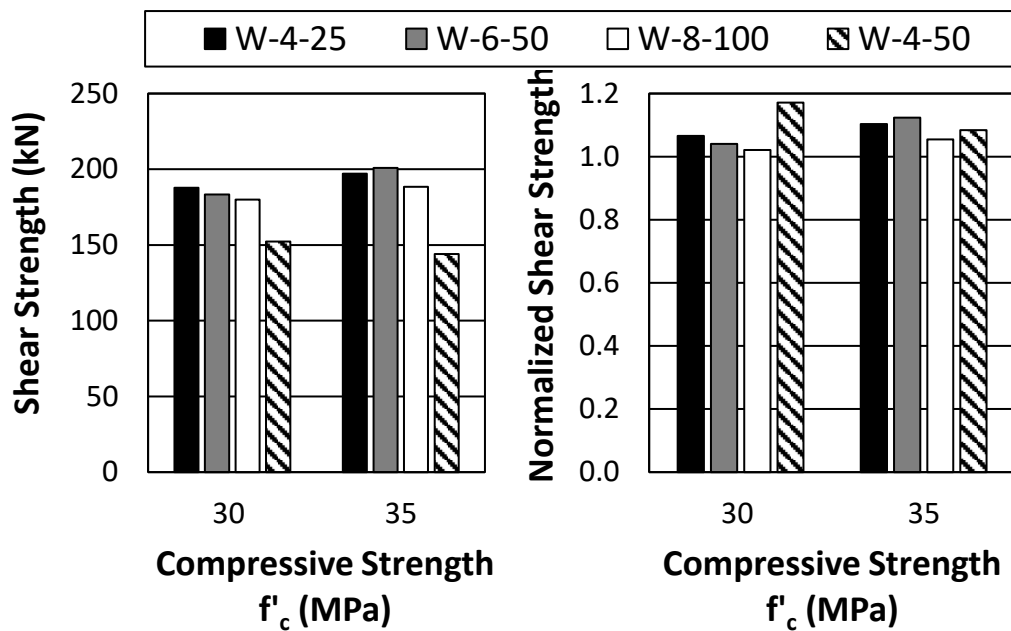


Figure 129: Effect of concrete compressive strength on shear strength.

7.3. Ductility

Ductility is a structural element's ability to sustain load at high level of deformation without collapse. This aspect is beneficial for structures where energy dissipation is required and important for the stability of a structural element at loads approaching ultimate. Ductile members exhibit signs of warning and allow inhabitants to leave the structure prior to failure. Ductility in a structural member can be quantified by the ductility index, μ . There are different definitions in the published literature of μ , one of which is given below based on the deflection of a beam:

$$\mu = \frac{(\Delta_{0.85})_{post}}{(\Delta_{0.85})_{prior}} \quad (28)$$

where $(\Delta_{0.85})_{post}$ represents the deflection of the beam when the load is 85% of the peak load after the peak load is reached, and $(\Delta_{0.85})_{prior}$ denotes the deflection of the beam when the load is 85% of the peak load before the peak load is reached on the load-deflection curve. Figure 130 shows graphically the definition of $(\Delta_{0.85})_{post}$ and $(\Delta_{0.85})_{prior}$, based on a load-deflection relationship obtained from experimental testing of a beam specimen. Traditionally, ductility has often been discussed by researchers more extensively in members subjected to flexure than to shear. This is because when a member is properly designed for flexure and shear per the relevant code, the flexural ductility will govern because of the lower strength reduction factor for flexure compared to shear (e.g. in the ACI 318 code: $\phi_f=0.90$ versus $\phi_s=0.75$). Nevertheless, in this study the ductility of tested beams in shear will be investigated for the WWF reinforced beams and their corresponding stirrup reinforced beams.

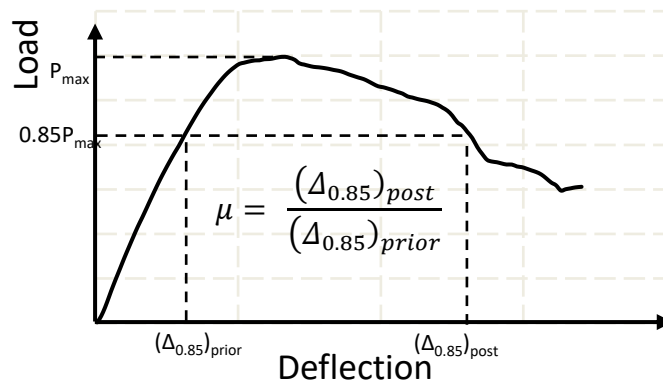


Figure 130: Points considered for determining ductility of a typical beam.

The ductility analysis in this research is particularly important because the behavior of welded wire fabric on the material level is not as ductile as rebars of which stirrups are made of. For WWF to be a viable alternative to conventional stirrups, not only it should have comparable strength, it should also have comparable ductility.

Using the previously presented formula, the ductility indices of the 23 tested specimens are computed and tabulated in Table 17. Moreover, a bar chart is plotted in Figure 131 to allow for comparison of the results, among the WWF reinforced beams and with the equivalent stirrup reinforced beams. Note that the stirrup reinforced beam S-6-103.5 and its corresponding WWF reinforced beam W-4-50 from Group 1 are not included in the figure because the stirrup reinforced beam failed prematurely in flexure

and the recorded results do not reflect the shear strength and ductility of the tested beam. Also, not included in the figure are the beams that do not contain any lateral shear reinforcement because they are unimportant to the ductility analysis.

In general, Figure 131 shows that the ductility of the WWF and stirrups reinforced beams are comparable. The ductility indices for the WWF reinforced beams varied between 1.65 and 2.95, while the same for the stirrup reinforced beams ranged between 1.86 and 2.77. Comparing beams of Groups 1 and 2, beams tested at a shear span-to-depth ratio of 2.5 resulted in ductility higher than beams tested at a shear span-to-depth ratio of 3.0 by about 45%. Although the beams that were tested at $a/h=2.5$ exhibited higher ductility than those at $a/h=3.0$, this finding cannot be generalized because the span length was not the same in these two groups. Further, beams that had a lower compressive strength ($f'_c = 30$ MPa) reported higher ductility indices than beams that had a higher compressive strength ($f'_c = 35$ MPa) by about 10%, on average. This is possibly because the stress-strain relationship of the lower strength concrete is more ductile than that of the higher strength concrete. The effect of the vertical wire reinforcement ratio on the ductility can be evaluated by comparing the ductility indices of the beams W-4-25 and W-4-50 within group 2 and 3, which shows that the average ductility index for the former case is 2.22 and the latter case 1.79.

The normalized ductility, shown in Figure 132, of WWF reinforced beams with respect to stirrup reinforced reveal that the ductility of WWF reinforced beams is better than the stirrups reinforced beams in some case but not others. For example, in Group 1, beam W-8-100 had a lower ductility index than the stirrup reinforced beams and in Group 2 and 3 beams W-6-50 had a lower ductility index than the stirrup reinforced beams. In Group 1, the WWF beams (all of which $(A_w f_{yw}/g)_v = 505$ N/mm) reinforced with grid size opening of 25 mm, 50 mm, and 100 mm exhibited ductility indices that are 6% higher, 16% higher, and 23% lower than corresponding stirrup reinforced beam ($A_s f_{ys}/s = 505$ N/mm), respectively.

7.4. Theoretical Studies

Five different theoretical procedures are used in this study to predict the shear strength of the 20 transversely reinforced tested beams and compare the results with the experimental findings. The 3 beams that did not contain WWF or stirrups are not considered in the theoretical component of the study. They include the ACI 318 code [5, 6], Eurocode2 [7], CSA23.3 [8], BS 8110 [9], and the MCFT as presented in

Table 17: Details of the calculations of ductility indices.

Group	Beam ID.	0.85P _{MAX} (kN)	($\Delta_{0.85}$) _{prior} (mm)	($\Delta_{0.85}$) _{post} (mm)	μ
Group 1 <i>L</i> = 1700mm <i>a/h</i> = 2.5 <i>f_c</i> = 35MPa	W-4-25-2.5-35	314	6.19	16.74	2.71
	W-6-50-2.5-35	283.7	5.38	15.87	2.95
	W-8-100-2.5-35	283.7	6.12	11.97	1.96
	S-8-91.5-2.5-35	277.3	5.14	13.09	2.55
	W-4-50-2.5-35	222.0	5.71	12.09	2.12
	S-6-103.5-2.5-35*	190.1	7.07	34.37	4.86
	S-10-73-2.5-35	432.1	7.91	21.93	2.77
	N-2.5-35	78.0	2.36	3.43	1.45
Group 2 <i>L</i> = 1850mm <i>a/h</i> = 3.0 <i>f_c</i> = 35MPa	W-4-25-3.0-35	326.6	5.37	10.94	2.04
	W-6-50-3.0-35	332.8	6.12	11.28	1.84
	W-8-100-3.0-35	312.2	5.15	10.16	1.97
	S-8-91.5-3.0-35	295.9	5.89	10.95	1.86
	W-4-50-3.0-35	238.6	5.75	11.05	1.92
	S-6-103.5-3.0-35	220.2	6.35	12.55	1.98
	S-10-73-3.0-35*	381.5	8.60	17.74	2.06
	N-3.0-35	90.9	4.54	9.36	2.06
Group 3 <i>L</i> = 1850mm <i>a/h</i> = 3.0 <i>f_c</i> = 30MPa	W-4-25-3.0-30	311.2	5.45	13.02	2.39
	W-6-50-3.0-30	303.8	6.09	12.36	2.03
	W-8-100-3.0-30	298.6	5.64	13.70	2.43
	S-8-91.5-3.0-30	291.9	5.90	12.85	2.18
	W-4-50-3.0-30	252.3	5.68	9.36	1.65
	S-6-103.5-3.0-30	215.1	5.98	12.79	2.14
	N-3.0-30	92.2	4.56	9.58	2.10

* Beams failed in flexure.

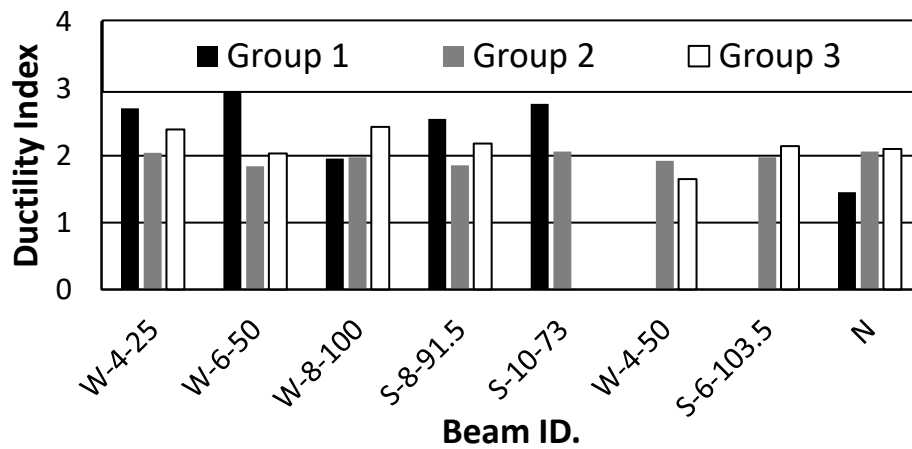


Figure 131: Ductility indices of the WWF and stirrup reinforced beams.

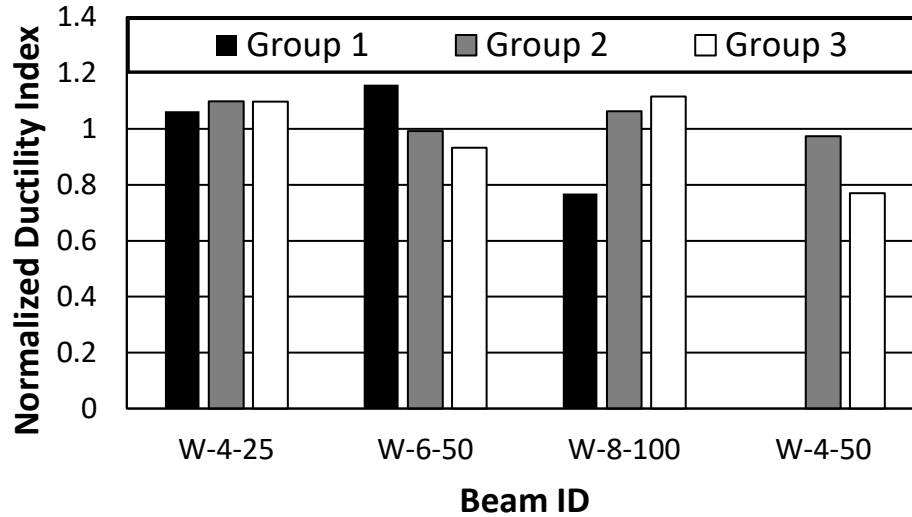


Figure 132: Normalized ductility indices of the WWF reinforced beams.

the AASHTO LRFD Specifications [10]. The considered procedures were discussed in detail in Chapter 3, with numerical examples. Note that the presented results were computed using actual material properties instead of nominal values. Table 18 shows the experimental shear strength of the tested beam specimens and their corresponding theoretical predictions. Plots of predicted shear strength versus observed shear strength are displayed in Figure 133. Ratios of the experimental-to-predicted shear strength for the 20 tested beams are presented in Table 19. It also demonstrates the overall accuracy of the predictive approaches in reference to the experimental results. Note that the beam S-10-73 is not included in all the analysis and calculations because it failed in flexure at a load much lower than the load corresponding to shear failure.

In general, Figure 133 shows that the predicted shear strength by all methods is close to the actual strength obtained by the experiments, although some methods are more accurate than others. The statistical analysis at the bottom of Table 19 reveals that the average experimental-to-theoretical shear strength ratio ranged between 0.891 and 1.124. The lower ratio is predicted by the MCFT [21] and the higher ratio is predicted by the Eurocode2 [7]. The standard deviation varied between 0.077 (based on the CSA23.3) and 0.12 (based on Eurocode2). The most accurate methods are the ACI 318-14 and CSA23.3, which gave average ratios very close to 1.0 and standard deviations approximately equal to 0.08. The method that gave the most scatter from the average is the MCFT, resulting in a coefficient of variation equal to 0.11.

Table 18: Experimental and predicted shear strength results based on actual f_y .

Group	Beam ID.	Experimental Shear (kN)	Predicted Shear based on actual f_y (kN)					
			ACI 318		Eurocode2	CSA 23.3	BS 8110	MCFT
			14	19				
Group 1 $L = 1700$ $a/h = 2.5$ $f'_c = 35$	W-4-25	206.4	206.4	203.3	181.8	207.4	192.6	227.9
	W-6-50	186.4	200.7	197.8	176.9	201.6	187.3	236.5
	W-8-100	186.2	199.4	196.8	176.0	200.4	186.4	236.0
	S-8-91.5	182.0	197.7	195.1	174.5	198.7	184.8	239.4
	W-4-50	145.8	131.8	119.6	106.7	135.4	113.1	140.0
	S-6-103.5*	124.8	127.5	115.6	103.1	131.2	109.3	137.6
	S-10-73	283.9	325.3	328.3	294.5	323.7	311.6	317.7
Group 2 $L = 1850$ $a/h = 3.0$ $f'_c = 35$	W-4-25	197.2	200.7	204.9	183.4	200.8	194.3	214.4
	W-6-50	200.9	195.1	199.4	178.5	195.1	189.1	232.4
	W-8-100	188.5	193.8	198.2	177.6	193.8	188.1	213.8
	S-8-91.5	178.8	192.2	196.6	176.1	192.2	186.6	234.4
	W-4-50	144.0	128.3	124.0	110.6	131.1	117.4	133.5
	S-6-103.5	132.8	124.1	120.1	107.1	126.9	113.6	133.5
	S-10-73*	230.3	323.2	327.8	294.2	323.3	311.3	293.5
Group 3 $L = 1850$ $a/h = 3.0$ $f'_c = 30$	W-4-25	187.8	197.2	200.7	180.8	196.8	191.6	220.0
	W-6-50	183.4	191.6	195.2	176.0	191.2	186.4	217.6
	W-8-100	180.0	190.4	194.0	175.1	190.0	185.5	216.0
	S-8-91.5	176.2	188.7	192.4	173.6	188.3	183.9	220.9
	W-4-50	152.2	125.4	123.2	111.1	127.0	117.8	141.5
	S-6-103.5	130.0	121.2	119.3	107.5	122.8	114.1	140.0

* Beams failed in flexure.

Furthermore, analysis shows that theoretical predictions for beams that are tested at $a/h=3.0$ are a little closer to the experimental results than the ones that are tested at $a/h=2.5$. This could be because as a/h ratio reduces the behavior of the beam becomes closer to a deep beam, which is not account for by most of the considered methods. The effect of variations in the concrete compressive strength did not affect the accuracy of theoretical predictions. Generally, it can be concluded that the ACI 318, CSA and BS 8110 are equally applicable to beams transversely reinforced for shear with either stirrups or WWF with high level of accuracy. The Eurocode2 predictions were a little on the conservative side. The MCFT unexpectedly gave unconservative predictions, resulting about 10% deviation from the experimental values.

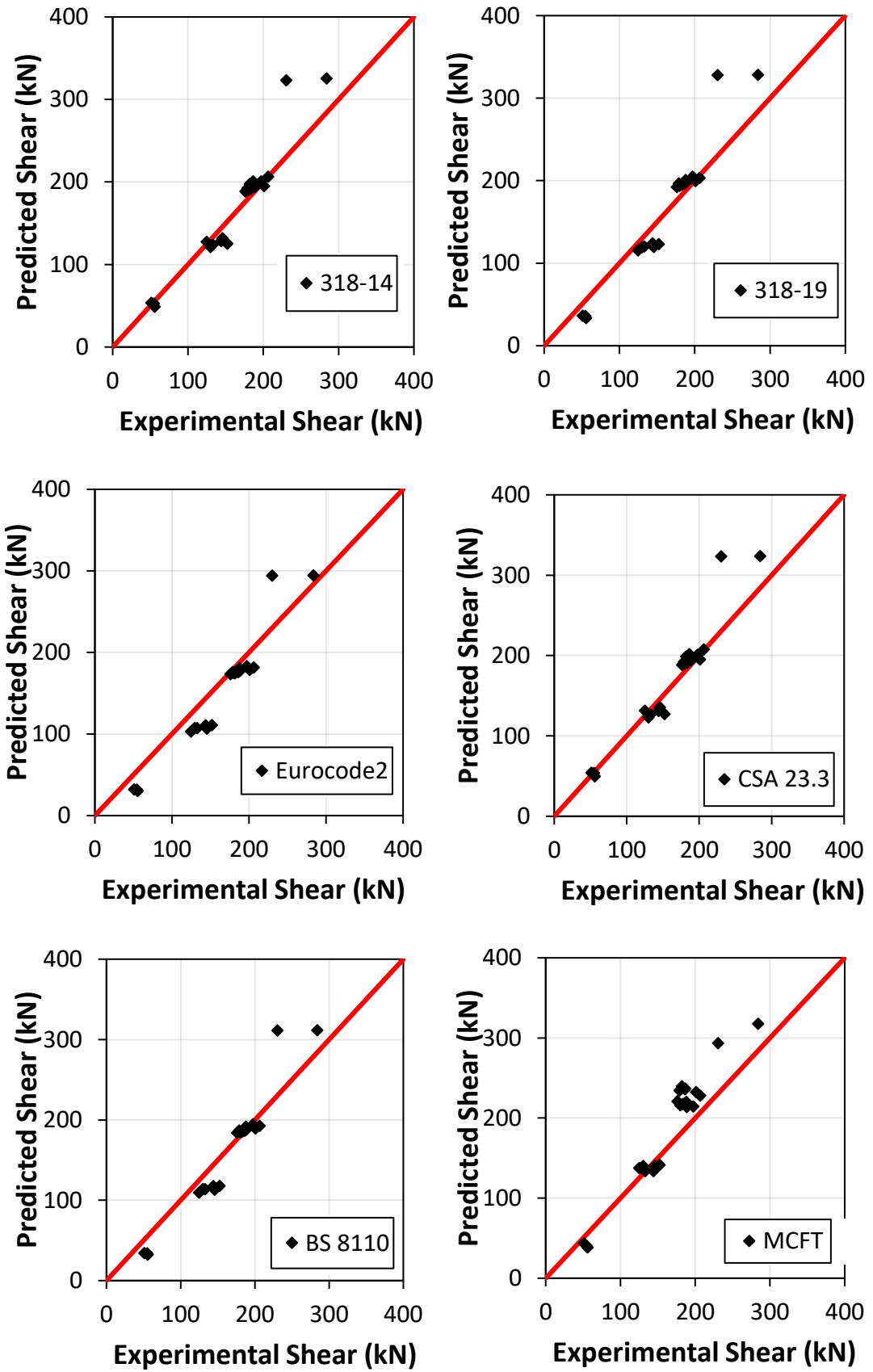


Figure 133: Predicted versus actual shear capacities for ACI 318-14 model.

Table 19: Experimental to predicted shear strength results based on actual f_y .

Group	Beam ID.	ACI		Eurocode2	CSA 23.3	BS 8110	MCFT
		318-14	318-19				
Group 1 $L = 1700$ $a/h = 2.5$ $f_c = 35$	W-4-25-2.5-35	1.00	1.02	1.13	1.00	1.07	0.91
	W-6-50-2.5-35	0.93	0.94	1.05	0.92	0.99	0.79
	W-8-100-2.5-35	0.93	0.95	1.06	0.93	1.00	0.79
	S-8-91.5-2.5-35	0.92	0.93	1.04	0.92	0.98	0.76
	W-4-50-2.5-35	1.11	1.22	1.37	1.08	1.29	1.04
	S-6-103.5-2.5-35*	0.98	1.08	1.21	0.95	1.14	0.91
	S-10-73-2.5-35	0.87	0.86	0.96	0.88	0.91	0.89
Group 2 $L = 1850$ $a/h = 3.0$ $f_c = 35$	W-4-25-3.0-35	0.98	0.96	1.08	0.98	1.01	0.92
	W-6-50-3.0-35	1.03	1.01	1.13	1.03	1.06	0.86
	W-8-100-3.0-35	0.97	0.95	1.06	0.97	1.00	0.88
	S-8-91.5-3.0-35	0.93	0.91	1.02	0.93	0.96	0.76
	W-4-50-3.0-35	1.12	1.16	1.30	1.10	1.23	1.08
	S-6-103.5-3.0-35	1.07	1.11	1.24	1.05	1.17	1.00
	S-10-73-3.0-35*	0.71	0.70	0.78	0.71	0.74	0.78
Group 3 $L = 1850$ $a/h = 3.0$ $f_c = 30$	W-4-25-3.0-30	0.95	0.94	1.04	0.95	0.98	0.85
	W-6-50-3.0-30	0.96	0.94	1.04	0.96	0.98	0.84
	W-8-100-3.0-30	0.95	0.93	1.03	0.95	0.97	0.83
	S-8-91.5-3.0-30	0.93	0.92	1.02	0.94	0.96	0.80
	W-4-50-3.0-30	1.21	1.24	1.37	1.20	1.29	1.08
	S-6-103.5-3.0-30	1.07	1.09	1.21	.06	1.14	0.93
Average		0.995	1.008	1.124	0.989	1.059	0.891
Standard Deviation		0.083	0.107	0.120	0.077	0.113	0.098
Coefficient of Variation		0.083	0.106	0.107	0.078	0.107	0.110

* Beams failed in flexure, but observed strength is close to shear strength.

The theoretical analysis is also conducted in this study on the tested beam specimens but with consideration of the nominal yield strength of the steel used. This approach results in a nominal shear strength, which is lower in magnitude than the corresponding strength based on the actual yield strength. The nominal yield strength of the steel material was specified in Chapter 5. For the WWF, it is equal to $f_{yw} = 500$ MPa for the 4mm and 8mm diameter wires, and equal to $f_{yw} = 450$ MPa for the 6mm diameter wires. For the stirrups, the nominal yield strength is equal to $f_{yst} = 460$ MPa. Table 20 and Table 21 show the predicted shears and experimental-to-predicted ratios

of all considered design specifications using nominal yield strength of transverse reinforcement. In general, the experimental-to-theoretical shear strength ratio based on nominal yield strength is 10-15% lower than corresponding ratio based on actual yield strength for all the considered codes. This shows that when the nominal values of steel strength are used, the codes are able to safely predict the shear capacity of the WWF reinforced and stirrup reinforced beams. To capture the effectiveness of design codes developed for stirrups in computing the shear capacity of beams reinforced with WWF, the average experimental-to-predicted ratios of each type is separately presented in Table 22. On average, the design codes predict shear capacity of beams reinforced with WWF with similar accuracy to that of beams reinforced with conventional stirrups.

Table 20: Experimental and predicted shear strength results based on nominal f_y .

Group	Beam ID.	Experimental Shear (kN)	Predicted Shear based on nominal f_y (kN)					
			ACI		Eurocode2	CSA 23.3	BS 8110	MCFT
			318-14	318-19				
Group 1 $L = 1700$ $a/h = 2.5$ $f_c = 35$	W-4-25	206.4	183.3	180.2	161.0	184.3	170.6	204.7
	W-6-50	186.4	183.4	180.6	161.4	184.4	171.0	215.5
	W-8-100	186.2	180.4	177.8	158.9	181.4	168.3	214.0
	S-8-91.5	182.0	181.1	178.5	159.5	182.1	169.0	218.4
	W-4-50	145.8	119.8	107.6	96.0	123.5	101.8	127.0
	S-6-103.5*	124.8	118.9	107.0	95.4	122.6	101.2	126.5
	S-10-73	283.9	294.0	297.0	266.4	292.4	281.9	288.1
Group 2 $L = 1850$ $a/h = 3.0$ $f_c = 35$	W-4-25	197.2	178.3	182.5	163.2	178.3	172.9	192.8
	W-6-50	200.9	178.4	182.7	163.5	178.4	173.3	212.0
	W-8-100	188.5	175.4	179.8	161.0	175.4	170.6	194.1
	S-8-91.5	178.8	176.1	180.5	161.6	176.1	171.3	214.1
	W-4-50	144.0	116.7	112.4	100.2	119.5	106.4	121.3
	S-6-103.5	132.8	115.8	111.7	99.6	118.5	105.7	122.9
	S-10-73*	230.3	291.9	296.5	266.1	292.0	281.6	266.1
Group 3 $L = 1850$ $a/h = 3.0$ $f_c = 30$	W-4-25	187.8	174.8	178.2	160.6	174.4	170.2	197.6
	W-6-50	183.4	174.9	178.5	160.9	174.5	170.6	198.4
	W-8-100	180.0	171.9	175.6	158.5	171.5	168.0	195.9
	S-8-91.5	176.2	172.6	176.3	159.1	172.2	168.6	201.6
	W-4-50	152.2	113.8	111.7	100.6	115.4	106.8	128.5
	S-6-103.5	130.0	112.9	111.0	100.0	114.5	106.2	128.8

* Beams failed in flexure.

Table 21: Ratio of experimental to predicted shear strength based on nominal f_y .

Group	Beam ID.	ACI		Eurocode2	CSA 23.3	BS 8110	MCFT
		318-14	318-19				
Group 1 $L = 1700$ $a/h = 2.5$ $f_c = 35$	W-4-25-2.5-35	1.13	1.15	1.28	1.12	1.21	0.99
	W-6-50-2.5-35	1.02	1.03	1.15	1.01	1.09	1.16
	W-8-100-2.5-35	1.03	1.05	1.17	1.03	1.11	1.15
	S-8-91.5-2.5-35	1.00	1.02	1.14	1.00	1.08	1.20
	W-4-50-2.5-35	1.22	1.35	1.52	1.18	1.43	0.87
	S-6-103.5-2.5-35*	1.05	1.17	1.31	1.02	1.23	1.01
	S-10-73-2.5-35	0.97	0.96	1.07	0.97	1.01	1.01
Group 2 $L = 1850$ $a/h = 3.0$ $f_c = 35$	W-4-25-3.0-35	1.11	1.08	1.21	1.11	1.14	0.98
	W-6-50-3.0-35	1.13	1.10	1.23	1.13	1.16	1.06
	W-8-100-3.0-35	1.07	1.05	1.17	1.07	1.10	1.03
	S-8-91.5-3.0-35	1.02	0.99	1.11	1.02	1.04	1.20
	W-4-50-3.0-35	1.23	1.28	1.44	1.21	1.35	0.84
	S-6-103.5-3.0-35	1.15	1.19	1.33	1.12	1.26	0.93
	S-10-73-3.0-35*	0.79	0.78	0.87	0.79	0.82	1.16
Group 3 $L = 1850$ $a/h = 3.0$ $f_c = 30$	W-4-25-3.0-30	1.07	1.05	1.17	1.08	1.10	1.05
	W-6-50-3.0-30	1.05	1.03	1.14	1.05	1.08	1.08
	W-8-100-3.0-30	1.05	1.02	1.14	1.05	1.07	1.09
	S-8-91.5-3.0-30	1.02	1.00	1.11	1.02	1.05	1.14
	W-4-50-3.0-30	1.34	1.36	1.51	1.32	1.42	0.84
	S-6-103.5-3.0-30	1.15	1.17	1.30	1.14	1.22	0.99
Average		1.079	1.091	1.218	1.071	1.149	1.039
Standard Deviation		0.110	0.135	0.151	0.103	0.142	0.108
Coefficient of Variation		0.102	0.123	0.124	0.097	0.124	0.104

* Beams failed in flexure, but observed strength is close to shear strength.

Table 23 shows the shear strength contribution of the concrete and transverse reinforcement based on the experimental testing and ACI 318-19. The experimental V_c is determined from the maximum shear strength of the beams that do not contain transverse reinforcement. The experimental V_s is obtained by deducting the shear strength of the beams that did not contain transverse reinforcement from the corresponding shear strength of the beams that contained transverse reinforcement. While this may not be very accurate since such values do not occur at the same level of

Table 22: Average experimental-to-predicted shear strength.

Group	Beam ID.	Average Experimental-to-Predicted					
		ACI318-14	ACI318-19	Eurocode2	CSA 23.3	BS 8110	MCFT
Group 1	WWF beams	0.993	1.033	1.153	0.983	1.088	0.883
	Stirrups beams	0.923	0.957	1.07	0.917	1.01	0.853
Group 2	WWF beams	1.025	1.02	1.143	1.02	1.075	0.935
	Stirrups beams	1	1.01	1.13	0.99	1.065	0.88
Group 3	WWF beams	1.018	1.013	1.12	1.015	1.055	0.9
	Stirrups beams	1	1.005	1.115	1	1.05	0.865

Table 23: Shear strength contribution of concrete and shear reinforcement.

Group	Beam ID.	Experimental		ACI 318-19	
		V_c	V_s	V_c	V_s
Group 1 $L = 1700$ mm $a/h = 2.5$ $f_c = 35$ MPa	W-4-25-2.5-35	51.1	155.3	51.6	151.7
	W-6-50-2.5-35	51.1	135.3	51.4	146.4
	W-8-100-2.5-35	51.1	135.1	51.3	145.6
	S-8-91.5-2.5-35	51.1	130.9	51.3	143.9
	W-4-50-2.5-35	51.1	94.7	41.4	78.1
	S-6-103.5-2.5-35*	51.1	73.7	41.3	74.3
	S-10-73-2.5-35	51.1	232.8	57.3	271.0
Group 2 $L = 1850$ mm $a/h = 3.0$ $f_c = 35$ MPa	W-4-25-3.0-35	54.8	142.4	57.7	147.2
	W-6-50-3.0-35	54.8	146.1	57.4	142.0
	W-8-100-3.0-35	54.8	133.7	57.1	141.2
	S-8-91.5-3.0-35	54.8	124.0	57.1	139.5
	W-4-50-3.0-35	54.8	89.2	48.1	75.9
	S-6-103.5-3.0-35	54.8	78.0	48.0	72.1
	S-10-73-3.0-35*	54.8	175.5	56.8	271.0
Group 3 $L = 1850$ mm $a/h = 3.0$ $f_c = 30$ MPa	W-4-25-3.0-30	55.6	132.2	53.4	147.2
	W-6-50-3.0-30	55.6	127.8	53.2	142.0
	W-8-100-3.0-30	55.6	124.4	52.9	141.2
	S-8-91.5-3.0-30	55.6	120.6	52.9	139.5
	W-4-50-3.0-30	55.6	96.6	47.4	75.9
	S-6-103.5-3.0-30	55.6	74.4	47.2	72.1

* Beams failed in flexure, but observed strength is close to shear strength.

loading, they can provide a good idea about such contributions. The results in Table 23 show very close agreement between the experimental and predicted values of V_c and V_s . This suggests that the shear strength predictive equations in the latest edition of the ACI 318 code for both V_c and V_s are reasonably accurate.

Chapter 8. Conclusions and Recommendations

8.1. Summary

The most common method to strength a concrete beam against shear is by means of rectilinear stirrups for all cross-sections except circular. This study is conducted to study an alternative method of shear reinforcement that utilizes welded wire fabric. To do so, a WWF sheet is cold formed into the shape of steel cage with additional rebars placed in the tensile zone caused by flexure. A total of 23 half-scale beams having 200mmx300mm cross-section and span length either equal to 1700 mm or 1850 mm are tested inside a UTM under displacement-controlled conditions with consideration of different variables. The beams were subjected point loads from the actuator head at a loading rate 1 mm/minute. The UTM was programmed to stop once the applied load drops to 50% of the peak load, on the descending part of the load-deflection relationship. Out of the 23 beams, 12 were transversely reinforced with WWF, 8 with stirrups and 3 without any transverse reinforcement. To preclude flexural failure and enforce shear failure in the beams, 15.2mm diameter high strength steel strands were utilized as flexural reinforcement (without prestressing). The variables that are considered in the study are the wire diameter (4-8mm), grid opening (25-100mm), concrete compressive strength (30 and 35 MPa, shear span-to-total depth ratio (2.5 and 3.0), and transverse steel reinforcement ratio ($A_v f_y / s = 251$ and 505 N/mm). Equivalent stirrup reinforced beams having the same transverse steel reinforcement ratio and total WWF weight, with correction for different steel yield strength among the WWF and stirrups, are also considered. The beams are instrumented with three LVDTs, of which two are attached to one side of the beams at 40-degree angles from the horizontal axis to measure the average width of the diagonal cracks at a location between the load and near support. The third LVDT is placed vertically just below the loading point to measure the beam deflection. Five strain gauges are placed on the vertical transverse steel reinforcement to monitor the strain in the WWF or stirrups within the shear critical region within 600 mm from the point of load application. Output of the experimental program yielded plots of load-deflection, load-average crack opening, load-strain. The applied load was converted to shear force based on the load-shear relationship (shear diagram) obtained from statics. The experimental results were processed and addressed shear-deflection relationships, ultimate shear strength, stiffness on the ascending part

of the load-deflection curve, and ductility. The experimental program was complemented with a theoretical component that addressed the shear strength of the tested beams based on the procedures included in the ACI 318 building code, Eurocode2, CSA 23.3, BS 8110, and the modified compression field theory model.

8.2. Conclusions

Based on the results of the experimental and theoretical components of the study, the following conclusions are drawn:

1. The manual work conducted in the laboratory showed that erecting steel cages for concrete beams made from WWF sheets entails shorter time and consumes less labor than assembling steel cages made from steel rebars and stirrups. Also, the end product from WWF is more uniform and consistent (leading to less tolerances) than corresponding one from conventional reinforcement utilizing rebars. If automated, the process will be enhanced by trimming further on labor costs and production time; thus, resulting in greater economy.
2. The strain gauge records showed that some of the instrumented vertical reinforcement within the high shear force region of the beams did not reach the yield point, even at peak shear force. Out of the 12 tested WWF reinforced beams, there were 7 in which none of the instrumented vertical wires exhibited yielding, although the stress in such wires reached at least 90% of the yield strength. For the stirrup reinforced beams, 6 out of the 8 beams had at least one stirrup reaching the yield point during the tests.
3. The angle of inclination of shear cracks is between 26.5 degrees and 48.5 degrees. The larger angles were observed in the beams that were loaded at a small shear span. Furthermore, the crack width at ultimate shear capacity for the WWF reinforced was generally smaller than the corresponding crack width in the stirrup reinforced beams.
4. In general, the test results showed that WWF reinforced beams possess 2-17% higher shear strength than corresponding stirrup reinforced beams in which the area of the stirrups is equivalent to that of the vertical wires of WWF. The elastic stiffness and post-elastic stiffness on the ascending part of the curve before the peak for the WWF reinforced beams are similar to those for the stirrups reinforced beams. The ductility index of WWF reinforced beams matched and, in some cases, exceeded the ductility index of corresponding stirrup reinforced

beams, which averaged around 2.0. This finding should alleviate any concerns related to the lack of adequate ductility at the material level in WWF.

5. As expected, stirrups reinforced beams in which the size and spacing of vertical stirrups are equivalent to the total volume of vertical and horizontal wires in WWF reinforced beams exhibited 33% higher shear strength than the WWF reinforced beams, although the ductility of the two different type of beams was similar.
6. The grid size in WWF reinforced beams has some impact on the shear strength. Beams containing WWF cages that consist of smaller diameter wires at narrow spacing exhibit higher shear strength than corresponding ones containing larger diameter wires at wide spacing. The normalized shear strength of the WWF reinforced beams with respect to the stirrup reinforced beams ranged 1.07-1.13 for the 25 mm mesh, 1.02-1.12 for of the 50 mm mesh, and 1.02-1.05 for the 100 mm mesh. This is because the concrete confinement in the core is enhanced by small mesh openings by protecting the concrete from excessive cracking and causing it to carry higher shear loads. However, caution should be exercised against the use of meshes made up of very small openings, as concrete infiltration during casting becomes problematic.
7. As expected, the effect of the vertical wire reinforcement ratio on the shear strength of WWF reinforced beams is significant. An increase in $(A_w f_{yw}/g)_v$ from 251 to 505 N/mm results in an average increase in the shear strength equal to 34%, which compares well with the 38% shear strength enhancement of corresponding stirrup reinforced beams.
8. Test results showed no consistent trend with regard to the effect of the shear span-to-depth ratio on shear strength. In some cases, beams loaded at $a/h = 2.5$ had higher strength than their corresponding counterparts that are loaded at $a/h = 3.0$ and in some other cases the opposite was witnessed. This finding support the new concrete shear strength provisions in the ACI318-19, which are independent of shear span.
9. The study showed that the WWF is about 5% more effective than stirrups in resisting shear when the concrete compressive strength is high ($f'_c=35$ MPa) than when it is low ($f'_c=30$ MPa). However, beams that had a lower compressive

strength reported approximately 10% higher ductility indices than corresponding beams that had a higher compressive strength.

10. The predicted shear strength by the ACI 318, Eurocode2, CSA23.3 and BS 8110 is within 6% of the actual strength obtained by the experiments. This shows that the current approaches in these structural design codes for computing the shear strength of stirrup reinforced beams can be safely used for computing the shear capacity of WWF reinforced beams without modifications.

Overall the results of this study show a promising future for utilizing WWF as shear reinforcement in concrete beams as an alternative to rectilinear stirrups.

8.3. Recommendations

Overall, the results of this study showed a promising potential for utilizing WWF as shear reinforcement in concrete beams as an alternative to rectilinear stirrups. Therefore, this study recommends the use of WWF as shear reinforcement without reservation. This is because WWF reinforced beams possess slightly higher shear strength and approximately the same ductility when compared to corresponding stirrup reinforced beams. The shear strength design provisions concerning concrete and transverse steel in structural design codes for beams subjected to gravity loads can be effectively used for calculating the shear capacity of WWF reinforced beams without adjustment. While the WWF used in the study was smooth-surfaced and galvanized, the findings of the study should be applicable also for WWF utilizing uncoated and/or deformed wires.

8.4. Suggested Future Research

Aside from investigating the flexural behavior of WWF reinforced beams, which is currently being conducted at AUS under the same research grant, the following proposed topics on the subject may be tackled in the future:

- Performance of WWF as shear reinforcement in beam cross-sections other than considered in the current study, such as T-section, box or circular.
- Shear strength of concrete beams transversely reinforced with WWF made with deformed wires.
- Investigation of epoxy-coated WWF as shear reinforcement in concrete beams.
- Researching high strength steel WWF (yield strength larger than 700 MPa) as shear reinforcement in concrete beams.

- Performance of axially loaded columns that are transversely reinforced with WWF instead of ties.
- Consideration of WWF reinforced beams made with high strength concrete (larger than 50 MPa).
- Impact of cyclic loading on the shear strength and ductility of WWF reinforced beams.
- Consideration of WWF in shear walls under the actions of bending, shear and axial compression.

References

- [1] L. E. Bernold and P. Chang, "Potential gains through welded-wire fabric reinforcement," *Journal of Construction Engineering and Management*, vol.118, no. 2, pp. 244-257, 1992.
- [2] S. W. Tabsh, "Stress-strain model for high-strength concrete confined by welded wire fabric," *Journal of Materials in Civil Engineering*, vol. 19, no. 4, pp. 286-294, 2007.
- [3] A. Griezic, W. D. Cook, and D. Mitchell, "Tests to determine performance of deformed welded wire fabric stirrups," *Structural Journal*, vol. 91, no. 2, pp. 211-220, 1994.
- [4] X. Y. Xuan, S. Rizkalla, and K. Maruyama, "Effectiveness of welded wire fabric as shear reinforcement in pretensioned prestressed concrete T-beams," *ACI Structural Journal*, vol. 85, no. 3, pp. 429-436, 1988.
- [5] ACI Committee 318, "ACI 318-11 Building Code Requirements for Structural Concrete," *American Concrete Institute, Retrieved*, vol. 8, 2012.
- [6] ACI Committee 318, "ACI 318-19 Building Code Requirements for Structural Concrete," *American Concrete Institute, Retrieved*, vol. 1, 2019.
- [7] W. H. Mosley, R. Hulse, and J. H. Bungey, *Reinforced concrete design: to Eurocode 2*. Macmillan International Higher Education, 2012.
- [8] Canadian Standards Association, *Design of concrete structures*. Mississauga, Ont.: Canadian Standards Association, 2004.
- [9] British Standard Institute, "BS 8110-1: 1997" *Structural Use of Concrete–Part 1: Code of Practice for Design and Construction*.
- [10] F. J. Vecchio and M. P. Collins, "The modified compression-field theory for reinforced concrete elements subjected to shear," *ACI Journal*, vol. 83, no. 2, pp. 219-231, 1986.
- [11] Technical Committee of the Wire Reinforcement Institute, *Structural Welded Wire Reinforcement*, ed. Hartford, CT: Wire Reinforcement Institute, 2016.
- [12] "Steel Concrete Reinforcement Brc Welded Wire Mesh Panel." Internet. [Online]. Available: <https://yaqiwiremesh.en.made-in-china.com> [Accessed: July 17, 2019].
- [13] P. University. "Welded Wire Reinforcement." Internet. [Online]. Available: <http://wpvecn3id01.itap.purdue.edu> [Accessed: October 1, 2019].
- [14] Unbox Factory. "How It's Made - Welded Wire Mesh and Chain Link Fencing Manufacturing." Internet. [Online]. Available: <https://www.youtube.com> [Accessed: September 25, 2019].
- [15] "Vinyl Coated Welded Wire Fabric." Internet. [Online]. Available: <https://www.weldedwiresupplier.com> [Accessed: September 20, 2019].
- [16] ASTM A1064/1065M-18a, "Standard Specification for Carbon-Steel Wire and Welded Wire Reinforcement, Plain and Deformed, for Concrete," ed. West Conshohocken, PA: ASTM International, 2018.
- [17] BS 4483, "Steel fabric for the reinforcement of concrete. Specification," ed. British Standard Institute, 2005.
- [18] ASTM A322-13, "Standard Specification for Steel Bars, Alloy, Standard Grades," ed. West Conshohocken, PA: ASTM International, 2018.
- [19] DIN 488-1, "Reinforcing Steels - Part 1: Grades, Properties, Marking," ed. Berlin, Germany: German Institute for Standardization, 2009.

- [20] Wikipedia, "Welded Wire Mesh," Internet. [Online]. Available: https://en.wikipedia.org/wiki/Welded_wire_mesh [Accessed: November 24, 2019].
- [21] AASHTO Committee, "AASHTO LRFD Bridge Design Specifications," ed. Washington, DC: American Association of State Highway and Transportation Officials, 2017.
- [22] J. G. MacGregor, J. K. Wight, S. Teng, and P. Irawan, *Reinforced concrete: Mechanics and design*. Prentice Hall Upper Saddle River, NJ, 1997.
- [23] D. Mitchell and M. P. Collins, "Diagonal compression field theory-a rational model for structural concrete in pure torsion," in *Journal Proceedings*, 1974, vol. 71, no. 8, pp. 396-408.
- [24] E. C. Bentz, F. J. Vecchio, and M. P. Collins, "Simplified modified compression field theory for calculating shear strength of reinforced concrete elements," *ACI Materials Journal*, vol. 103, no. 4, p. 614, 2006.
- [25] C. G. Karayannis and C. E. Chalioris, "Shear tests of reinforced concrete beams with continuous rectangular spiral reinforcement," *Construction and Building Materials*, vol. 46, pp. 86-97, 2013.
- [26] C. Lee, J.-Y. Kim, and S.-Y. Heo, "Experimental observation on the effectiveness of fiber sheet strip stirrups in concrete beams," *Journal of Composites for Construction*, vol. 14, no. 5, pp. 487-497, 2010.
- [27] S. Ahmed, "Use of Internal Structural Steel Strip Bands as Shear Reinforcement in Concrete Beams," M.S. thesis, American University of Sharjah, UAE, 2017.
- [28] S. Suwanpanjasil, T. Nakamura, K. Matsumoto, and J. Niwa, "Replacement of Conventional Steel Stirrups by Internal Reinforcing CFRP Grids in Shear of Concrete Beams," *Journal of JSCE*, vol. 5, no. 1, pp. 377-391, 2017.
- [29] R. Deivanai and R. Sathia, "A comparative study of welded and tied shear reinforcement in beams," *Journal of Chemical and Pharmaceutical JCPS*, vol. 9, no. 3, pp. 1535-1537, 2016.
- [30] M. M. Al-Nasra and N. M. Asha, "Shear reinforcements in the reinforced concrete beams," *American Journal of Engineering Research (AJER)*, vol. 2, no. 10, pp. 191-199, 2013.
- [31] J. A. Pincheira, S. H. Rizkalla, and E. K. Attiogbe, "Performance of welded wire fabric as shear reinforcement under cyclic loading," *ACI Structural Journal*, vol. 86, no. 6, pp. 728-735, 1989.
- [32] Y. Ladi and P. Mohite, "Experimental evaluation of reinforced concrete beam retrofitted with ferrocement," *International journal of research in engineering and technology*, vol. 2, no. 3, 2013.
- [33] S. Yuksel, "Behavior of Reinforced Concrete Walls with Mesh Reinforcement Subjected to Cyclic Loading," in *Fifth International Symposium on Innovative Technologies in Engineering and Science, Baku, Azerbaijan, 2017*, pp. 1308-1318.
- [34] M. Ajin and H. Gokulram, "Flexural Behaviour of RC Beam with Welded Mess as Shear Reinforcement," *International Journal of Engineering Sciences & Research Technology*, pp. 242-246, 2015.
- [35] N. KR and S. Kumar, "Flexural Behaviour of Self Compacting Concrete Beam using Welded Wire Mesh as Shear Reinforcement," *International Journal of Science and Research*, vol. 5, no. 6, p. 6 2016.

- [36] N. Lambert-Aikhionbare and S. W. Tabsh, "Confinement of high-strength concrete with welded wire reinforcement," *Structural Journal*, vol. 98, no. 5, pp. 677-685, 2001.
- [37] N. Lambert-Aikhionbare and S. W. Tabsh, "Ductility enhancement of high strength concrete columns with welded wire mesh," in *Structures 2004: Building on the Past, Securing the Future*, 2004, pp. 1-20.
- [38] B. Kusuma and P. Suprobo, "Axial load behavior of concrete columns with welded wire fabric as transverse reinforcement," *Procedia engineering*, vol. 14, pp. 2039-2047, 2011.
- [39] J. B. Mander, M. J. Priestley, and R. Park, "Theoretical stress-strain model for confined concrete," *Journal of structural engineering*, vol. 114, no. 8, pp. 1804-1826, 1988.
- [40] J. Hoshikuma, K. Kawashima, K. Nagaya, and A. Taylor, "Stress-strain model for confined reinforced concrete in bridge piers," *Journal of Structural Engineering*, vol. 123, no. 5, pp. 624-633, 1997.
- [41] F. Légeron and P. Paultre, "Uniaxial confinement model for normal-and high-strength concrete columns," *Journal of Structural Engineering*, vol. 129, no. 2, pp. 241-252, 2003.
- [42] B.-S. Han and S.-W. Shin, "Confinement effects of high-strength reinforced concrete tied columns," *International Journal of Concrete Structures and Materials*, vol. 18, no. 2E, pp. 133-142, 2006.
- [43] R. G. Delalibera and J. S. Giongo, "Theoretical and numerical analysis of reinforced concrete beams with confinement reinforcement," *Revista IBRACON de Estruturas e Materiais*, vol. 1, no. 1, pp. 17-30, 2008.
- [44] K. Jaafar, "Utilising confinement reinforcement for shear resistance in reinforced concrete structures," 2013.
- [45] ASTM A370-18, "Standard Test Methods and Definitions for Mechanical Testing of Steel Products," ed. West Conshohocken: ASTM International, 2018.
- [46] ASTM E8/E8M-16a, "Standard Test Methods for Tension Testing of Metallic Materials," ed. West Conshohocken: ASTM International, 2018.
- [47] G. Russo, D. Mitri, and M. Pauletta, "Shear strength design formula for RC beams with stirrups," *Engineering Structures*, vol. 51, pp. 226-235, 2013.

Vita

Yazan Lutfi Alhoubi was born in Dubai, in June 1995. He studied in several international schools and graduated from The International School of Choueifat in 2013. Mr Alhoubi joined the American University of Sharjah fall of 2013 and graduated fall of 2016, where he studied Bachelor of Science degree in Civil Engineering. He then started his master program in the American University of Sharjah spring of 2017 and was awarded a graduate teaching assistantship.